MOISTURE EFFECTS ON THE HIGH STRAIN-RATE BEHAVIOR OF SAND

By

BRADLEY E. MARTIN

A THESIS DISSERTATION PRESENTED TO THE GRADUATE SCHOOL
OF THE UNIVERSITY OF FLORIDA IN PARTIAL FULFILLMENT
OF THE REQUIREMENTS FOR THE DEGREE OF
MASTER OF ENGINEERING

UNIVERSITY OF FLORIDA

2007

ACKNOWLEDGMENTS

I would like to thank each member of the supervisory committee for their suggestions and support. Considerable appreciation is extended to Dr. Oana Cazacu for her willingness, support and friendship throughout this study at such short notice. Special thanks and gratitude is given to Dr. Weinong Chen of Purdue University for the support, friendship and help to become knowledgeable and proficient with conducting split-Hopkinson pressure bar experiments. This research would not have been possible without the generosity of Dr. Weinong Chen for the use of his facilities and for the many fruitful conversations during this work. I have great appreciation for Dr. Mary L. Hughes from Auburn University for the many valuable conversations, friendship, and continuous persistence to have me pursue this Master's Thesis. I sincerely appreciate the U.S. Air Force Research Laboratory, Damage Mechanisms Branch (AFRL/MNMW) for there financial support, for providing the opportunity to pursue this research, and for future opportunities to pursue my Doctorate Degree.

This research would not have been possible without the help and assistance from my colleagues Dr. Bo Song of Purdue University, Dr. Steven Akers of U.S. Army Engineering Research and Development Center and Mr. Mark Green from the Air Force Research Laboratory, AFRL/MNMW. I am very appreciative for there help and willingness to support me in this research.

This degree is not possible without the friendship and moral support of fellow graduate student Stefan Soare and colleague Brian Plunkett. I would like to acknowledge that without the love and support of my wife Jessica Martin during the duration of this degree program it would not have been possible. I finally give all thanks to God for giving me the will and desire to accomplish this degree.

TABLE OF CONTENTS

LIST OF TABLES

LIST OF FIGURES

Abstract of Thesis Presented to the Graduate School
of the University of Florida in Partial Fulfillment of the
Requirements for the Degree of Master of Engineering

MOISTURE EFFECTS ON THE HIGH STRAIN-RATE BEHAVIOR OF SAND

By

Bradley E. Martin

August 2007

Chair: Oana Cazacu
Major: Mechanical Engineering

The behavior of soils in the quasi-static regime is well characterized and fairly well understood. However, for the dynamic behavior of soils is less known and understood. The goal of this research is to characterize the effects of moisture content on the high strain rate deformation and strength of fine grain sand. To this end, split-Hopkinson pressure bar tests were conducted at a given strain-rate of 400/s using the equipment at Purdue University. The material studied has a dry density of 1.50 g/cc. The range of moisture contents investigated was from 3% to 20%. In addition, the specimens were confined using (1) confinement applied using a steel tube, (2) confinement applied using a polycarbonate tube. The experimental protocol varied from that traditionally followed in that pulse shaping was used to acquire stress equilibrium and constant strain-rate within the specimen.

The experiments indicate that the moist/partially saturated sand is more compressible (less stiff) than dry sand. The softening of the moist/partially saturated sand may occur due to the pore water acting as a lubricant between the sand particles that cause a reduction in shear loads. Similar trends were reported for the behavior in the quasi-static regime based on results of tests performed at the U.S. Army Engineering Research and Development Center.

CHAPTER 1
INTRODUCTION

1.1 Background

In today's society geo-materials are widely used in engineering applications ranging from military to construction uses. For instance, in military applications soils are important because they are often used as either over-burdens for protective structures, or they affect the overpressure region associated with weapon effects (Felice et al. [1]). Compared to traditional engineering materials such as metals, the mechanical behavior of geo-materials are much less characterized and are consequently less understood, in particular, when subject to high loading rates. A better understanding of the dynamic response of soils will aid in the military's ability to better predict the response of soils by incorporating associated physics into current or new constitutive models for geo-materials.

Geo-materials are also widely used in the commercial areas of mining and earthquake engineering (Hampton et al. [2]). If a structure is to be designed to survive a certain level of ground motion such as those generated by an earthquake, it is important to have quantitative knowledge of the dynamic loading transmitted to the structure through its foundation. Better predictive methods are needed to specify the dynamic load histories on which the building design will be based. For this reason, again, improved knowledge and characterization of the dynamic response of soils is necessary.

A common predictive method is numerical simulation of the high-rate behavior of the entire soil system with a foundation described with a continuum scale model. However, the predictive capabilities of current soil models are limited due to the complexity of the material. In addition, models may not represent all the phenomenology associated with the dynamic response of soils or even incorporate all of the necessary parameters that influence the behavior e.g.

moisture content, different densities, etc. For example, unsaturated soils under loading exhibit a multiphase behavior due to four different constituents interacting to give the total material response (1) soil skeleton, (2) pore water, (3) grain stiffness, and (4) pore air (Hampton et al. [2]), and so realistic constitutive models will have to account for the mechanical response that reflects each of these constituents and the interactions among them. Furthermore, other parameters, such as stress states, loading rates, and grain refining may affect the mechanical response significantly. Such a model will have to be multi-scale and multi-physics in nature and currently does not exist.

Physics-based constitutive material models for high-rate applications are thus needed. However, geo-materials are traditionally not characterized at high strain rates. Sand, for example, has been sporadically investigated to characterize the high rate behavior over the past three or four decades. Although no theoretical or numerical methods are available for accurately predicting the dynamic response of sand, some experimental explorations have been performed to probe the sand response to high-rate loading (Veyera [3], and Felice et al. [1]). As will be pointed out later, due to different applications or limited experimental conditions, few of these results are suitable for the development of reliable rate-dependent constitutive models.

A complete set of systematically designed experiments for constitutive model development purposes will have to account for the effects of different geo-materials, loading rates, densities, stress states, temperatures, moisture levels and uncertainties in specimens and testing conditions. Due to the currently limited knowledge base the testing matrix for an extensive examination of the various effects can be prohibitively large. In this research, we focus our effort on investigating the effects of moisture/saturation content on the compressive

response of one kind of sand at one high strain rate, with one initial dry density, and two confining pressures (stress states).

1.2 Purpose

The research described herein is an experimental effort to investigate the behavior of unsaturated fine grained sand with various moisture/saturation levels subjected to dynamic compression with lateral confinement at one particular high strain rate using the Split Hopkinson Pressure Bar (SHPB). The SHPB has been shown to be a viable experimental method to investigate the dynamic properties of soils (Felice et al. [1]). The results of this research will contribute to a better fundamental understanding of the dynamic behavior of moist/partially saturated sand at high strain rates and aid in improving current and future constitutive models for geo-materials.

Chapter 2 consists of a survey of major contributions to the investigation of the dynamic response of soils. Although research has been conducted in this area for three to four decades many of the contributors did not have their focus specifically on the mechanical response of unsaturated sand at high strain rates. Previous research generally investigated various parameters instead of conducting controlled experiments to determine the effects of a single parameter such as saturation/moisture content. Due to limited experimental methods at the time of these efforts only a few could contribute to the development of rate-dependent constitutive models. Therefore, we pointed out the needs to conduct systematically designed experimental programs to form a basis of physics and data for the development of reliable constitutive models for this class of materials. In particular, the scope of this thesis research is limited mainly on the effects of moisture on the high rate compressive response of fine sand. The research is primarily experimental, using a split Hopkinson pressure bar to apply the dynamic loading and to record the sand specimen behavior.

Chapter 3 is devoted to the experimental method used in this research. This chapter will describe the history of the SHPB apparatus and a description of the one-dimensional wave theory used to reduce the data collected in experiments using the SHPB. To satisfy the conditions for a valid SHPB experiment, the necessity and a description of the pulse shaping technique used will be explained. In addition, a description of the confinement methods used will be discussed in conjunction with a discussion of the stress-states that are implemented with the different confinement methods. The material studied in this research and the procedure for specimen preparation will be discussed. A description of the material is provided to give the reader a general understanding of the material gradation and the physical properties for the material of choice. It will be illustrated that, in SHPB experiments, the specimen thickness is much smaller as compared to those commonly used in quasi-static experiments because the specimen is loaded by stress waves propagating and being reflected inside it. In dealing with small aspect ratios it is also recognized that inertia and/or frictional effects may exist, which will also be discussed. Additionally, the procedure for specimen fabrication and assembly is explained and shown for each confinement.

The experimental results are presented in Chapter 4. After presenting typical raw experimental records and validity checks, the primary results are presented in terms of stress-strain curves obtained at a high strain rate on fine grained sand with a wide range of moisture/saturation conditions. The experimental results obtained from dry sand, 0% saturation, and the moist/partially saturated sand will be compared to identify the trends and to understand the moisture effects on the mechanical response of the material. Also, confinement effects will be investigated to identify the effects of differences in confining conditions. Lastly, unusual phenomenon in the data will be pointed out.

Chapter 5 will give discussions of the results and any recommendations for future work, respectively. The discussions will illustrate how the current results may contribute to a better understanding of the dynamic mechanical behavior of the sand with the support of newly obtained quantitative experimental results. The recommendations are made based on a detailed analysis of the experimental work presented in this research. These recommendations will help to better plan for future research and to increase the level of fidelity of the data obtained to aid in further improving modeling efforts.

CHAPTER 2
STATE OF THE ART IN RESEARCH ON DYNAMIC RESPONSE OF SOILS

The split-Hopkinson pressure bar technique, originally developed by Kolsky [4-5], has been used as a tool by investigators in the last five decades to evaluate the dynamic response of materials at high strain rates. The technique has been extensively used to study the plastic behavior of metals at strain rates between $10^2 – 10^4$ s^{-1} (Nemat-Nasser [6]) and recently has been used for evaluating the dynamic response of soils at the same strain rates.

The conventional split-Hopkinson pressure bar consists of a striker bar, an incident bar and a transmitter bar with the specimen located between the incident and transmitter bars. A gas gun launches the striker bar into the incident bar and propagates an elastic wave down the incident bar towards the specimen. As the wave arrives at the end of the incident bar if the impedance of the specimen is less than that of the incident bar, a compressive wave will be transmitted through the specimen to the transmitter bar, and, a tension wave reflected back in the incident bar. After the compressive wave traverses the specimen length and reaches the transmitter bar, part of the wave will be reflected back through the specimen as a compressive wave in the specimen, which builds up the stress in the specimen, and part will be transmitted as a compressive wave in the transmitter bar. If the elastic compressive wave in the bars is nondispersive, and if the specimen undergoes uniform deformation at a constant strain rate under dynamically equilibrated stress, then one-dimensional (1-D) wave propagation theory can be utilized to determine the specimen's dynamic response.

Attaining dynamic equilibrium in the test specimen may not be an issue of concern in conventional/classical split-Hopkinson pressure bar experiments on materials with high wave speeds, in which the stresses in the specimen rise quickly, However, for geo-materials, in which the wave speeds are quite low compared to common engineered materials, the loading durations

and rise times of the incident pulse needs to be longer to ensure the specimen is in stress equilibrium and at constant strain rate before significant behavior such as damage, compaction, or failure occurs. The material investigated in this research has a wave speed of approximately 500 m/s depending on the material conditions (Pierce [7]), which is an order of magnitude lower than those in a steel or an aluminum alloy. To ensure that constant strain rate and stress equilibrium are acquired the classical split-Hopkinson pressure bar will have to be modified before reliable dynamic data can be produced. To accomplish stress equilibrium and constant strain rate a pulse shaping method was implemented to increase the pulse rise time and loading duration.

This chapter consists of two sections in which previous work has been reviewed and cited for it's relevance to this research. The first section will include a discussion of previous work using various experimental techniques to evaluate the dynamic behavior of both dry, 0% saturated sand and unsaturated/moist sand. The second section consists of a discussion on the history and purpose for implementing a pulse shaping technique for this research. The state of the art and history of the split-Hopkinson pressure bar will be presented in more details in Chapter 3.

2.1 Previous Studies on Dynamic Response of Soils

The dynamic response of soils has been sporadically investigated for the last four decades. The research efforts studied different types of soils for various experimental conditions (i.e., saturation levels, strain rates etc.) rather than conducting controlled experiments to determine the effects of a single parameter such as moisture/saturation content. Due to limited experimental techniques available at the time of these efforts, only a few could contribute to the development of rate-dependent constitutive models mainly because of changes in multiple experimental parameters and lack of data. These earlier experimental investigations using SHPB were

conducted in a conventional manner, without pulse shaping, prohibiting the soil specimens from obtaining constant strain-rate deformation possibly not producing accurate dynamic material data. The following discussion will give a brief history of the dynamic response of soils and point out any inaccuracies of the experimental research.

The SHPB has been used to characterize various parameters of soils subjected to dynamic loading. Charlie et al. [8] tested unsaturated 50/80 silica sand subjected to dynamic compressive loading using a SHPB. The sand specimens were compacted using a 1.36 kg steel hammer in four equal lifts to a dry density of 1600 kg/m^3 with a final specimen length of 10.16 cm (4.0 inches) and diameter of 5.08 cm (2.0 inches). The specimens were confined by a steel tube and held in place by steel wafers on both sides of the specimens with o-rings between the outer diameter of the steel wafer and the inner diameter of the steel confinement. The primary focus was to evaluate the effects of saturation levels on the material wave speed and transmission ratio (ration of the transmitted stress to the incident stress). Although such experimental data is needed for wave propagation studies in sand, the data does not provide sufficient information for the development of rate dependent material models. In earlier work by Ross et al. [9] a SHPB was used to evaluate a single short pressure pulse traveling through long soil specimens in order to assess the effects on the materials. Ross tested many different materials, specifically, 20/40 dry sand, 50/80 dry sand, silica flour, clay, glass beads, and steel balls. These materials were subjected to dynamic loadings to assess their effects on material properties (i.e., wave velocity, transmission ratio etc.). In addition, the effects of static and dynamic compaction methods were also investigated in conjunction with varying moisture contents. This work provided valuable data relating the force histories on both sides of the specimens. However, to improve predictive

capabilities using rate dependent models the material stress-strain response needs to be determined, which requires experiments designed for this purpose.

Pierce [7] in 1989 evaluated moisture and confining effects using a SHPB for 20-30 Ottawa sand and for Eglin sand. The specimens were subjected to a dynamic, single short compressive pulse to study the effects on the material's dynamic properties. All specimens were compacted dry, saturated, and then desaturated using the pressure plate method. Tri-axial confining pressures were applied to the specimens by applying axial pressure through the incident/transmitter bars in the axial direction and by pressurizing water between a thin membrane and the inner wall of the confining cell to apply the lateral confinement. The type of data obtained, was primarily, stress transmission ratio and wave speed data, collected at varying percent saturation levels and at confining pressures of 0 kPa and 310 kPa. This set of experiments again does not provide sufficient data to develop the needed rate-dependent material models for improving predictive capabilities.

Felice et al. [10] in 1987 conducted a small number of experiments using a split-Hopkinson pressure bar to evaluate the high strain-rate behavior of compacted soil. The stress-strain behavior was studied for a clayey sand with varying water contents to determine there effects. The samples were prepared from bulk quantities of clayey sand that was slaked to ensure a uniform mixture with large clumps of soil broken apart. Of the 26 experiments conducted, 10 had a specimen length of 12.7 mm with the remaining 6.35 mm in length, but all had the same diameter of 60.4 mm with each specimen size evaluated at varying moisture contents. In addition, the two specimen sizes were assessed at two different loading stresses by changing the velocity of the striker bar, and hence the strain-rate. Although the clayey sand is characterized dynamically limited experiments were conducted at one specimen size, one strain

rate and moisture content. There is clearly a need to conduct a statistically sufficient amount of experiments in order to acquire a representative material response to one set of experimental conditions. Although the data presented (Felice et al. [10]) is the type needed for developing a constitutive model, the effects of additional moisture contents need to be evaluated at one particular strain rate and specimen size to ensure a true material response due to moisture effects.

In 1994, Veyera [3] studied the uniaxial stress-strain behavior of compacted moist soils. The soils were undrained, confined compression SHPB tests conducted at strain rates of 1000/s and 2000/s. Three types of soils were investigated: Eglin sand, Tyndall sand, and Ottawa 20-30 sand. Each of the specimens were 50.8 mm (2.0 inches) in diameter and compacted In Accordance With (IAW) ASTM D-698 to lengths of 12.7 mm (0.50 inches) and 6.4 mm (0.25 inches) for 1000/s and 2000/s strain rates, respectively, with all specimens having the same dry density. All materials were evaluated at varying levels of saturation from 0% - 100%, where 100% is fully saturated with no air voids. The typical data obtained from the SHPB experiments is shown in Figure 2-1. The loading pulse was square, with a short rise time, which is not typically associated with attaining constant strain rate deformation of a sand specimen. The reflected pulse had a short rise time followed by a negative decaying slope indicating that the specimens never acquired a constant strain rate. The author concluded that the stress-strain behavior appears to be strain-rate independent, but this conclusion could be inaccurate since the loading pulse did not produce a constant strain-rate in the specimen.

Work conducted by Lee et al. [11] of Sandia National Laboratories performed uniaxial strain tests to determine the effects of moisture content on the quasi-static behavior of the same material investigated herein. Lee investigated the sand at strain-rates of 10^{-4} s^{-1} to 10^{-5} s^{-1} and a dry density of 1.65 g/cc. The specimens were evaluated in a dry condition and were

moist/partially saturated with a moisture content of 7.5%. This is one of the first experimental efforts to study both dry and moist/partially saturated sand in the same research effort to determine the effects of moisture content. The specimens used in this research had diameters of 50.8 mm (2.0 inch), lengths of 101.6 mm (4.0 inch), and aspect ratios of 2.0. The uniaxial strain test uses a fluid to apply radial confinement to the specimen to prohibit lateral deformation of the specimens. While being confined radially the specimen is loaded simultaneously in the axial direction. The trends presented in the research by Lee agree with the trends presented in this report. Akers et al. [12], of Waterways Experiment Station, performed uniaxial strain tests at both dry and moist/partially saturated conditions for the same material. The specimen diameter was 50.8 mm (2.0 inch), 110 mm (4.33 inch) in length and an aspect ration of ~ 2.2. The dry density of all the specimens was 1.65 g/cc with the moist/partially saturated specimens having a moisture content of 7.0% and all tests conducted at strain-rates of 10^{-4} s^{-1} to 10^{-5} s^{-1}. The trends presented in the research by Akers et al. [12] also agrees with the trends obtained in this study and will be discussed in Chapter 4. Data obtained by Lee et al. [11] and Akers et al. [12] is essential to developing the quasi-static portion of the constitutive equation, but geo-materials have limited data at best that adequately describes the dynamic behavior of geo-materials.

Previous efforts by Whitman et al. [13] and Whitman [14] showed the relations between soil properties and crater size and shape, ground motions, and response of buried structures. The dynamic properties of soils were determined by rapidly loading the soil with a square pulse with varying rise times. The experiments conducted in these two reports evaluated many different types of soils at different loading conditions. Soils were studied using a triaxial apparatus developed by MIT that evaluated several different types of soils at both dry and wet conditions in order to determine the shear strength of the materials. Additional uniaxial strain experiments

were conducted using an oedometer (i.e., uniaxial strain apparatus) to study various soils stress-strain behavior at varying loading rates (i.e., 15 msec and higher rise time to peak load). In earlier work by Durbin [15] a modified shock tube was used to apply slow and fast rates of loading of two different types of sand with the samples loaded using a step pulse with a long duration. The samples were 12.85 inches long and 1.5 inches in diameter and confined laterally in the modified shock tube. The experiments measured the flow field properties of the materials due to the shock loading imparted by the shock tube apparatus. These research efforts (Whitman et al. [13], Whitman [14], and Durbin [15]) offer good insight into the quasi-static behavior of soils under various testing conditions, however, the strain-rates are much lower than a typical SHPB experiment.

High fidelity material modeling requires clear and accurate experimental results from well-designed and valid experiments. The motivation of this research is to conduct controlled experiments to evaluate the dynamic response of one material at a single high strain-rate with varying moisture contents and constant strain-rate deformation. The only parameter that is systematically varied is the moisture content. Stress state is varied, but only at two different conditions, through the change in confining jacket material. These experiments are part of a more complete experimental plan, which is beyond the scope of this thesis.

2.2 Pulse Shaping Experimental Technique

For conducting quasi-static compression experiments, the cross-head speed of the loading frame is typically controlled by closed-loop servo systems to ensure that the desired testing conditions are followed in the tests. In SHPB experiments, valid testing conditions are ensured through the control of the loading pulse profiles. The conventional SHPB typically has incident pulses with small rise times followed by nearly constant amplitudes overridden by high-frequency oscillations that introduce several complications depending upon the specimen

material under investigation. In the experiments on sand that will be presented later in this thesis, a longer rise time is needed to facilitate the porous specimen to achieve dynamic stress equilibrium; a longer pulse duration is necessary to deform the specimen to a significant strain level encountered in practical applications; and a smooth pulse profile is desired to load the specimen with a well-defined loading history and to minimize the uncertainties associated with dispersion correction.

To produce such desired incident pulses, we used an experimental technique called "pulse shaping". The pulse shaping technique was originally pioneered by Duffy et al. [16] in 1971. Duffy et al. [16] at that time wanted to evaluate rate effects in 1100-0 Aluminum using the split-Hopkinson torsion bar. It was determined that torsion instead of compression would eliminate the wave dispersion found in a conventional split-Hopkinson pressure bar due to the minimization of inertia effects associated with the propagation of the two types of waves in the bars, in addition to removing the radial inertia and frictional constraint in the specimens. The torsional-Hopkinson bar (Duffy et al. [16]) used a small explosively filled detonator to initiate the striker bar. Using this launching method it was discovered that the strain rate varied considerably due to high frequency components of large amplitude imbedded in the incident pulse. In order to study strain rate effects of materials the loading pulse needed to have a short rise time followed by a steady loading opposed to a short rise time followed by a decreasing amplitude. To mitigate the high frequency components thin lead strips were placed between the striker bar and the end of the Hopkinson bar and additionally a short length (0.25 mm) of tubing 0.76 mm in thickness (called a pulse smoother) was placed between the end of the incident bar and the specimen.

In 1982, pulse shaping was introduced to the conventional compression SHPB by Ellwood et al. [17]. The author wanted to modify the conventional split-Hopkinson pressure bar through pulse shaping to create a constant strain rate in the material of interest at high strain rates. The conventional SHPB was producing a flat-topped incident pulse rather than an incident pulse with a short rise time followed by a profile that facilitates constant strain rate in the specimen, so Ellwood et al. [17], modified the conventional SHPB to accommodate a third bar (Figure 2-2). A dummy specimen of the same material as the specimen was placed between the preloading bar and loading bar to function as a pulse shaper. Upon impact of the preloading bar the dummy specimen expanded radially and shortened allowing the high frequencies in the signal to be eliminated. The similar hardening behavior between the dummy and the real specimens resulted in a nearly flat reflected signal in the incident bar, which, as will be discussed in Chapter 3, indicates a constant strain-rate deformation in the specimen.

The pulse shaping technique was found to be quite adaptable to different types of pulse shapers other than circular disks. Christensen et al. [18] found that by replacing the typical right circular cylinder striker bar with a truncated cone striker bar they could obtain better resolution of the initial part of the stress-strain curve in evaluating the dynamic response of rocks. By holding the amount of truncation constant at 3.597 inch and varying the cylinder/cone area ratio the incident pulse loading could be varied (Figure 2-3). This technique discovered that the pulse shaping method could be easily modified to produce different types of desired input loading profiles.

In 1984 Frantz et al. [19] implemented several pulse shaping techniques to acquire a slow rise time pulse in order to reduce the effects of wave dispersion. The split-Hopkinson pressure bar used by the authors (Frantz et al. [19]) was a two bar system versus the three bar system

employed by Ellwood et al. [17]. The authors (Frantz et al. [19]) discovered that by machining a large radius at the end of the striker bar this would create a non-planar impact but eventually found that the effects of the non-planar impact become insignificant after traveling a short distance in the incident bar. The second pulse shaping method (Frantz et al. [19]) implemented was to place a pulse shaper on the impact end of the incident bar, which is the more applied technique currently used. The pulse shaper materials were paper, aluminum, brass or stainless steel. In addition, the authors (Frantz et al. [19]) show that by choosing the proper pulse shaping material that a constant strain rate could be achieved in an annealed 304 stainless steel.

By the early 1990s the pulse shaping technique was becoming a more accepted experimental technique to provide constant strain rates and allowing stress equilibrium to be obtained. In 1991 Nemat-Nasser et al. [20] introduced the pulse shaping technique to characterize brittle materials in addition to the first numerical code to predict the pulse shapes based on pulse shaper material and dimensions.

In determining the dynamic response of brittle materials it becomes difficult to use a conventional split-Hopkinson pressure bar due to the flat top of the incident pulse. If the stress in the specimen produced by the flat-top loading is below the compressive strength of the brittle material, the specimen will not fail during the dynamic loading. On the other hand, if that stress reaches the specimen compressive strength, the specimen fails during the rising portion of the incident pulse. Due to the short rise time in a conventional SHPB loading pulse, the specimen is typically not in stress equilibrium when failure occurs. The strain to failure for brittle materials generally occurs below one or two percent strain, and the stress-strain behavior before failure is nearly linear. To produce a constant strain rate deformation in such a specimen and let

damage/failure occur after dynamic stress equilibrium is achieved, a pulse with a ramped loading is required (Nemat-Nasser et al. [20]).

Using an OFHC pulse shaper of 4.8 mm (0.190 inch) diameter and 0.5 mm (0.020 inch) thickness a triangular pulse was created (Figure 2-4). The triangular pulse has an initial regime of positive strain rate, followed by a regime of zero strain rate and ending with a regime of negative strain rate. As shown in Figure 2-4 the numerical simulation is in good agreement with the incident pulse. By introducing this technique it was shown that constant strain-rate deformation can be achieved in brittle specimens using a split-Hopkinson pressure bar.

In the more recent present the pulse shaping technique has been extended to the use of a two material compound pulse shaper. Frew et al. [21] showed that a combination of copper and steel pulse shapers is essential to conduct valid SHPB experiments on high-strength steel specimens. The impact end of the incident bar was equipped with an assembled pulse shaper consisting of a copper (C11000) disk attached to a M42 tool steel disk and then to a 4340 steel disk (Figure 2-5). In addition, the analytical model (Frew et al. [22]) was modified to accommodate a two material compound pulse shaper. The experimental data and analytical model are in good agreement showing that the model is capable of predicting the incident pulse and minimizing trial experiments.

In the application of the pulse shaping technique, a trial test needs to be performed to examine the specimen behavior under dynamic loading. The desired incident pulse should have the shape of the transmitted pulse (specimen behavior) but higher in amplitude such that the reflected signal, which is proportional to the strain rate, is nearly flat, indicating constant strain rate. The analytical models developed by Frew et al. [21, 22] can serve as effective tools in determining the proper pulse shaper material and dimensions. Without the guidance of such

predicting tools, a large amount of trial experimental work or extensive laboratory experience is needed to find proper pulse shapers.

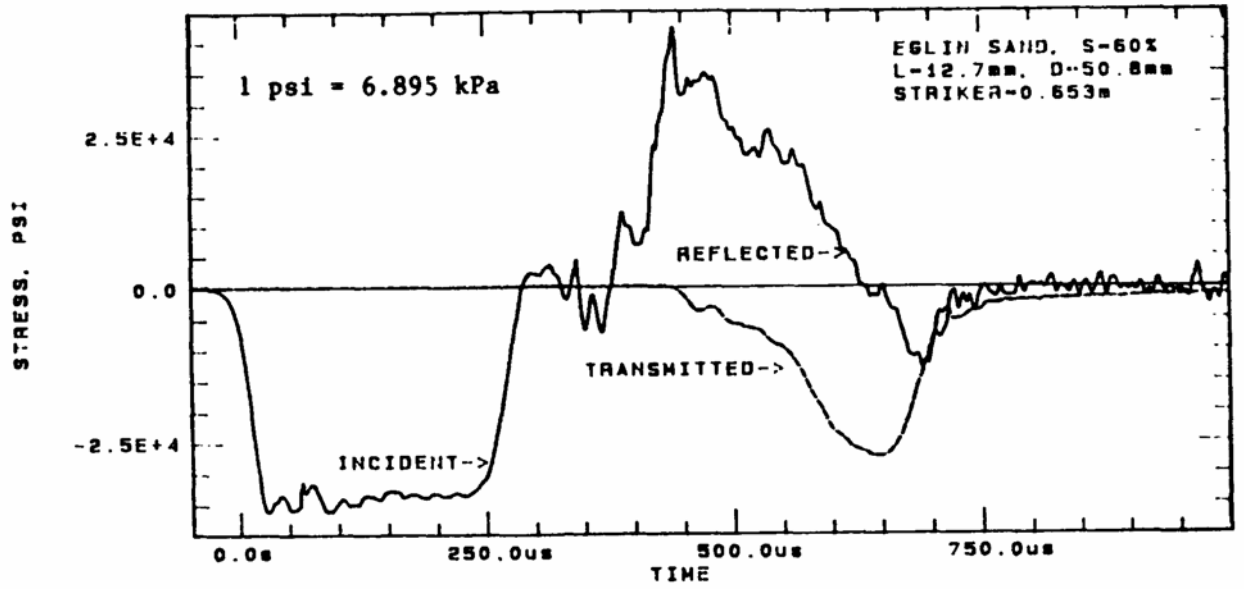

Figure 2-1. Raw data of a typical experiment conducted using the classical split Hopkinson Pressure Bar. [Reprinted from Veyera, G.E., 1994, "Uniaxial Stress-Strain Behavior of Unsaturated Soils at High Strain Rates," WL-TR-93-3523, Wright Laboratory Flight Dynamics Directorate, Tyndall AFB, FL. (Figure 6)]

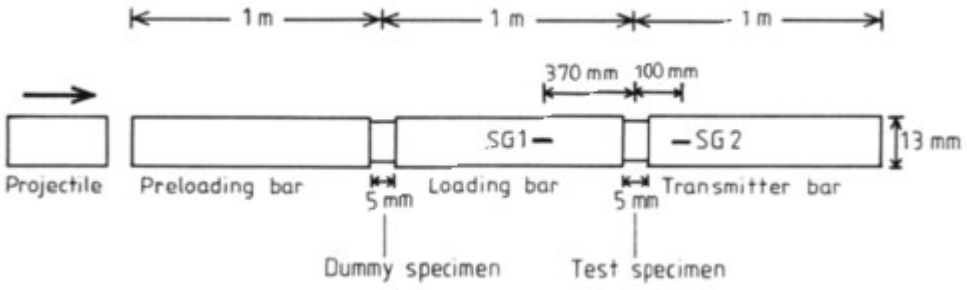

Figure 2-2. Modified split-Hopkinson bar with a third bar with and a dummy specimen simulating a pulse shaper. [Reprinted from Ellwood, S., Griffiths, L.J., and Parry, D.J., 1982, "Materials Testing at High Constant Strain Rates," J. Phys. E: Sci. Instrum., 15, pp. 280-282. (Figure 2)]

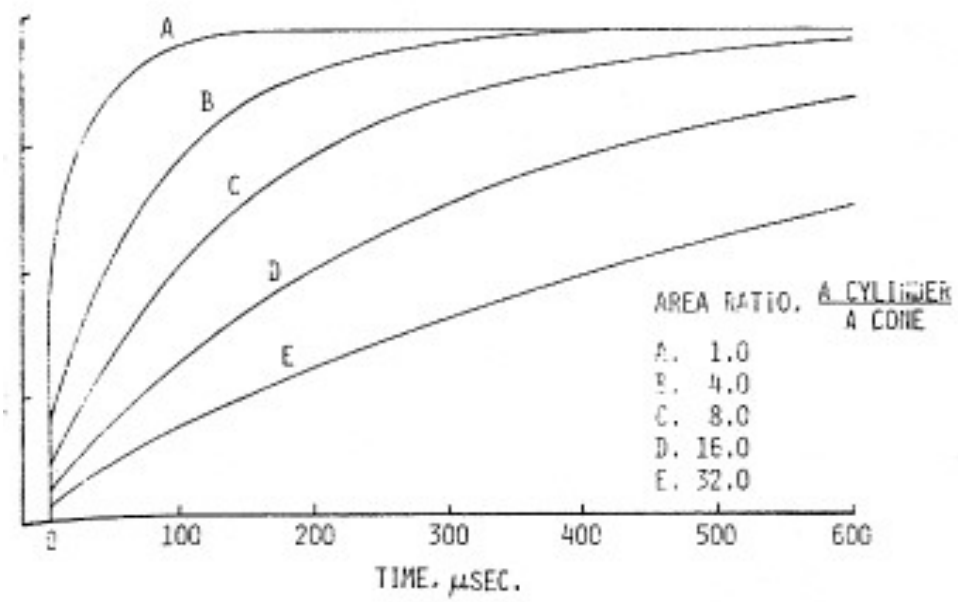

Figure 2-3. The modified input stress wave by Christensen et al. The pulses were obtained using a truncated conical tipped striker bar. [Reprinted from Christensen, R.J., Swanson, S.R., and Brown, W.S., 1972, "Split-Hopkinson-bar Tests on Rock under Confining Pressure," Exp. Mech., pp. 508-513. (Figure 6)]

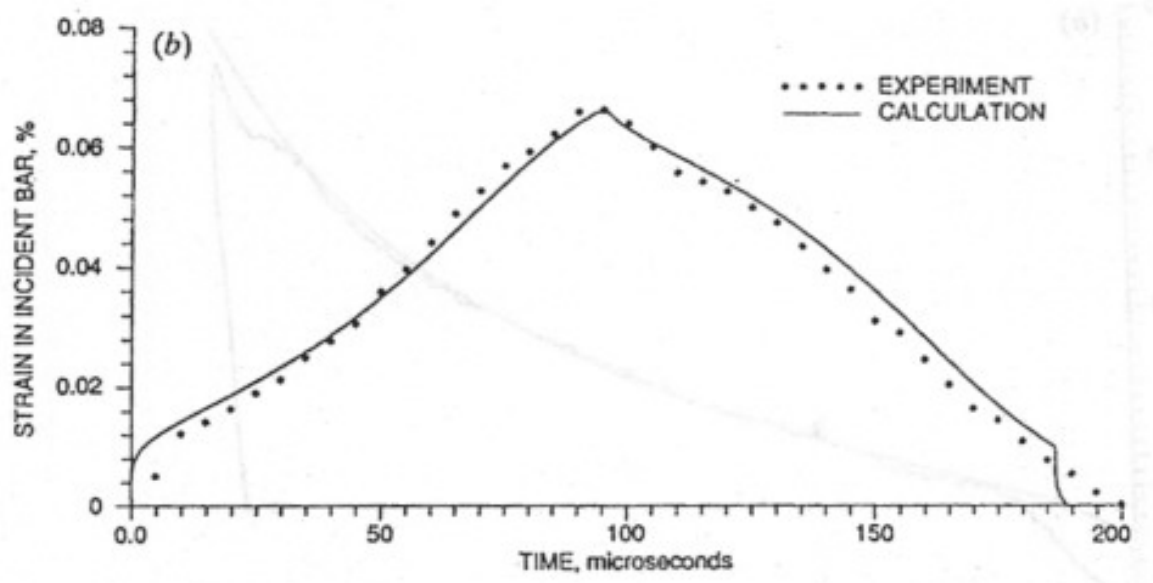

Figure 2-4. Triangular ramp strain profile determined by Nemat-Nasser et al. This profile was obtained using an OFHC pulse shaper with a 0.190 in. diameter and 0.20 in. thickness. [Reprinted from Nemat-Nasser, S., Isaacs, J.B., and Starrett, J.E., 1991, "Hopkinson Techniques for Dynamic Recovery Experiments," Proc. R. Soc. London, Ser. A, **A435**, pp. 371-391. (Figure 4b)]

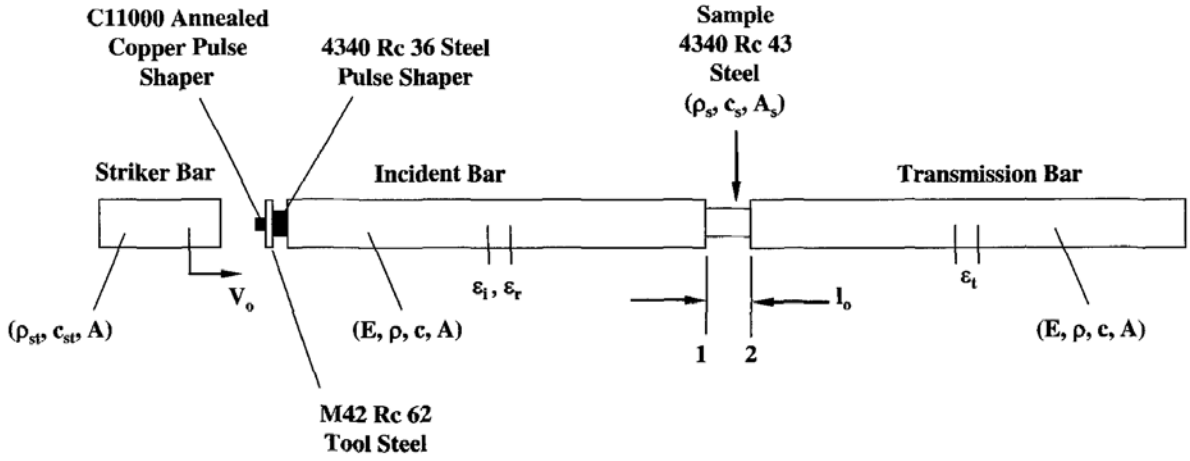

Figure 2-5. Modified split-Hopkinson bar using an assembled pulse shaper made of C11000 copper, M42 Tool Steel and Hardened 4340. [Reprinted from Frew, D.J, Forrestal, M.J., and Chen, W., 2005, "Pulse Shaping Techniques for Testing Elastic-Plastic Materials with a Split Hopkinson Pressure Bar," Exp. Mech., **45**, pp. 186-195. (Figure 1)]

CHAPTER 3
EXPERIMENTAL METHOD

The experimental method selected for this study is the split Hopkinson pressure bar (SHPB). Although, there are other high-rate experimental techniques such as Charpy tests, drop-weight tower tests, and ultrasonic evaluation, the split-Hopkinson pressure bar method remains the only method that can provide complete stress-strain relationships as a function of strain-rate information that is necessary to quantify strain-rate effects on deformation and strength and to develop models that account for strain-rate influence. To obtain valid dynamic compressive response of the fine sand with a variety of moisture levels, we modified the conventional SHPB with a pulse shaping technique to subject the sample to desired loading conditions and a jacketed test section to contain the sand specimen. The discussions in this chapter focus on the specific high-rate technique of SHPB. Since the principles of the SHPB have been well documented (Kolsky and Gray), only brief descriptions are given here.

3.1 Split-Hopkinson Pressure Bar History

The SHPB was developed to study the dynamic response of materials at high strain rates. The response of engineering materials may change with increasing strain rates showing the need for an experimental technique that can study material responses at much higher strain rates than the more common quasi-static experiments. Using SHPB techniques, typically strain-rates of 10^2 – 10^4 (Nemat-Nasser [6]) can be achieved. The SHPB has been developed in order to study the dynamic response of metallic materials, and within the last decades it has been adapted such as to allow the study of the dynamic behavior of geologic and cementitious materials (i.e., concrete, soils, ceramics, etc.). In this section a brief history of the SHPB method and the main contributors in the development of this experimental technique are presented.

The history of the SHPB begins with the pioneering work by Bertram Hopkinson [23] in 1914. Bertram Hopkinson developed an experimental technique where a long elastic bar was used to measure the pressure produced by a bullet impact and/or detonation wave produced by gun cotton. This bar with stress waves carrying pressure signals came to be known as the Hopkinson bar. The experimental apparatus developed by Hopkinson is shown in Figure 3-1. The impact induced by the detonation of gun cotton (A) creates a compressive loading pulse that propagates down the steel rod (B). At the end of the steel rod (B) a piece, referred as the *"time piece"*, of the same material and diameter (C) as the steel rod is magnetically mounted to the end with a little grease on the interface. When the compressive pulse propagates down the steel rod the pulse will reflect at the end of the *time piece* (C) as a tension wave, which propagates back towards the steel rod (B) and separates the two bars at the interface since the interface cannot bear tension. The momentum from the compressive wave is then trapped in the *time piece* (C), which, once separated, flies into a ballistic momentum trap (D) that enables the momentum of the *time piece* (C) to be measured. Once the momentum is determined the average pressure applied by the detonation loading pulse is known when the duration of the pulse (wavelength) is determined. Hopkinson was able to determine the maximum pressure and pulse duration through varying the *time piece* (C) length, but was unable to establish a complete pressure-time history of the pulse as it propagated through the rod.

In 1948, R.M. Davies [24] modified the Hopkinson bar by incorporating parallel plate and cylindrical condensers to measure the dynamic radial and axial strains in the bar as a function of time. The data from the condensers was collected electrically using a cathode-ray oscilloscope. This enabled Davies to replace the *time piece* and the grease at the interface. The general set-up of the Davies bar is shown in Figure 3-2. Implementing the one-dimensional wave propagation

in a bar with a free end, Davies showed that the particle velocity of the end of the bar and the radial displacement were related to the compressive pressure in the bar, p as : $\xi = 2p/\rho c_0$ (Davies [24]) and $\zeta = vap/E$ (Davies [24]), where ρ is the bar density, c_0 is the bar wave speed, v is Poisson's ratio, E is the Young's modulus and a is the bar radius. By incorporating the parallel plated and cylindrical condensers the pressure-time history of the compressive pulse could be determined.

In 1949, Kolsky [4] modified the Davies bar in order to make stress-strain measurements of engineering materials. Kolsky extended the *time piece* and/or extension bar and put a thin disc of material between the extension bar (i.e., transmitter bar) and pressure bar (i.e. incident bar). The dynamic compressive loading was applied by firing a detonator placed against a hardened steel anvil (Fig. 3-3). The compressive pulse propagates down the pressure bar where it passes through a cylindrical condenser microphone that measures the amplitude of the pressure pulse as a function of time with the data recorded to a cathode ray oscilloscope. The compressive pulse upon reaching the specimen reflects a pulse back into the pressure bar with a compressive pulse traveling through the extension bar. The extension bar is equipped with a parallel plate condenser that enabled the axial displacements at the free end of the extension bar to be measured and collected by the cathode ray oscilloscope. This apparatus became known as the "Split Hopkinson Pressure Bar" or Kolsky bar. Kolsky using the measured displacement-time histories was able to obtain the stress-strain relationship of the material sandwiched between the pressure bar and extension bar using one-dimensional elastic wave propagation theory. Kolsky also noted that thin specimens were required in order to acquire a constant loading across the specimen.

These three scientists (Hopkinson [23], Davies [24], and Kolsky [4]) are the pioneers of what today is called the split-Hopkinson pressure bar (SHPB) technique. The SHPB has been modified since its inception to load specimens in uniaxial tension, torsion, simultaneous torsion compression/tension and simultaneous compression/torsion (note: since torsion or shear waves travel slower than the normal waves, the sample is usually loaded by compression of tension before the torsion waves arrive, not simultaneous) (Gray [25]). The classical SHPB (Kolsky bar) has additionally been modified by implementing pulse shaping techniques as described in the previous chapter. Pulse shaping has allowed researchers to acquire dynamic stress equilibrium and constant strain-rate deformation in various kinds of specimens that would not deform under the desired conditions in classical SHPB tests due to uncontrolled loading. The research presented in this report uses a classical SHPB with pulse shaping in order to obtain constant strain-rate deformation in soils under nearly uniform stress loading.

3.2 1-D Stress Wave Propagation in Rods

The elastic bar waves are used to load the specimen, to sense the specimen response, and to reduce the data in an SHPB experiment. In this section the one-dimensional elastic stress wave propagation analysis for rods is presented. The 1-D stress wave propagation theory in long rods is governed by a fundamental assumption that the rod is homogeneous, isotropic and linear elastic. Furthermore, any transverse deformation of the rods is neglected. This implies that the bar properties remain the same throughout the entire length of the rod and is dispersion free. The material can not be stressed beyond its proportional limit and parallel cross-sections remain plane and parallel in conjunction with a uniform state of stress in the rod. The rod is unconfined, so lateral effects will be present, but for simplicity will be ignored. Figure 3-4 shows a differential element with an applied dynamic stress σ. The equation of motion in the x-direction is,

$$-\sigma A + \left(\sigma + \frac{\partial \sigma}{\partial x}\Delta x\right)A = \rho A \Delta x \frac{\partial^2 u}{\partial t^2} \tag{3.1}$$

where A is the cross-sectional area of the bar, ρ is the density of the bar, and u is the displacement of the bar. Equation (3.1) reduces to,

$$\frac{\partial \sigma}{\partial x} = \rho \frac{\partial^2 u}{\partial t^2} \tag{3.2}$$

Since the linear material is not stressed beyond its elastic range, Hooke's law can be utilized.

$$\sigma = E\varepsilon \tag{3.3a}$$

where E is Young's Modulus and ε is the axial strain given in small strains by,

$$\varepsilon = \frac{\partial u}{\partial x} \tag{3.3b}$$

Substituting equations (3.3) into the equation of motion (3.1) we obtain,

$$\frac{\partial}{\partial x}\left(E\frac{\partial u}{\partial x}\right) = \rho \frac{\partial^2 u}{\partial t^2} \tag{3.4}$$

If the rod is homogeneous where E and ρ do not vary along the rod, then the equation of motion can be written as the classical one-dimensional wave equation,

$$\frac{\partial^2 u}{\partial x^2} = \frac{1}{c_0^2}\frac{\partial^2 u}{\partial t^2} \tag{3.5}$$

where the wave speed of the rod is defined as $c_0 = \left(E/\rho\right)^{1/2}$. The general solution of equation (3.5) using D'Alembert's method is given by,

$$u_1(x,t) = f(x + c_0 t) + g(x - c_0 t) = u_r + u_i \tag{3.6}$$

where f and g are arbitrary functions for a left and right traveling waves, respectively and c_0 again represents the bar wave speed, u_r is the displacements of the reflected wave, and u_i is the displacements of the incident waves along the rod. The solution in equation (3.6) applies only to

the incident bar in contact with the specimen. Through the transmitter bar, there is only a right traveling wave, so

$$u_2(x,t) = h(x - c_0 t) = u_t \tag{3.7}$$

where u_t is the displacement of the transmitted wave along the rod.

Indeed as shown in Figure 3-5, a SHPB consists of a striker bar, incident bar, and transmitter bar with a sample sandwiched between the incident and transmitter bars. Compressed air released using a quick releasing valve launches the striker bar into the incident bar creating an elastic compressive wave that travels towards the sample. When the impedance of the sample is less than the impedance of the bars part of the compressive wave is transmitted through the specimen to the transmitter bar and part is reflected back into the incident bar as a reflected wave. If the elastic stress waves in the bars are nondispersive then waves measured at strain gage locations on the bar surfaces away from the specimen can be used as those at the interfaces between the bars and the sample. One-dimensional wave theory can be used to determine the response of the specimen using strain measurements obtained by strain gages.

In this study the incident and transmitter bars were made of the same material. As shown in Figure 3-5 the incident and transmitter bars have the same area A, density ρ and wave speed c_0. The ends of the sample are represented by the subscripts 1 and 2 as shown. The subscripts *i, r, t* designate the incident, reflected and transmitted waves, respectively. Due to the nature of the compression tests, the stress is taken positive in compression, strain positive in contraction, and velocity positive in the right direction.

The strains in the incident bar and transmitter bar can be determined by differentiating equations (3.6) and (3.7) with respect to x.

$$\frac{\partial u_1}{\partial x} = f'(x + c_0 t) + g'(x - c_0 t) = \varepsilon_r + \varepsilon_i \tag{3.8}$$

$$\frac{\partial u_2}{\partial x} = h'(x - c_0 t) = \varepsilon_t \tag{3.9}$$

Taking the time derivative of the same equations yields,

$$v_1 = \frac{\partial u_1}{\partial t} = c_0 f'(x + c_0 t) - c_0 g'(x - c_0 t) = c_0(\varepsilon_r - \varepsilon_i) \tag{3.10}$$

$$v_2 = \frac{\partial u_2}{\partial t} = -c_0 h'(x - c_0 t) = -c_o \varepsilon_t \tag{3.11}$$

which represents the bar velocities for the incident bar and transmitter bar. For homogeneous deformation the strain rate in the specimen is given by,

$$\dot{\varepsilon} = \frac{v_1 - v_2}{l_s} \tag{3.12}$$

where l_s is the instantaneous length of the specimen. Substituting equations (3.10) and (3.11) into equation (3.12) the strain rate becomes,

$$\dot{\varepsilon} = \frac{c_0}{l_s}(-\varepsilon_i + \varepsilon_r + \varepsilon_t) \tag{3.13}$$

After an initial "ringing up" period, where the duration is dependent upon the wave speed of the material and its geometry, the specimen is assumed to be in stress equilibrium, so if the specimen is in a state of homogeneous deformation then the forces on both sides of the specimens are equal, i.e. $P_1 = P_2$ (Gray [26]). The forces in the incident and transmitter bars are given by,

$$P_1 = \frac{A}{A_s} E(\varepsilon_i + \varepsilon_r) \tag{3.14}$$

$$P_2 = \frac{A}{A_s} E(\varepsilon_t) \tag{3.15}$$

where A is the rod cross-sectional area and A_s is the specimen cross-sectional area. Setting these two equations equal to one another yields,

$$\varepsilon_t = \varepsilon_i + \varepsilon_r \tag{3.16}$$

Substituting equation (3.16) into equation (3.13) the strain rate can be rewritten,

$$\dot{\varepsilon} = \frac{2c_0}{l_s}\varepsilon_r \tag{3.17}$$

The compressive pulse traveling in the incident and transmitter bars has to be elastic, so the stress in the sample is given by,

$$\sigma_s = \frac{A}{A_s}E\varepsilon_t \tag{3.18}$$

Integrating equation (3.17) the strain in the specimen can be determined.

$$\varepsilon_s = \frac{2c_o}{l_s}\int_o^t \varepsilon_r dt \tag{3.19}$$

Using equations (3.18) and (3.19) the stress-strain relationship can be determined. Determining the stress-strain relation using these equations is termed a "1D-wave" analysis since the specimen stress is obtained using only the transmitted strain and the specimen strain is obtained using only the reflected strain. Before utilizing equations (3.17), (3.18) and (3.19) one should know it is assumed that the specimen is in stress equilibrium as discussed by Gray [25] and Gray and Blumenthal [27]. The stress equilibrium can be assessed by comparing the stresses on both sides of the specimen. If the stresses are in good agreement then equations (3.17), (3.18) and (3.19) may be utilized to evaluate the specimen response to dynamic loading.

3.3 Split-Hopkinson Pressure Bar Set-up

The split-Hopkinson pressure bar utilized to perform this research was built at Purdue University in the AAE/MSE Department. The system shown in Figure 3-6 was built initially for the evaluation of engineering materials (i.e., metals, brittle composites etc.) and until recently

used to study the dynamic stress-strain behavior of geologic materials (i.e., limestone, sand etc.). Figure 3-7 is a photograph of the actual SHPB system used for these experiments.

The bars are supported by a frame consisting of six "A-Frame" structures, spaced accordingly, that in turn support several steel beams. The steel beams have high rigidity with the top and bottom of the beams parallel to one another to ensure that all the equipment mounted to either surface is level. The steel beams are mounted together at the ends by aligning the machined slots on each side of the beams and fastening the two together using a piece of steel and bolting the steel piece into the machined grooves using large socket cap screws to prohibit the beams from coming apart. After mounted the beam together the pads located on the bottom of the "A-Frames" are adjusted to ensure that all the surfaces are level with one another.

The barrel for housing the striker bar and the incident and transmission bars rest on aluminum supports with brass bushings for the barrel and bars to rest in. The bushing design allowed adequate clearance between the bushings and the bars to allow the stress pulses to travel through the bars without interference. The striker bar and incident bars were aligned by adjusting the tops of the gun barrel and incident bar supports until they were flush with one another and the incident bar was allowed to move freely through all of the brass bushings. Finally the aluminum mounts are fastened to the steel beams using 5-inch C-Clamps. The transmitter bars is mounted and aligned in the same manner as the incident bar.

The gas gun launcher consists of a gas tank and quick releasing valve. The gas tank has a maximum pressure rating of 20 MPa (3000 psi) with the operating pressure supplied to the tank using compressed air and read by a digital pressure gage. The striker bar barrel has an outer diameter of 31.75 mm (1.25 inch) and an inner diameter of 25.4 mm (1.0 inch) with a vented section at the end of the barrel to prohibit secondary impacts from the striker bar following

impact. The striker bar is loaded from the muzzle end of the barrel and pushed back to appropriate distance, depending upon the strain-rate required, using a tape measure. The striker bar is mounted with several plastic sabots placed at the front and rear and depending upon the length of the striker bar a sabot is located in the middle. The sabots take up the volume between the striker bar and the inner diameter of the gun barrel enabling the striker bar to travel down the gun barrel in addition to aligning the striker bar upon impact with the incident bar. The rear sabot is also used to ensure that a gas seal is produced at the end of the striker bar to prohibit gases from flowing between the plastic sabots and the inner diameter of the gun barrel.

The bars were fabricated of a VascoMax C350 maraging steel (HRC = 53) with a yield strength, Young's Modulus and density of 2.5 GPa (362 ksi), 200 GPa (20 Mpsi) and 8100 kg/m^3 (0.283 lb/in^3), respectively. The bars have an outer diameter of 19.1 mm (0.75 inch) with the ends of the bars faced to length and polished. The lengths of the striker bar, incident bar and transmitter bar for these experiments were 0.685 m (27.0 inch), 4.15 m (163.0 inch) and 2.44 m (96.0 inch), respectively. Diametrically opposed strain gages were located on the incident bar and transmitter bar to nullify bending strains in the bar. The strain gages were located approximately 1.30 m (51.0 inch) from the front (bar end in contact with the specimen) of the incident bar and approximately 0.20 m (7.8 inch) from the front of the transmitter bar. The strain gages were manufactured by Vishay Micro-Measurements Group in Raleigh, NC with each set of strain gages forming a Wheatstone bridge excited by a 24 V power supply. Finally, the signal is run to an in-house fabricated Pre-amplifier and recorded by a high speed digital oscilloscope.

3.4 SHPB Experiments

The experiments conducted for this study used the SHPB arrangement shown previously in Figure 3.6. The experiments were conducted at different levels of confinement using a polycarbonate plastic tube and a hardened 4340 steel tube. The polycarbonate and 4340 steel

tubes both had outer diameters of 25.4 mm (1.0 inch), inner diameters of 19.1 mm (0.75 inch) and lengths of approximately 50.8 mm (2.0 inch). The specimens for this study all had a dry density of 1.50 g/cc (0.054 lb/in^3) with varying mass percent moisture contents. The specimens had outer diameters of 19.1 mm (0.75 inch) and lengths of 9.3 mm (0.366 inch). All experiments were conducted at a strain rate of approximately 400/s and used the pulse shaping technique to acquire constant strain rate deformation of the specimen.

For a Hopkinson bar experiment measurements to be considered valid and accurate, two conditions must be met (1) the specimen must be compressed uniformly and/or be in a state of stress equilibrium, (2) the strain-rate of the specimen should be constant. When testing materials with low ductility (e.g., soils, rocks, cementitious materials) with a classical SHPB set-up, it is difficult to satisfy these two conditions simultaneously without changing the loading pulse is difficult. As mentioned previously a classical SHPB experiment typically produces a square loading pulse with a short time to peak load. Materials with slow sound speeds, such as soils, require longer loading durations to acquire stress equilibrium. For example, in the study reported by Veyera [3] using several different sands and two different strain rates is was not possible to acquire a constant strain rate with a classical SHPB. As shown in Figure 3-8, the raw data obtained from those experiments show a fast rise time to peak load or a square incident pulse. In addition, the reflected pulse is continuously decreasing and constant strain-rate is never reached. Earlier work by Felice et al. [1] used a classical SHPB to develop an experimental technique to study the dynamic stress-strain behavior of sand. Figure 3-9 shows the raw data obtained from a typical experiment under this study. Again, the incident pulse is a square pulse with a short rise to peak load, while the reflected pulse has a continuously declining slope, thus not achieving

constant strain rate. These two studies are representative of the state-of-the-art in characterization soils at high strain rates using the SHPB technique.

To utilize the SHPB testing method modifications must be made to ensure that the specimen meets the before mentioned constraints. To satisfy these conditions in this study, a pulse shaping technique was implemented in order to change the shape of the loading pulse or incident pulse. The pulse shaper is a thin disc of copper, 7.1 mm Ø x 0.81 mm thick (0.28" Ø x 0.03 thick), that is placed on the impact end of the incident bar as shown in Figure 3-6. The material and dimensions of the pulse shaper depends on the strain rate required and the specimen material being evaluated. When the striker bar impacts the copper disc it deforms plastically filtering out the high frequencies (dispersion) (Gray [25]) inherent in the loading pulse and increases the time to peak load allowing the specimen to acquire stress equilibrium. The typical raw data obtained from these experiments is shown in Figure 3-10. The incident pulse clearly illustrates a slower and more gradual increase to peak load than a conventional SHPB. The reflected pulse also confirms that constant strain rate was acquired during the experiment. Figure 3-11 shows the dynamic load equilibrium history of the specimen. The overlapped loads on the front and back of the specimen clearly indicate that the specimen achieved stress equilibrium. At dynamic stress equilibrium, the reflected pulse represents the strain-rate history of the specimen (Eq. 3.17). Figure 3-12 shows the strain and strain-rate histories of the specimen. The strain-rate of the specimen was nearly constant (380/s) from approximately 200 μs to 325 μs and is associated with strains from approximately 3.5% to 8.5%. During this time, the specimen was loaded under stress equilibrium and constant strain-rate conditions, so the stress-strain measurements (Figure 3-13) are correct. Sand can sometimes have different responses to the same loading depending on the specimen preparation. Controlled specimen

needed to ensure that repeatable material responses can be obtained for a particular confinement and moisture content. Figure 3-14 shows the variation of stresses at 5% and 9% for the polycarbonate confinement and Figure 3.15 shows the variation of stresses at 5% and 8% for steel confinement. These results show that reasonably repeatable measurements were obtained in all of the experiments.

3.5 Material Description

The material used for this study is a white fine grain sand purchased from Quikrete Company, Atlanta, GA. The sand is silica based, kiln dried and poorly graded. The physical properties of the sand are summarized in Table 3-1. The physical properties were determined using standard laboratory procedures designated by the American Society of Testing and Materials (ASTM). The grain size distribution is shown in Figure 3-16. Based on the grain size distribution the sand is classified as SP or poorly graded sand according to the Unified Soil Classification System (USCS). The sand was studied at various moisture contents ranging from 3% to 20%. All specimens had a dry density of 1.50 g/cc (0.054 lb/in^3) with the appropriate mass percent of water added to the specimen to achieve the specified moisture content. All specimens were in an undrained condition where the water is not allowed to drain from the specimen. Table 3-2 shows the test matrix conducted in this study.

3.6 Confinement Methods

. The specimens were confined using a polycarbonate plastic tube and a hardened 4340 steel tube. The polycarbonate tube was commercially purchased from McMaster-carr with an outer diameter of 25.4 mm (1.0 inch) and inner diameter of 19.1 mm (0.75 inch). For the experiments performed, the polycarbonate tube was cut into 50.8 mm (2.0 inch) long individual pieces. The polycarbonate tube provides some confinement to the specimen, but is also allowed to expand in the radial direction during the compaction of the specimen as shown by Song et al.

[28]. The boundary conditions associated with the polycarbonate tube are unknown quantitatively, thus the low strength of the polycarbonate plastic in comparison to the loads created in the sand specimen during loading is neither one-dimensional stress nor one-dimensional strain. The unknown boundary conditions add further difficulties in analyzing the data since it is not known if the boundary conditions significantly affect the material response. This will be further discussed in the results portion of this report. The second method used for imposing confinement to the specimen is through a hardened 4340 steel having the same dimensions as the polycarbonate tube. The 4340 steel tube creates is more rigid around the outer diameter of the specimen than the previous polycarbonate tube. The steel tube is used in order to achieve higher confinement levels and to simulate a one-dimensional, confined uniaxial loading condition.

3.7 Specimen Dimensions

Prior to characterizing the dynamic properties of the sand the specimen size must be accurately determined. As previously mentioned, to have a valid SHPB experiment the specimen must reach stress equilibrium or uniform deformation. In materials, such as sand, that have low wave speeds it is difficult to acquire uniform deformation with long specimens. Earlier work was performed by Song et al. [28] on the same material for dry conditions, specimen preparation, confinement methods and experimental set-up in order to determine the adequate specimen dimensions. Song et al. [28] used a Cordin 550 high speed digital camera running at 80,000 frames per second to capture the stress pulse traveling through the sand confined in a polycarbonate tube. Specimen lengths of 28.4 mm (1.1 inch), 25.4 mm (1.0 inch), 15.2 mm (0.60 inch) and 13.1 mm (0.51 inch) were used. These experiments indirectly confirm that uniform deformation is more easily acquired with the short specimen, e.g. 13.1 mm long specimen, than the longer sand specimens, e.g. 28.4 mm long sand specimen. The digital images

obtained from the camera for the different specimen lengths are shown in Figures 3-17 thru 3-20. The corresponding stress histories of the 13.1 mm long sand specimen can be seen in Figure 3-21. On the basis of these results, Song et al. [28], recommended that a specimen length of 9.3 mm be used, since in the shorter specimen uniform deformation and stress equilibrium can be acquired.

However, the use of a short specimen length enabled the specimen to acquire both stress equilibrium and constant strain during the experiment, the shorter length specimens also may introduce problems associated with longitudinal and radial inertia as well as frictional effects. Before addressing these issues it should be stated that when testing porous materials, such as sand, some level of confinement is needed to prepare the specimens. Thus, steel platens were used to bound the media on each end of the sample. The steel platens were machined flat and parallel to ensure that the platens were collinear with the incident and transmitter bars when the specimen was placed between the two bars. To ensure that the measurements are representative of the bulk behavior of the material, the dimensions of the specimen needed to be at least ten times the representative constituent size (Gray [25]). The longitudinal and radial inertia caused by the particle acceleration at high strain rates can influence the accuracy of the measurements. The errors caused by the longitudinal and radial inertia were analyzed by Davies and Hunter [29] in 1963 with corrections derived for these errors and given by the following equation:

$$\sigma(t) = \sigma_m(t) + \rho_s \left[\frac{L^2}{6} - \upsilon_s \frac{D^2}{8} \right] \frac{d^2\varepsilon(t)}{dt^2} \tag{3.20}$$

where σ_m is the measured stress, ρ_s is the specimen density, v_s is Poisson's ratio, L is the specimen length and D is the specimen diameter. If constant strain rate is obtained then the inertial effects will be minimized and a simpler expression of equation (3.20) may be used and is given by,

$$\frac{L}{D} = \sqrt{\frac{3\nu_s}{4}} \tag{3.21}$$

The material studied in this research is considered moist/partially saturated and tested in an undrained condition. Its Poisson's ratio is 0.3[1] if the material is considered elastic. Using equation (3.21) we obtain that the minimum *L/D* ratio for which inertial effects are minimized is 0.47. Thus, all the specimens for this research had an *L/D* ratio of 0.49.

The friction between the specimen and the bars is typically maximized when small aspect ratios are used so a brief explanation of this is required since our specimen aspect ratio does not meet the requirements of ASTM standard E 9. This standard recommends an aspect ratio of $1.5 < l_s/d < 2.0$ in order to minimize frictional effects. Since the conditions for inertial and frictional effects cannot be satisfied simultaneously, specimen aspect ratios that satisfy $0.5 < l_s/d < 1.0$ as suggested by Gray [25] can be used. Note also that in order to minimize the frictional effects the recommendations of ASTM Standard E 9 could be utilized in conjunction with lubrication, but this would create additional problems. Indeed, this would require a minimum specimen length of ~28.5 mm and as previously mentioned this would imply that uniform deformation cannot be achieved or inertial effects be reduced. Also, lubrication cannot be used for sand since the material is porous and thus allowing the lubrication to fill voids in the material altering the material properties. Achieving uniform deformation was considered to be more critical than frictional effects since a non-uniform deformation would not satisfy a valid SHPB experiment.

3.8 Specimen Preparation

The specimens used in this research used the material described in section 3.5 with a dry density of 1.50 g/cc and the appropriate mass percent of water added depending on the moisture

[1] The poisson ratio for sand was determined during a personal communication with Mark L. Green of the Air Force Research Laboratory, Eglin AFB, FL on March 13, 2007.

content. The specimens were not compacted IAW any standard and were tested in an undrained state. Since the specimens were tested in an undrained state the moisture content was not reevaluated following the experiments. The specimen preparation associated with each confinement will be discussed in the following.

3.8.1 Polycarbonate Confinement

The polycarbonate confinement tubes used, have outer diameters of 25.4 mm, inner diameters of 19.1 mm and lengths of 50.8 mm. Each tube has a set of holes drilled on one end of the tube and 180 degrees apart. A 6.35 mm (0.25 inch) thick steel platen was placed close to the end of the polycarbonate tube and placed between the incident and transmitter bars. The steel platen was held in place by the polycarbonate tube and collinear with the bars by applying pressure with the incident and transmitter bars. The polycarbonate tube was then slid back and forth to ensure that movement of the platens is not hindered. The pre-drilled holes were located in the middle of the steel platen and fastened in place to the steel platen by using set screws. The polycarbonate tube is then removed from the SHPB and placed vertically on top of a 19.1 mm diameter rod fixture. A piece of paper is placed on top of the scale, tared and a mass of 4.0 g of sand weighted. The sand is then poured into the polycarbonate tube and tapped lightly such that the top surface is even. Using a 1 ml syringe the appropriate mass percent (i.e., 0.28 ml for 7% moisture) of water is obtained with all air voids removed from the syringe. The water is slowly released from the syringe into the dry sand and evenly distributed over the top of the sand located in the polycarbonate tube. Using a toothpick the sand and water was mixed until all of the dry sand was mixed thoroughly with the water to acquire as uniform water distribution as possible. The second steel platen is then placed on top of the moist sand and slightly pressed to ensure the interface between the platen and moist sand is flat. The specimen is shown in the polycarbonate confinement in Figure 3-22. The polycarbonate tube is then removed from the rod

fixture and carried vertically to the SHPB. One drop of super glue was placed on the incident bar and spread over ~ 70% of the diameter. The super glue is used to ensure that the steel platen is held in place when the reflected tensile wave arrives at the incident bar/steel platen interface. The specimen is then placed between the incident and transmitter bars and the super glue allowed to dry. The specimen length is measured using digital calipers. If the specimen length is not correct light pressure is applied using the incident and transmitter bars and the length measured again. This process was repeated until the desired specimen length was obtained. The positioning screws are then removed prior to impact loading. Following each experiment the steel platens were removed from the polycarbonate tube cleaned of all excess sand and super glue and reused for the next experiment. A new polycarbonate tube was used for each experiment.

3.8.2 Steel Confinement

A 4340 steel confinement tube having an outer diameter of 25.4 mm, inner diameter of 19.1 mm and length of 50.8 mm was used. This steel tube has a set of holes drilled 14.8 mm from the end of the tube and 180 degrees apart. A 6.35 mm thick steel platen is placed close to the end of the steel tube and placed between the incident and transmitter bars. A striation is put on the incident and transmitter bars at 14.0 mm (0.55 inch) and 14.8 mm (0.58 inch), respectively from the end of each bar. The steel platen is held in place in the steel tube and collinear with the bars by applying pressure with the incident and transmitter bars. The steel tube is then slid back and forth to ensure that movement of the platens is not hindered. The bottom of the steel tube is then aligned with the striation on the transmitter bar and the steel platen fastened in place by using set screws. The steel tube is then removed from the SHPB and placed vertically on top of a 19.1 mm diameter rod fixture. A piece of paper is then placed on top of the scale, tared and a mass of 4.0 g of sand weighted. The sand is then poured into the

steel tube and tapped lightly to even the top surface. Using a 1 ml syringe, the appropriate mass percent (i.e., 0.28 ml for 7% moisture) of water is obtained with all air voids removed from the syringe. The water is slowly released from the syringe into the dry sand and evenly distributed over the top of the sand located in the steel tube. Using a toothpick the sand and water was mixed until all of the dry sand was mixed thoroughly with the water to acquire as uniform water distribution as possible. The second steel platen is then placed on top of the moist sand and slightly pressed to ensure the interface between the platen and moist sand is flat. The specimen is shown in the steel confinement in Figure 3-23. The steel tube is removed from the rod fixture and carried vertically to the SHPB. One drop of super glue was placed on the incident bar and spread over ~ 70% of the diameter. The super glue is used to ensure that the steel platen is held in place when the reflected tensile wave arrives at the incident bar/steel platen interface. Holding the top steel platen with fingers the specimen is turned horizontally and placed between the incident and transmitter bars and super glue allowed to dry. If the striations and the ends of the steel tube do not align then apply light pressure using the incident and transmitter bars until the ends of the steel tube is aligned with the striations. Therefore, the specimen length is 50.8 – 14.0 – 14.8 – (6.35 x 2) = 9.3 mm. The positioning screws are then removed prior to impact loading. Following each experiment the steel confinement tube and steel platens were cleaned to remove any excess sand and super glue and reused for the next experiment.

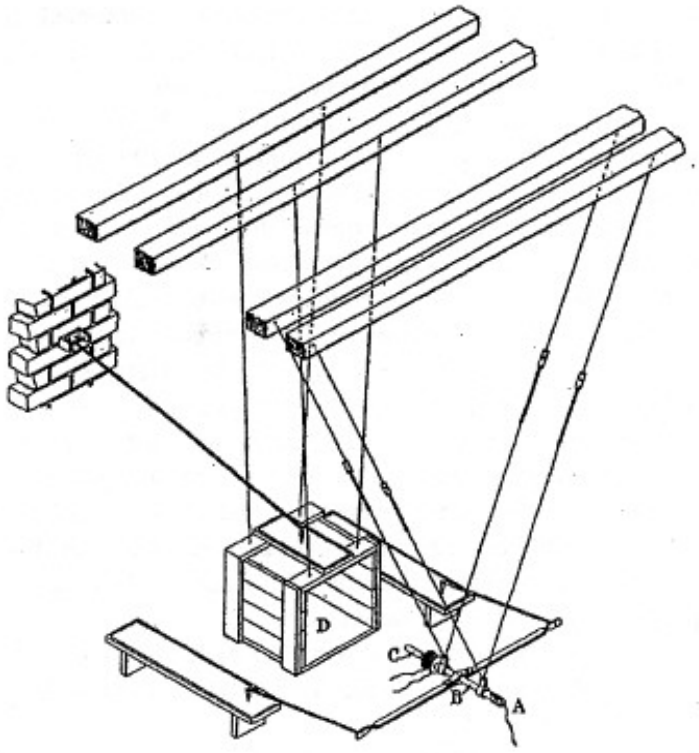

Figure 3-1. Apparatus designed by Bertram Hopkinson to measure the pressure produced by the detonation of gun cotton. [Reprinted from Hopkinson, B., 1914, "A Method of Measuring the Pressure Produced in the Detonation of High Explosives or by the Impact of Bullets," Philos. Trans. R. Soc. London, Ser. A, 213, pp. 437-456. (Figure 12)]

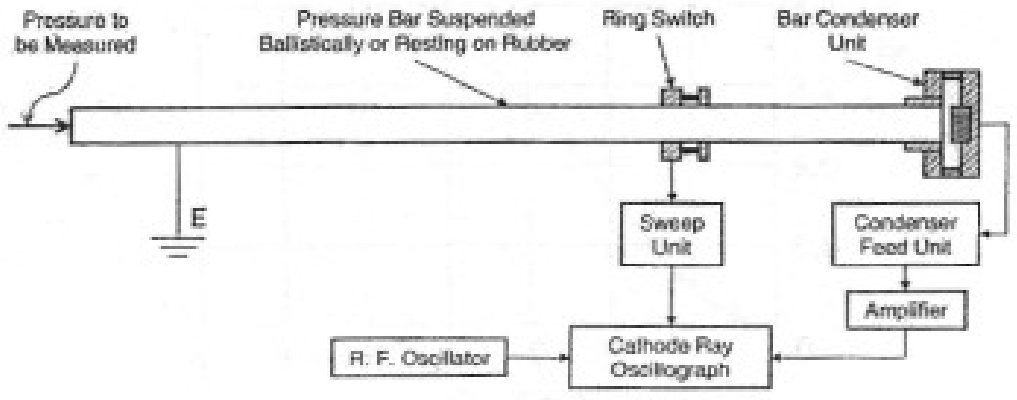

Figure 3-2. General arrangement of the Davies Bar. [Reprinted from Davies, R.M., 1948, "A Critical Study of the Hopkinson Pressure Bar," Philos. Trans. R. Soc. London, Ser. A, 240, pp. 375-457. (Figure 1)]

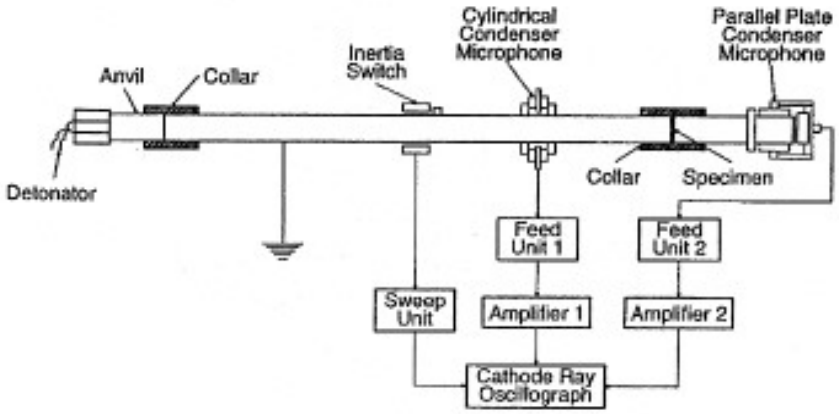

Figure 3-3. General arrangement of the Kolsky Bar. [Reprinted from Kolsky, H., 1949, "An Investigation of the Mechanical Properties of Materials at very High Rates of Loading," Proc. Phys. Soc. London, B62, pp. 676-700. (Figure 1)]

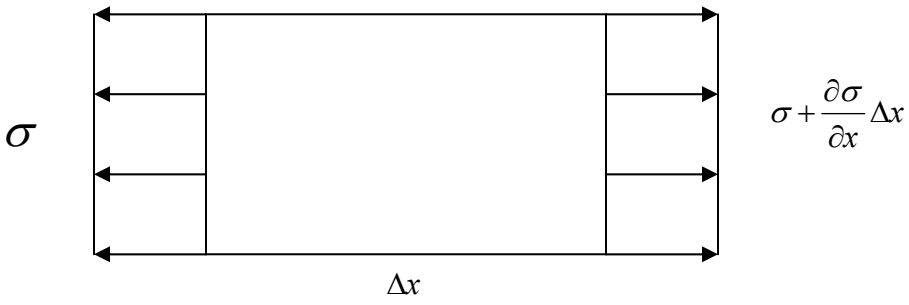

Figure 3-4. Stresses acting on a differential element in the bar.

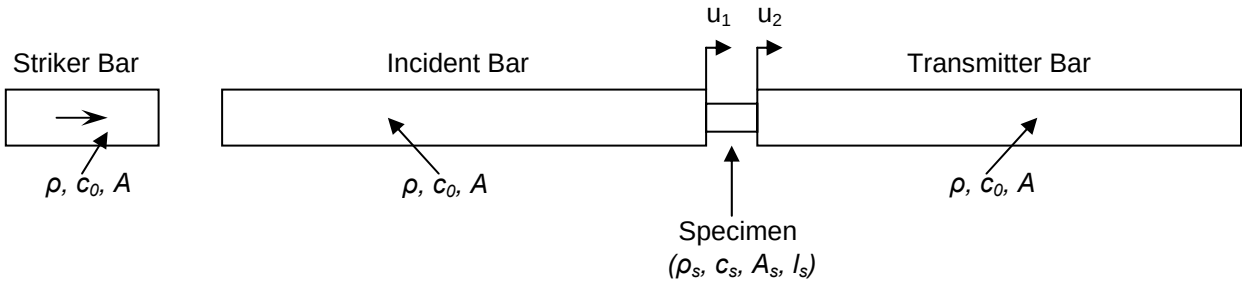

Figure 3-5. General arrangement of a conventional split Hopkinson Pressure Bar (SHPB).

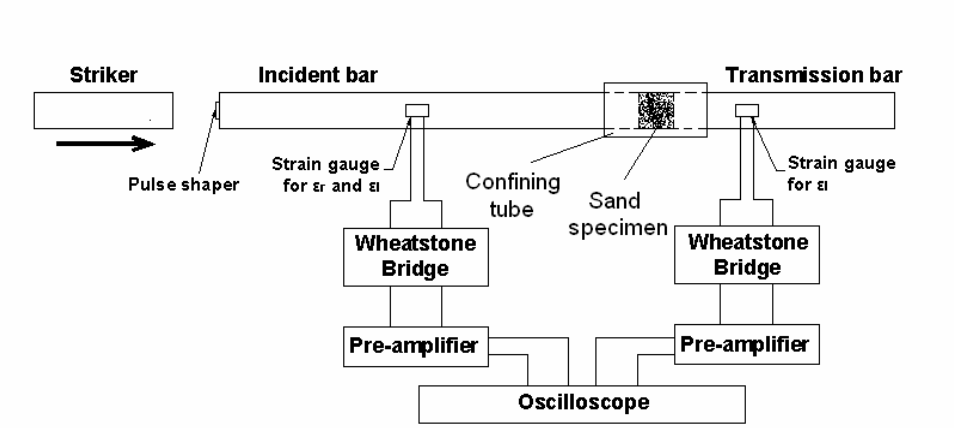

Figure 3-6. Arrangement of the modified split Hopkinson Pressure Bar implementing pulse shaping. [Reprinted from Song, B., and Chen, W., 2006, "Dynamic Compressive Behavior of Sands," Unpublished technical report, School of Aeronautics and Astronautics and School of Materials Engineering, Purdue University. (Figure 1)]

Figure 3-7. Photograph of the modified split Hopkinson Pressure Bar used in this research. [Reprinted from Song, B., and Chen, W., 2006, "Dynamic Compressive Behavior of Sands," Unpublished technical report, School of Aeronautics and Astronautics and School of Materials Engineering, Purdue University. (Figure 2)]

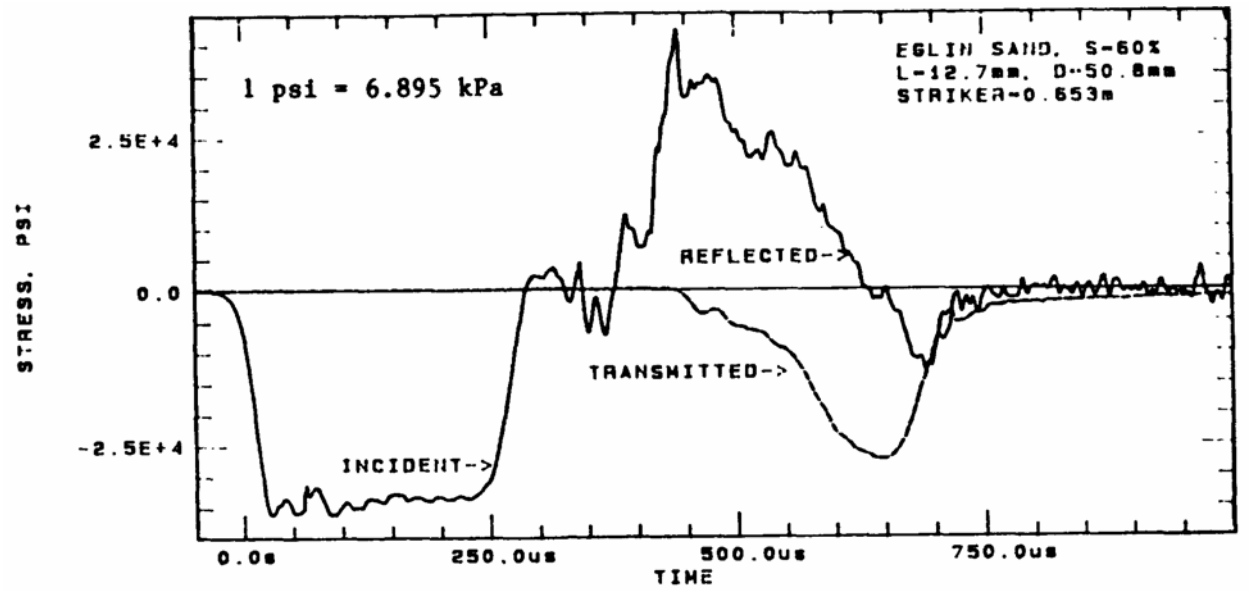

Figure 3-8. Raw data of a typical experiment conducted using the classical split Hopkinson Pressure Bar. [Reprinted from Veyera, G.E., 1994, "Uniaxial Stress-Strain Behavior of Unsaturated Soils at High Strain Rates," WL-TR-93-3523, Wright Laboratory Flight Dynamics Directorate, Tyndall AFB, FL. (Figure 6)]

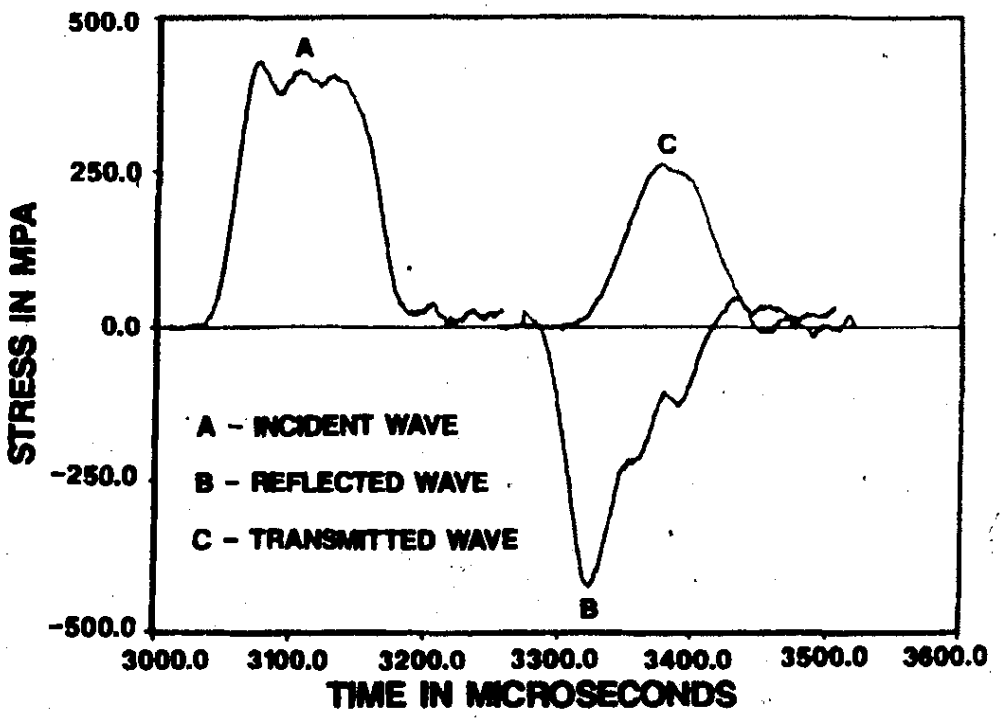

Figure 3-9. Raw data of a typical experiment conducted using the classical split Hopkinson Pressure Bar. [Reprinted from Felice, C.W., Gaffney, E.S., Brown, J.A., and Olsen, J.M., 1987, "Dynamic High Stress Experiments on Soil," Geotechnical Testing Journal, GTJODJ, 10, No. 4, pp. 192-202. (Figure 6)]

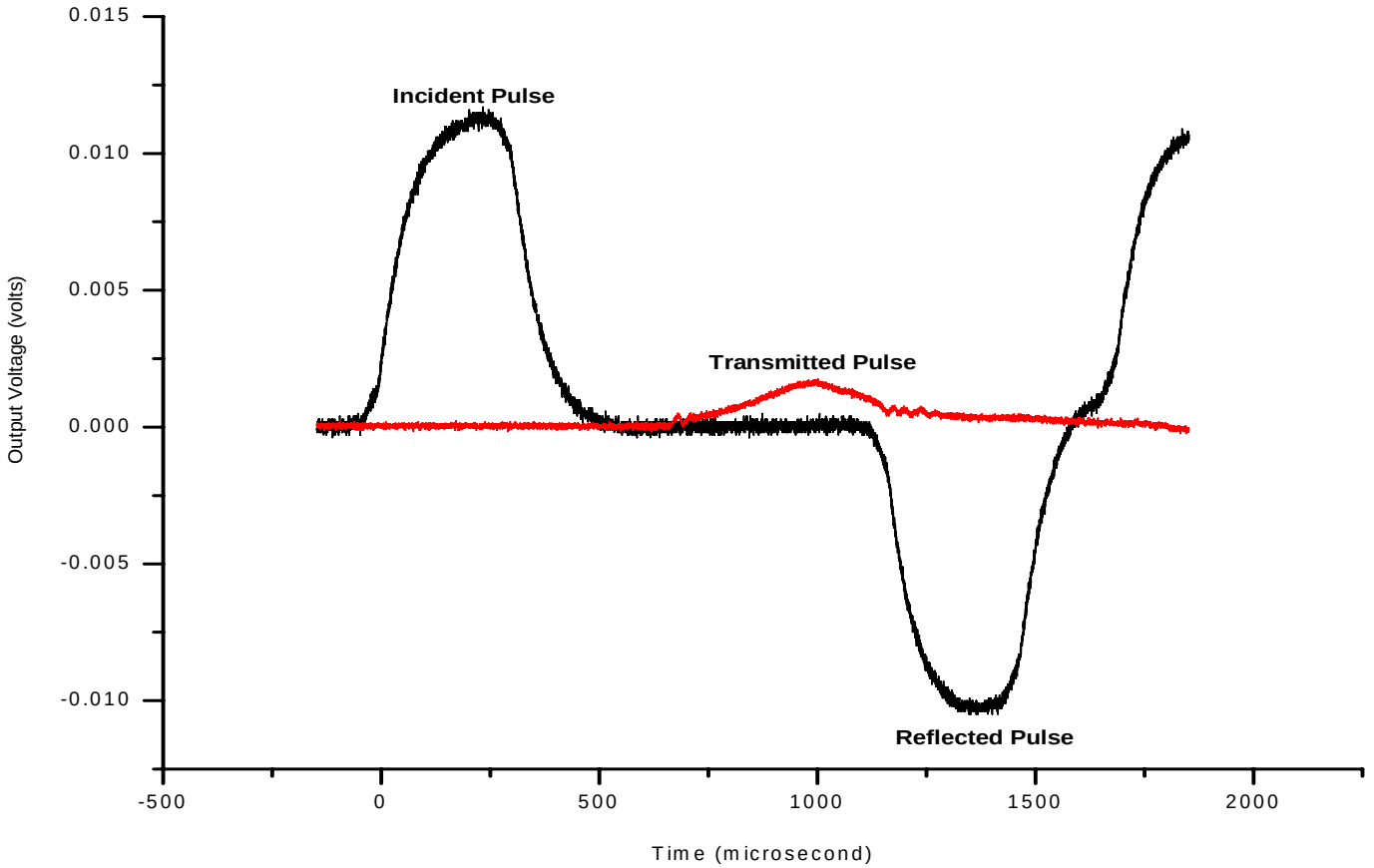

Figure 3-10. Typical raw data obtained for all experiments herein using the modified split Hopkinson Pressure Bar.

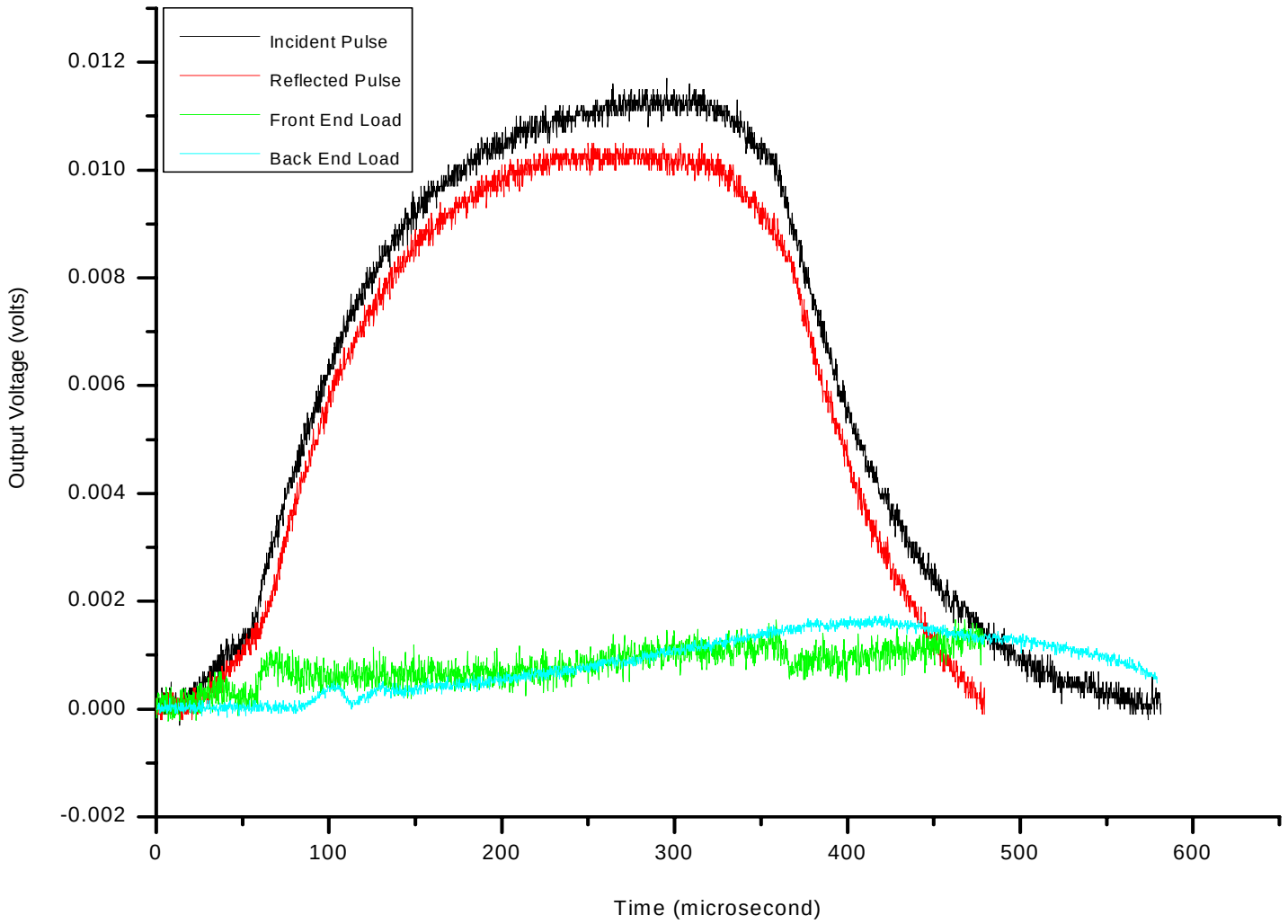

Figure 3-11. Typical stress equilibrium history for the experiments herein using the modified split Hopkinson Pressure Bar.

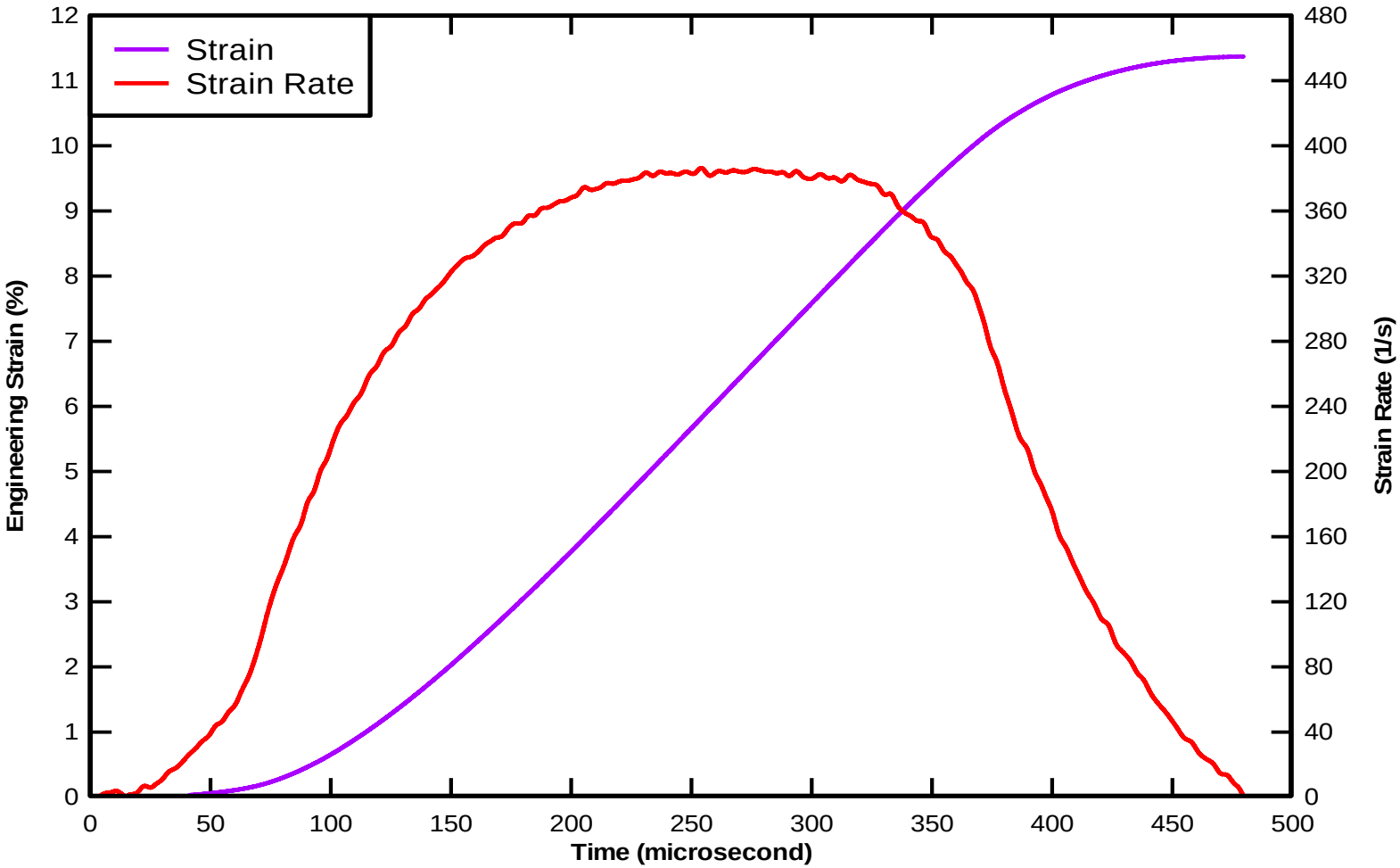

Figure 3-12. Typical strain and strain-rate histories of the experiments using the modified split Hopkinson Pressure Bar.

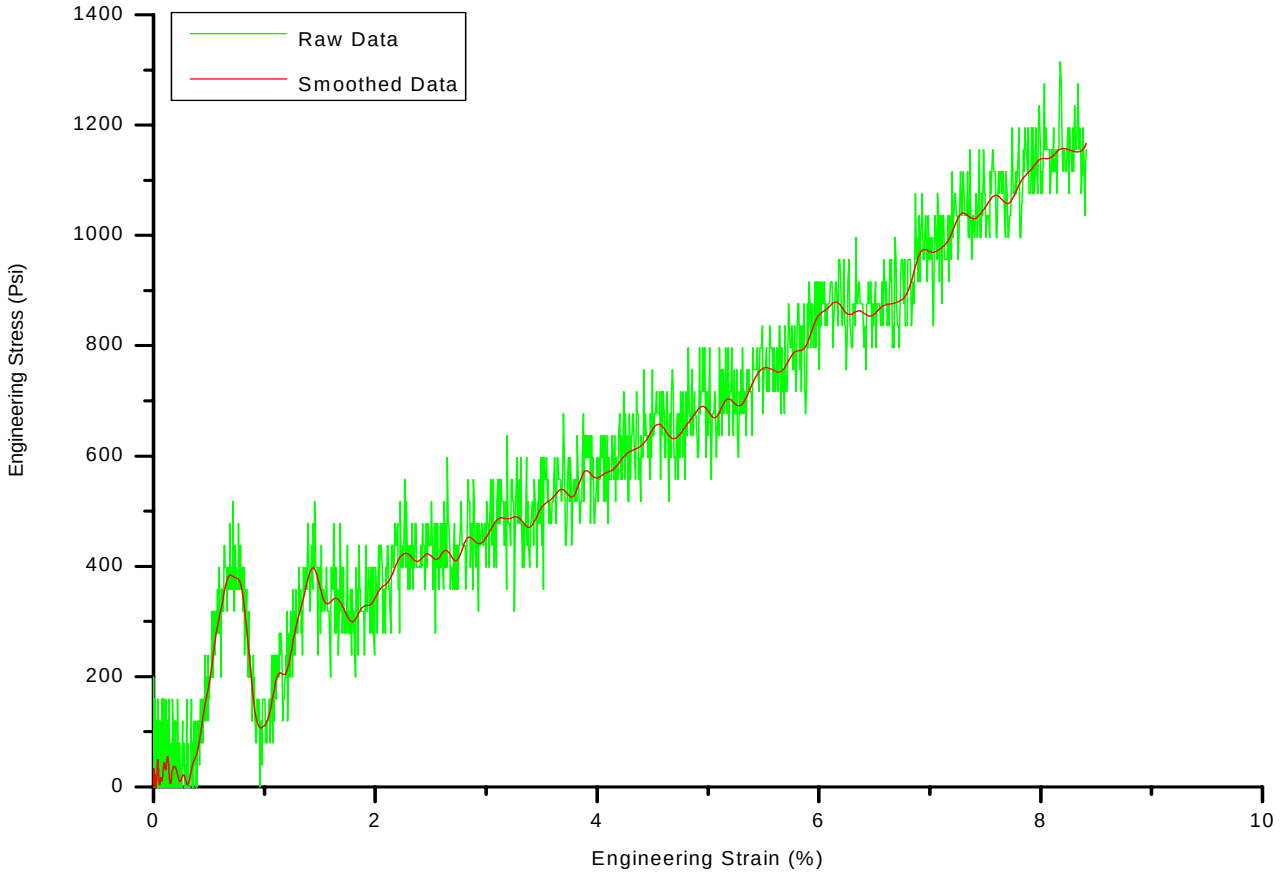

Figure 3-13. Stress-strain relationship showing the raw data and the smoothed data obtained for moist sand using the modified split Hopkinson Pressure Bar.

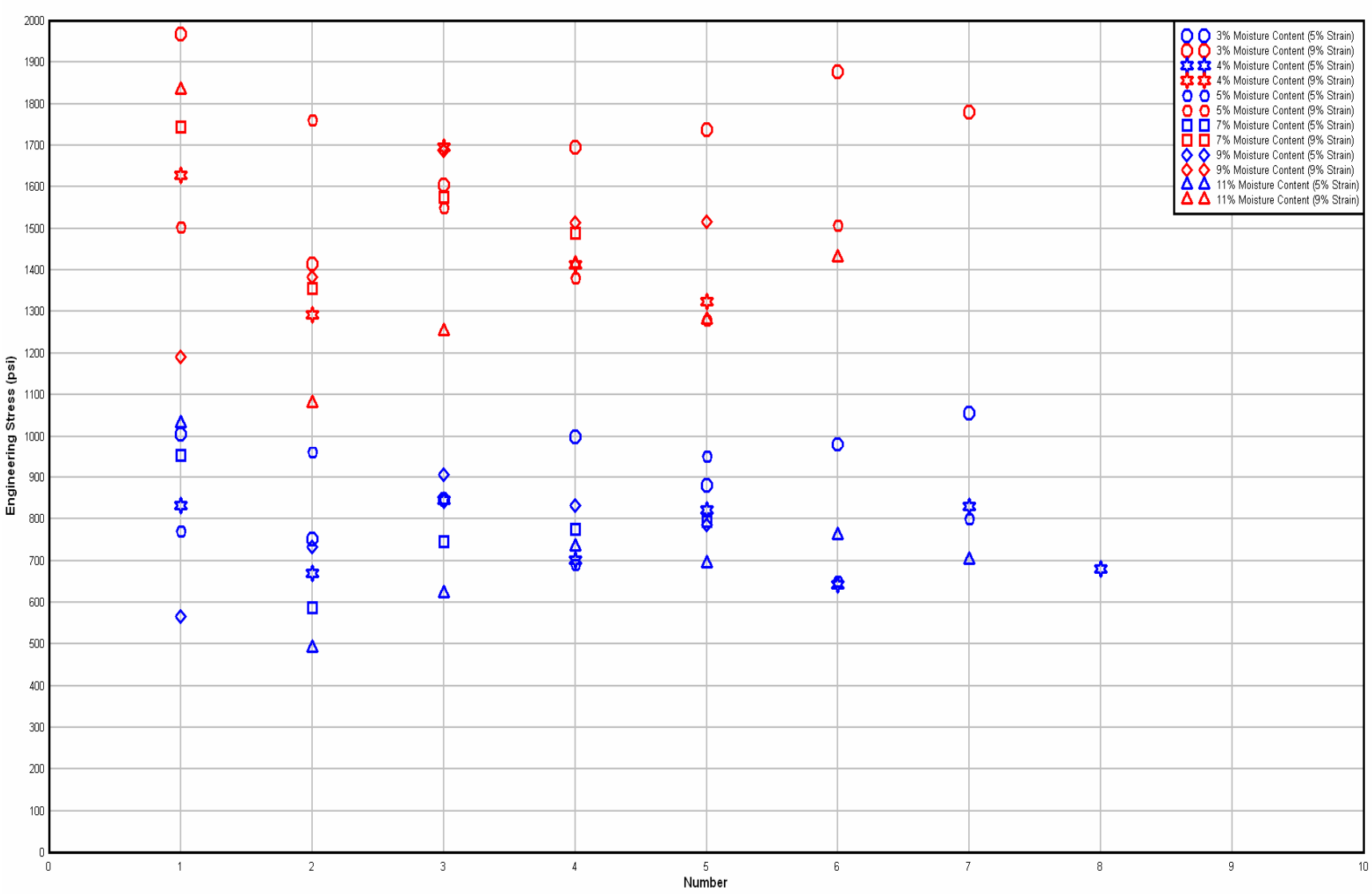

Figure 3-14. Stress distributions at 5% and 9% strain for polycarbonate tube confinement.

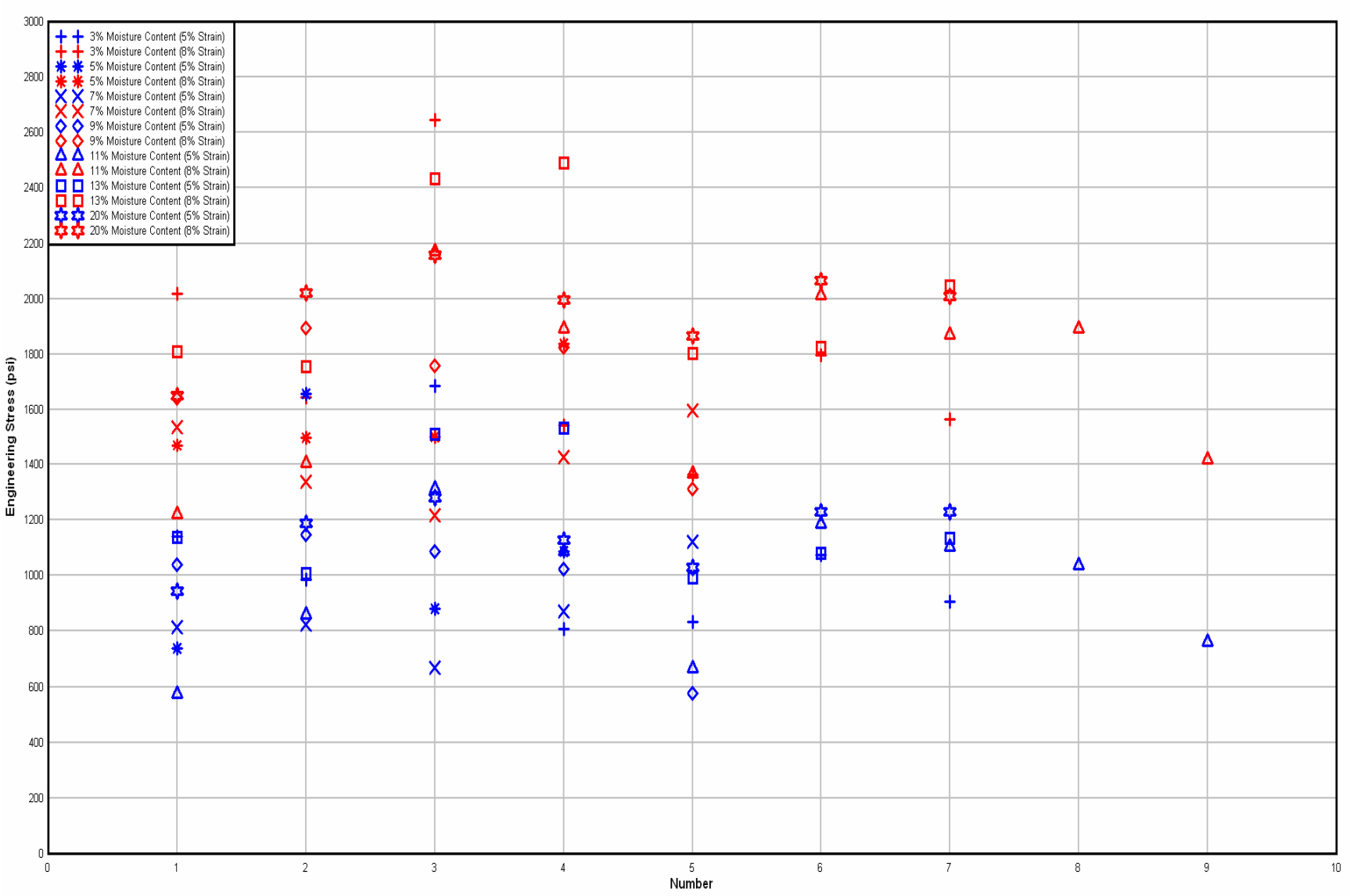

Figure 3-15. Stress distributions at 5% and 8% strain for 4340 steel tube confinement.

Table 3-1. Quikrete #1961 properties

[a]USCS Classification	SP
Specific Gravity	2.72
D_{10} Particle Size (mm)	0.137
D_{30} Particle Size (mm)	0.211
D_{50} Particle Size (mm)	0.281
D_{60} Particle Size (mm)	0.320
[b]C_u	2.33
[c]C_c	1.02
[d]Percent Passing #100 sieve (%)	12.5
[d]Percent Passing #200 sieve (%)	2.7
[e]Maximum Dry Density (kg/m^3)	1630
[e]Minimum Dry Density (kg/m^3)	1400

Notes:

a. Unified Soil Classification System

b. Coefficient of Uniformity

c. Coefficient of Curvature

d. ASTM D4253

e. ASTM D4254

Table 3-2. Dynamic Experiments conducted on sand

Test No.	Moisture Content	Dry Weight	Pulse Shaper	Confinement	Striker Length/Depth	Air Press.	Specimen Dimensions	Specimen Density	Notes
SDDT-1	7%	4 g	0.28125" DIA x 0.032" T Copper disk	Polycarbonate Tube	27"/ 33"	11 psi	19.10 mm Dia x 9.3 mm L	1.61g/cc	Trial experiment Steel SHPB
SDDT-2	7%	4 g	0.28125" DIA x 0.032" T Copper disk	Polycarbonate Tube	27"/ 33"	11 psi	19.10 mm Dia x 9.3 mm L	1.61g/cc	~390/s Steel SHPB
SDDT-3	7%	4 g	0.28125" DIA x 0.032" T Copper disk	Polycarbonate Tube	27"/ 33"	11 psi	19.10 mm Dia x 9.3 mm L	1.61g/cc	~390/s Steel SHPB
SDDT-4	7%	4 g	0.28125" DIA x 0.032" T Copper disk	Polycarbonate Tube	27"/ 33"	11 psi	19.10 mm Dia x 9.3 mm L	1.61g/cc	~410/s Steel SHPB
SDDT-5	7%	4 g	0.28125" DIA x 0.032" T Copper disk	Polycarbonate Tube	27"/ 33"	11 psi	19.10 mm Dia x 9.3 mm L	1.61g/cc	~420/s Steel SHPB
SDDT-6	7%	4 g	0.28125" DIA x 0.032" T Copper disk	Polycarbonate Tube	27"/ 33"	11 psi	19.10 mm Dia x 9.3 mm L	1.61g/cc	~420/s Steel SHPB
SDDT-7	3%	4 g	0.28125" DIA x 0.032" T Copper disk	Polycarbonate Tube	27"/ 33"	11 psi	19.10 mm Dia x 9.3 mm L	1.55 g/cc	~410/s Steel SHPB
SDDT-8	3%	4 g	0.250" DIA x 0.032" T Copper Disk	Polycarbonate Tube	27"/ 33"	11 psi	19.10 mm Dia x 9.3 mm L	1.55 g/cc	~400/s Steel SHPB
SDDT-9	3%	4 g	0.375" DIA x 0.032" T Copper Disk	Polycarbonate Tube	27"/ 33"	11 psi	19.10 mm Dia x 9.3 mm L	1.55 g/cc	~410/s Steel SHPB
SDDT-10	3%	4 g	0.3125" DIA x 0.032" T Copper Disk	Polycarbonate Tube	27"/ 33"	11 psi	19.10 mm Dia x 9.3 mm L	1.55 g/cc	~400/s Steel SHPB
SDDT-11	3%	4 g	0.28125" DIA x 0.032" T Copper disk	Polycarbonate Tube	27"/ 33"	11 psi	19.10 mm Dia x 9.3 mm L	1.55 g/cc	~420/s Steel SHPB

Table 3-2. Continued

Test No.	Moisture Content	Dry Weight	Pulse Shaper	Confinement	Striker Length/Depth	Air Press.	Specimen Dimensions	Specimen Density	Notes
SDDT-12	3%	4 g	0.28125" DIA x 0.032" T Copper disk	Polycarbonate Tube	27"/ 33"	11 psi	19.10 mm Dia x 9.3 mm L	1.55 g/cc	~420/s Steel SHPB
SDDT-13	3%	4 g	0.28125" DIA x 0.032" T Copper disk	Polycarbonate Tube	27"/ 33"	11 psi	19.10 mm Dia x 9.3 mm L	1.55 g/cc	~420/s Steel SHPB
SDDT-14	3%	4 g	0.28125" DIA x 0.032" T Copper disk	Polycarbonate Tube	27"/ 33"	11 psi	19.10 mm Dia x 9.3 mm L	1.55 g/cc	~420/s Steel SHPB
SDDT-15	5%	4 g	0.28125" DIA x 0.032" T Copper disk	Polycarbonate Tube	27"/ 33"	11 psi	19.10 mm Dia x 9.3 mm L	1.58 g/cc	~420/s Steel SHPB
SDDT-16	5%	4 g	0.28125" DIA x 0.032" T Copper disk	Polycarbonate Tube	27"/ 33"	11 psi	19.10 mm Dia x 9.3 mm L	1.58 g/cc	~420/s Steel SHPB
SDDT-17	5%	4 g	0.28125" DIA x 0.032" T Copper disk	Polycarbonate Tube	27"/ 33"	11 psi	19.10 mm Dia x 9.3 mm L	1.58 g/cc	~430/s Steel SHPB
SDDT-18	5%	4 g	0.28125" DIA x 0.032" T Copper disk	Polycarbonate Tube	27"/ 33"	11 psi	19.10 mm Dia x 9.3 mm L	1.58 g/cc	~420/s Steel SHPB
SDDT-19	5%	4 g	0.28125" DIA x 0.032" T Copper disk	Polycarbonate Tube	27"/ 33"	11 psi	19.10 mm Dia x 9.3 mm L	1.58 g/cc	~410/s Steel SHPB
SDDT-20	11%	4 g	0.28125" DIA x 0.032" T Copper disk	Polycarbonate Tube	27"/ 33"	11 psi	19.10 mm Dia x 9.3 mm L	1.67 g/cc	~410/s Steel SHPB
SDDT-21	11%	4 g	0.28125" DIA x 0.032" T Copper disk	Polycarbonate Tube	27"/ 33"	11 psi	19.10 mm Dia x 9.3 mm L	1.67 g/cc	~440/s Steel SHPB
SDDT-22	11%	4 g	0.28125" DIA x 0.032" T Copper disk	Polycarbonate Tube	27"/ 33"	11 psi	19.10 mm Dia x 9.3 mm L	1.67 g/cc	~450/s Steel SHPB

Table 3-2. Continued

Test No.	Moisture Content	Dry Weight	Pulse Shaper	Confinement	Striker Length/Depth	Air Press.	Specimen Dimensions	Specimen Density	Notes
SDDT-23	11%	4 g	0.28125" DIA x 0.032" T Copper disk	Polycarbonate Tube	27"/ 33"	11 psi	19.10 mm Dia x 9.3 mm L	1.67 g/cc	~430/s Steel SHPB
SDDT-24	11%	4 g	0.28125" DIA x 0.032" T Copper disk	Polycarbonate Tube	27"/ 33"	11 psi	19.10 mm Dia x 9.3 mm L	1.67 g/cc	~420/s Steel SHPB
SDDT-25	11%	4 g	0.28125" DIA x 0.032" T Copper disk	Polycarbonate Tube	27"/ 33"	11 psi	19.10 mm Dia x 9.3 mm L	1.67 g/cc	~450/s Steel SHPB
SDDT-26	11%	4 g	0.28125" DIA x 0.032" T Copper disk	Polycarbonate Tube	27"/ 33"	11 psi	19.10 mm Dia x 9.3 mm L	1.67 g/cc	~410/s Steel SHPB
SDDT-27	11%	4 g	0.28125" DIA x 0.032" T Copper disk	Polycarbonate Tube	27"/ 33"	11 psi	19.10 mm Dia x 9.3 mm L	1.67 g/cc	~400/s Steel SHPB
SDDT-28	5%	4 g	0.28125" DIA x 0.032" T Copper disk	Polycarbonate Tube	27"/ 33"	11 psi	19.10 mm Dia x 9.3 mm L	1.58 g/cc	~440/s Steel SHPB
SDDT-29	5%	4 g	0.28125" DIA x 0.032" T Copper disk	Polycarbonate Tube	27"/ 33"	11 psi	19.10 mm Dia x 9.3 mm L	1.58 g/cc	~440/s Steel SHPB
SDDT-30	9%	4 g	0.28125" DIA x 0.032" T Copper disk	Polycarbonate Tube	27"/ 33"	11 psi	19.10 mm Dia x 9.3 mm L	1.64 g/cc	~420/s Steel SHPB
SDDT-31	9%	4 g	0.28125" DIA x 0.032" T Copper disk	Polycarbonate Tube	27"/ 33"	11 psi	19.10 mm Dia x 9.3 mm L	1.64 g/cc	~430/s Steel SHPB
SDDT-32	9%	4 g	0.28125" DIA x 0.032" T Copper disk	Polycarbonate Tube	27"/ 33"	11 psi	19.10 mm Dia x 9.3 mm L	1.64 g/cc	~440/s Steel SHPB
SDDT-33	9%	4 g	0.28125" DIA x 0.032" T Copper disk	Polycarbonate Tube	27"/ 33"	11 psi	19.10 mm Dia x 9.3 mm L	1.64 g/cc	~440/s Steel SHPB

Table 3-2. Continued

Test No.	Moisture Content	Dry Weight	Pulse Shaper	Confinement	Striker Length/Depth	Air Press.	Specimen Dimensions	Specimen Density	Notes
SDDT-34	9%	4 g	0.28125" DIA x 0.032" T Copper disk	Polycarbonate Tube	27"/ 33"	11 psi	19.10 mm Dia x 9.3 mm L	1.64 g/cc	~430/s Steel SHPB
SDDT-35	4%	4 g	0.28125" DIA x 0.032" T Copper disk	Polycarbonate Tube	27"/ 33"	11 psi	19.10 mm Dia x 9.3 mm L	1.56 g/cc	~440/s Steel SHPB
SDDT-36	4%	4 g	0.28125" DIA x 0.032" T Copper disk	Polycarbonate Tube	27"/ 33"	11 psi	19.10 mm Dia x 9.3 mm L	1.56 g/cc	~430/s Steel SHPB
SDDT-37	4%	4 g	0.28125" DIA x 0.032" T Copper disk	Polycarbonate Tube	27"/ 33"	11 psi	19.10 mm Dia x 9.3 mm L	1.56 g/cc	~420/s Steel SHPB
SDDT-38	4%	4 g	0.28125" DIA x 0.032" T Copper disk	Polycarbonate Tube	27"/ 33"	11 psi	19.10 mm Dia x 9.3 mm L	1.56 g/cc	~410/s Steel SHPB
SDDT-39	4%	4 g	0.28125" DIA x 0.032" T Copper disk	Polycarbonate Tube	27"/ 33"	11 psi	19.10 mm Dia x 9.3 mm L	1.56 g/cc	~400/s Steel SHPB
SDDT-40	4%	4 g	0.28125" DIA x 0.032" T Copper disk	Polycarbonate Tube	27"/ 33"	11 psi	19.10 mm Dia x 9.3 mm L	1.56 g/cc	~400/s Steel SHPB
SDDT-41	4%	4 g	0.28125" DIA x 0.032" T Copper disk	Polycarbonate Tube	27"/ 33"	11 psi	19.10 mm Dia x 9.3 mm L	1.56 g/cc	~380/s Steel SHPB
SDDT-42	4%	4 g	0.28125" DIA x 0.032" T Copper disk	Polycarbonate Tube	27"/ 33"	11 psi	19.10 mm Dia x 9.3 mm L	1.56 g/cc	~380/s Steel SHPB
SDDT-43	3%	4 g	0.28125" DIA x 0.032" T Copper disk	Steel Tube	27"/ 33"	11 psi	19.10 mm Dia x 9.3 mm L	1.55 g/cc	~410/s Steel SHPB
SDDT-44	3%	4 g	0.28125" DIA x 0.032" T Copper disk	Steel Tube	27"/ 33"	11 psi	19.10 mm Dia x 9.3 mm L	1.55 g/cc	~410/s Steel SHPB

Table 3-2. Continued

Test No.	Moisture Content	Dry Weight	Pulse Shaper	Confinement	Striker Length/Depth	Air Press.	Specimen Dimensions	Specimen Density	Notes
SDDT-45	3%	4 g	0.28125" DIA x 0.032" T Copper disk	Steel Tube	27"/ 33"	11 psi	19.10 mm Dia x 9.3 mm L	1.55 g/cc	~410/s Steel SHPB
SDDT-46	3%	4 g	0.28125" DIA x 0.032" T Copper disk	Steel Tube	27"/ 33"	11 psi	19.10 mm Dia x 9.3 mm L	1.55 g/cc	~430/s Steel SHPB
SDDT-47	3%	4 g	0.28125" DIA x 0.032" T Copper disk	Steel Tube	27"/ 33"	11 psi	19.10 mm Dia x 9.3 mm L	1.55 g/cc	~420/s Steel SHPB
SDDT-48	3%	4 g	0.28125" DIA x 0.032" T Copper disk	Steel Tube	27"/ 33"	11 psi	19.10 mm Dia x 9.3 mm L	1.55 g/cc	~390/s Steel SHPB
SDDT-49	3%	4 g	0.28125" DIA x 0.032" T Copper disk	Steel Tube	27"/ 33"	11 psi	19.10 mm Dia x 9.3 mm L	1.55 g/cc	~390/s Steel SHPB
SDDT-50	7%	4 g	0.28125" DIA x 0.032" T Copper disk	Steel Tube	27"/ 33"	11 psi	19.10 mm Dia x 9.3 mm L	1.61g/cc	~390/s Steel SHPB
SDDT-51	7%	4 g	0.28125" DIA x 0.032" T Copper disk	Steel Tube	27"/ 33"	11 psi	19.10 mm Dia x 9.3 mm L	1.61g/cc	~430/s Steel SHPB
SDDT-52	7%	4 g	0.28125" DIA x 0.032" T Copper disk	Steel Tube	27"/ 33"	11 psi	19.10 mm Dia x 9.3 mm L	1.61g/cc	~440/s Steel SHPB
SDDT-53	7%	4 g	0.28125" DIA x 0.032" T Copper disk	Steel Tube	27"/ 33"	11 psi	19.10 mm Dia x 9.3 mm L	1.61g/cc	~440/s Steel SHPB
SDDT-54	7%	4 g	0.28125" DIA x 0.032" T Copper disk	Steel Tube	27"/ 33"	11 psi	19.10 mm Dia x 9.3 mm L	1.61g/cc	~430/s Steel SHPB
SDDT-55	11%	4 g	0.28125" DIA x 0.032" T Copper disk	Steel Tube	27"/ 33"	11 psi	19.10 mm Dia x 9.3 mm L	1.67 g/cc	~440/s Steel SHPB

Table 3-2. Continued

Test No.	Moisture Content	Dry Weight	Pulse Shaper	Confinement	Striker Length/Depth	Air Press.	Specimen Dimensions	Specimen Density	Notes
SDDT-56	11%	4 g	0.28125" DIA x 0.032" T Copper disk	Steel Tube	27"/ 33"	11 psi	19.10 mm Dia x 9.3 mm L	1.67 g/cc	~430/s Steel SHPB
SDDT-57	11%	4 g	0.28125" DIA x 0.032" T Copper disk	Steel Tube	27"/ 33"	11 psi	19.10 mm Dia x 9.3 mm L	1.67 g/cc	~390/s Steel SHPB
SDDT-58	11%	4 g	0.28125" DIA x 0.032" T Copper disk	Steel Tube	27"/ 33"	11 psi	19.10 mm Dia x 9.3 mm L	1.67 g/cc	~400/s Steel SHPB
SDDT-59	11%	4 g	0.28125" DIA x 0.032" T Copper disk	Steel Tube	27"/ 33"	11 psi	19.10 mm Dia x 9.3 mm L	1.67 g/cc	~420/s Steel SHPB
SDDT-60	11%	4 g	0.28125" DIA x 0.032" T Copper disk	Steel Tube	27"/ 33"	11 psi	19.10 mm Dia x 9.3 mm L	1.67 g/cc	~400/s Steel SHPB
SDDT-61	11%	4 g	0.28125" DIA x 0.032" T Copper disk	Steel Tube	27"/ 33"	11 psi	19.10 mm Dia x 9.3 mm L	1.67 g/cc	~390/s Steel SHPB
SDDT-62	11%	4 g	0.28125" DIA x 0.032" T Copper disk	Steel Tube	27"/ 33"	11 psi	19.10 mm Dia x 9.3 mm L	1.67 g/cc	~380/s Steel SHPB
SDDT-63	11%	4 g	0.28125" DIA x 0.032" T Copper disk	Steel Tube	27"/ 33"	11 psi	19.10 mm Dia x 9.3 mm L	1.67 g/cc	~380/s Steel SHPB
SDDT-64	13%	4 g	0.28125" DIA x 0.032" T Copper disk	Steel Tube	27"/ 33"	11 psi	19.10 mm Dia x 9.3 mm L	1.70 g/cc	~400/s Steel SHPB
SDDT-65	13%	4 g	0.28125" DIA x 0.032" T Copper disk	Steel Tube	27"/ 33"	11 psi	19.10 mm Dia x 9.3 mm L	1.70 g/cc	~420/s Steel SHPB
SDDT-66	13%	4 g	0.28125" DIA x 0.032" T Copper disk	Steel Tube	27"/ 33"	11 psi	19.10 mm Dia x 9.3 mm L	1.70 g/cc	~390/s Steel SHPB

Table 3-2. Continued

Test No.	Moisture Content	Dry Weight	Pulse Shaper	Confinement	Striker Length/Depth	Air Press.	Specimen Dimensions	Specimen Density	Notes
SDDT-67	13%	4 g	0.28125" DIA x 0.032" T Copper disk	Steel Tube	27"/ 33"	11 psi	19.10 mm Dia x 9.3 mm L	1.70 g/cc	~390/s Steel SHPB
SDDT-68	13%	4 g	0.28125" DIA x 0.032" T Copper disk	Steel Tube	27"/ 33"	11 psi	19.10 mm Dia x 9.3 mm L	1.70 g/cc	~410/s Steel SHPB
SDDT-69	13%	4 g	0.28125" DIA x 0.032" T Copper disk	Steel Tube	27"/ 33"	11 psi	19.10 mm Dia x 9.3 mm L	1.70 g/cc	~400/s Steel SHPB
SDDT-70	13%	4 g	0.28125" DIA x 0.032" T Copper disk	Steel Tube	27"/ 33"	11 psi	19.10 mm Dia x 9.3 mm L	1.70 g/cc	~390/s Steel SHPB
SDDT-71	9%	4 g	0.28125" DIA x 0.032" T Copper disk	Steel Tube	27"/ 33"	11 psi	19.10 mm Dia x 9.3 mm L	1.64 g/cc	~400/s Steel SHPB
SDDT-72	9%	4 g	0.28125" DIA x 0.032" T Copper disk	Steel Tube	27"/ 33"	11 psi	19.10 mm Dia x 9.3 mm L	1.64 g/cc	~380/s Steel SHPB
SDDT-73	9%	4 g	0.28125" DIA x 0.032" T Copper disk	Steel Tube	27"/ 33"	11 psi	19.10 mm Dia x 9.3 mm L	1.64 g/cc	~410/s Steel SHPB
SDDT-74	9%	4 g	0.28125" DIA x 0.032" T Copper disk	Steel Tube	27"/ 33"	11 psi	19.10 mm Dia x 9.3 mm L	1.64 g/cc	~400/s Steel SHPB
SDDT-75	9%	4 g	0.28125" DIA x 0.032" T Copper disk	Steel Tube	27"/ 33"	11 psi	19.10 mm Dia x 9.3 mm L	1.64 g/cc	~400/s Steel SHPB
SDDT-76	20%	4 g	0.28125" DIA x 0.032" T Copper disk	Steel Tube	27"/ 33"	11 psi	19.10 mm Dia x 9.3 mm L	1.80 g/cc	~400/s Steel SHPB
SDDT-77	20%	4 g	0.28125" DIA x 0.032" T Copper disk	Steel Tube	27"/ 33"	11 psi	19.10 mm Dia x 9.3 mm L	1.80 g/cc	~390/s Steel SHPB

Table 3-2. Continued

Test No.	Moisture Content	Dry Weight	Pulse Shaper	Confinement	Striker Length/Depth	Air Press.	Specimen Dimensions	Specimen Density	Notes
SDDT-78	20%	4 g	0.28125" DIA x 0.032" T Copper disk	Steel Tube	27"/ 33"	11 psi	19.10 mm Dia x 9.3 mm L	1.80 g/cc	~390/s Steel SHPB
SDDT-79	20%	4 g	0.28125" DIA x 0.032" T Copper disk	Steel Tube	27"/ 33"	11 psi	19.10 mm Dia x 9.3 mm L	1.80 g/cc	~380/s Steel SHPB
SDDT-80	20%	4 g	0.28125" DIA x 0.032" T Copper disk	Steel Tube	27"/ 33"	11 psi	19.10 mm Dia x 9.3 mm L	1.80 g/cc	~400/s Steel SHPB
SDDT-81	20%	4 g	0.28125" DIA x 0.032" T Copper disk	Steel Tube	27"/ 33"	11 psi	19.10 mm Dia x 9.3 mm L	1.80 g/cc	~390/s Steel SHPB
SDDT-82	20%	4 g	0.28125" DIA x 0.032" T Copper disk	Steel Tube	27"/ 33"	11 psi	19.10 mm Dia x 9.3 mm L	1.80 g/cc	~380/s Steel SHPB
SDDT-83	5%	4 g	0.28125" DIA x 0.032" T Copper disk	Steel Tube	27"/ 33"	11 psi	19.10 mm Dia x 9.3 mm L	1.58 g/cc	~400/s Steel SHPB
SDDT-84	5%	4 g	0.28125" DIA x 0.032" T Copper disk	Steel Tube	27"/ 33"	11 psi	19.10 mm Dia x 9.3 mm L	1.58 g/cc	~410/s Steel SHPB
SDDT-85	5%	4 g	0.28125" DIA x 0.032" T Copper disk	Steel Tube	27"/ 33"	11 psi	19.10 mm Dia x 9.3 mm L	1.58 g/cc	~380/s Steel SHPB
SDDT-86	5%	4 g	0.28125" DIA x 0.032" T Copper disk	Steel Tube	27"/ 33"	11 psi	19.10 mm Dia x 9.3 mm L	1.58 g/cc	~370/s Steel SHPB

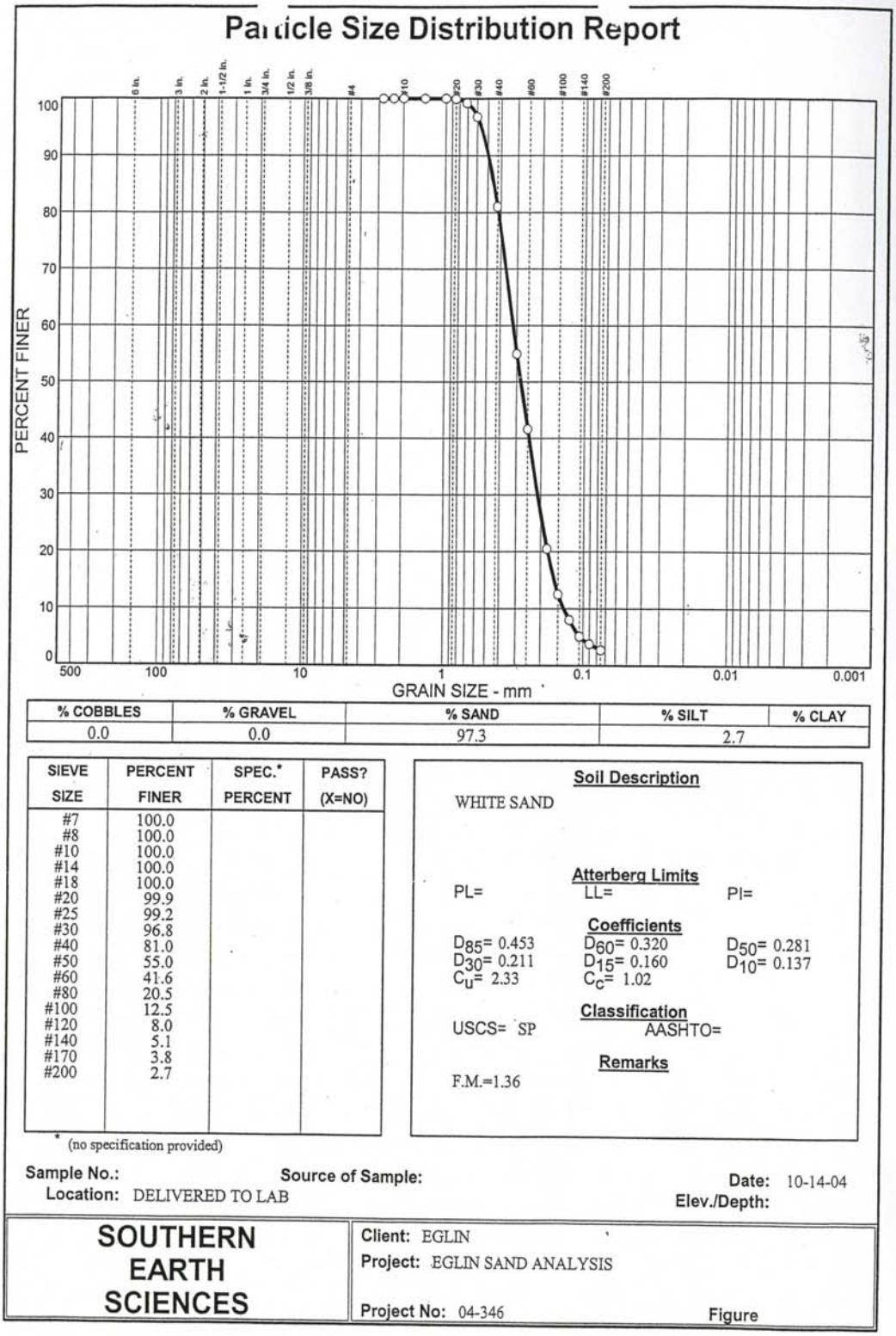

Figure 3-16. Gradation Curve for Quikrete #1961 Fine Grain Sand.

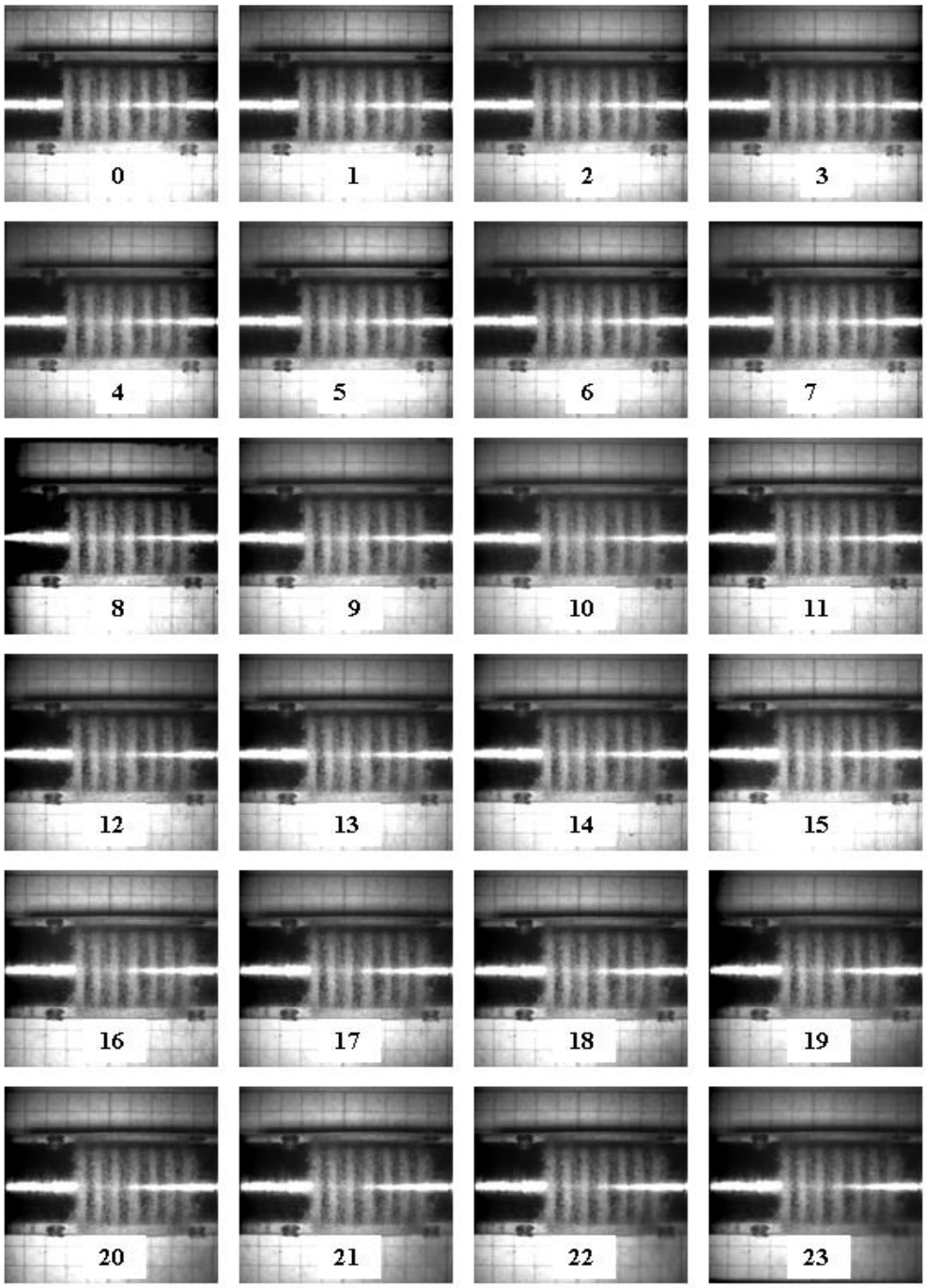

Figure 3-17. Dynamic deformation of a 28.4 mm long dry sand specimen (Duration: 12.3 microseconds). [Reprinted from Song, B., and Chen, W., 2006, "Dynamic Compressive Behavior of Sands," Unpublished technical report, School of Aeronautics and Astronautics and School of Materials Engineering, Purdue University. (Figure 3)]

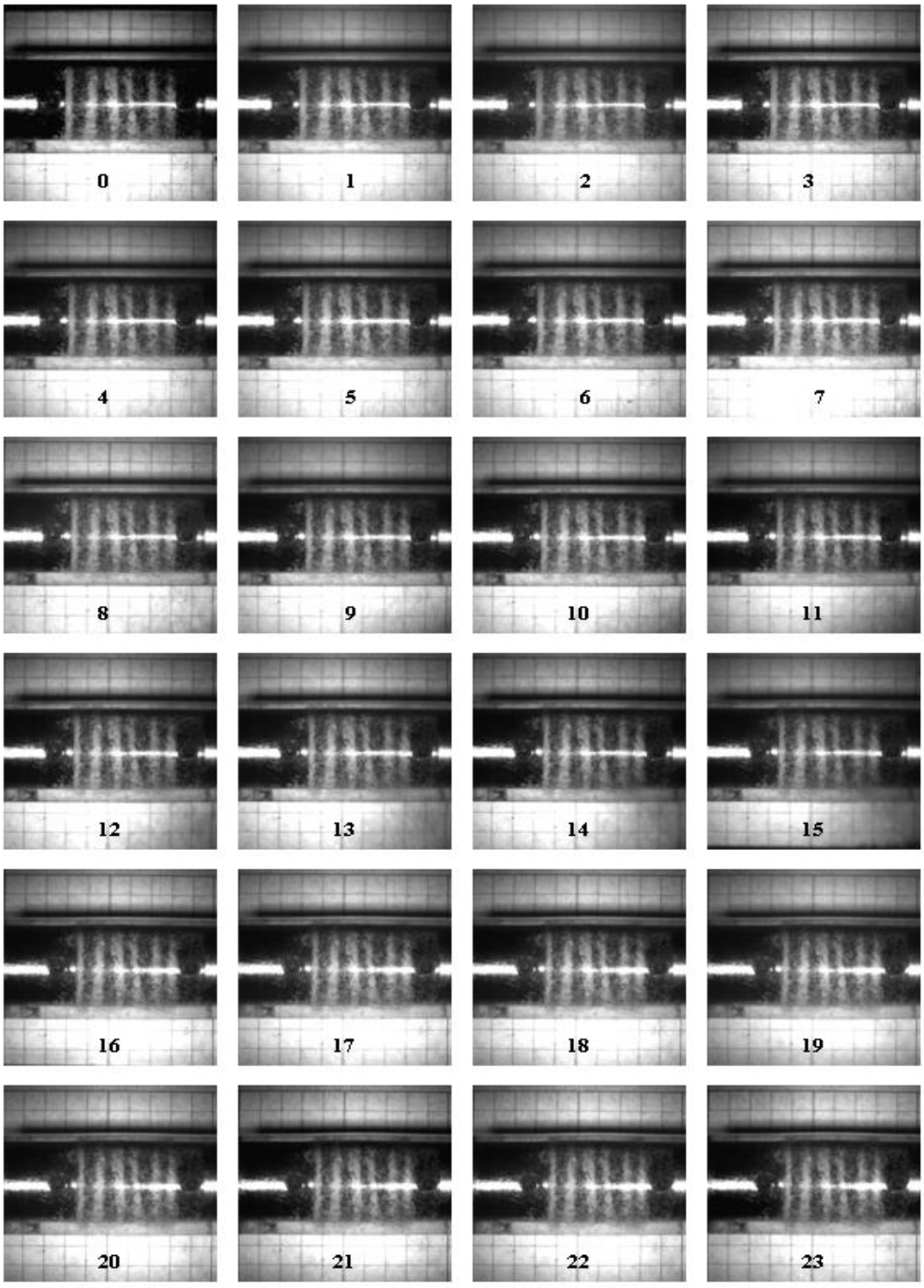

Figure 3-18. Dynamic deformation of a 25.4 mm long dry sand specimen (Duration: 12.4 microseconds). [Reprinted from Song, B., and Chen, W., 2006, "Dynamic Compressive Behavior of Sands," Unpublished technical report, School of Aeronautics and Astronautics and School of Materials Engineering, Purdue University. (Figure 4)]

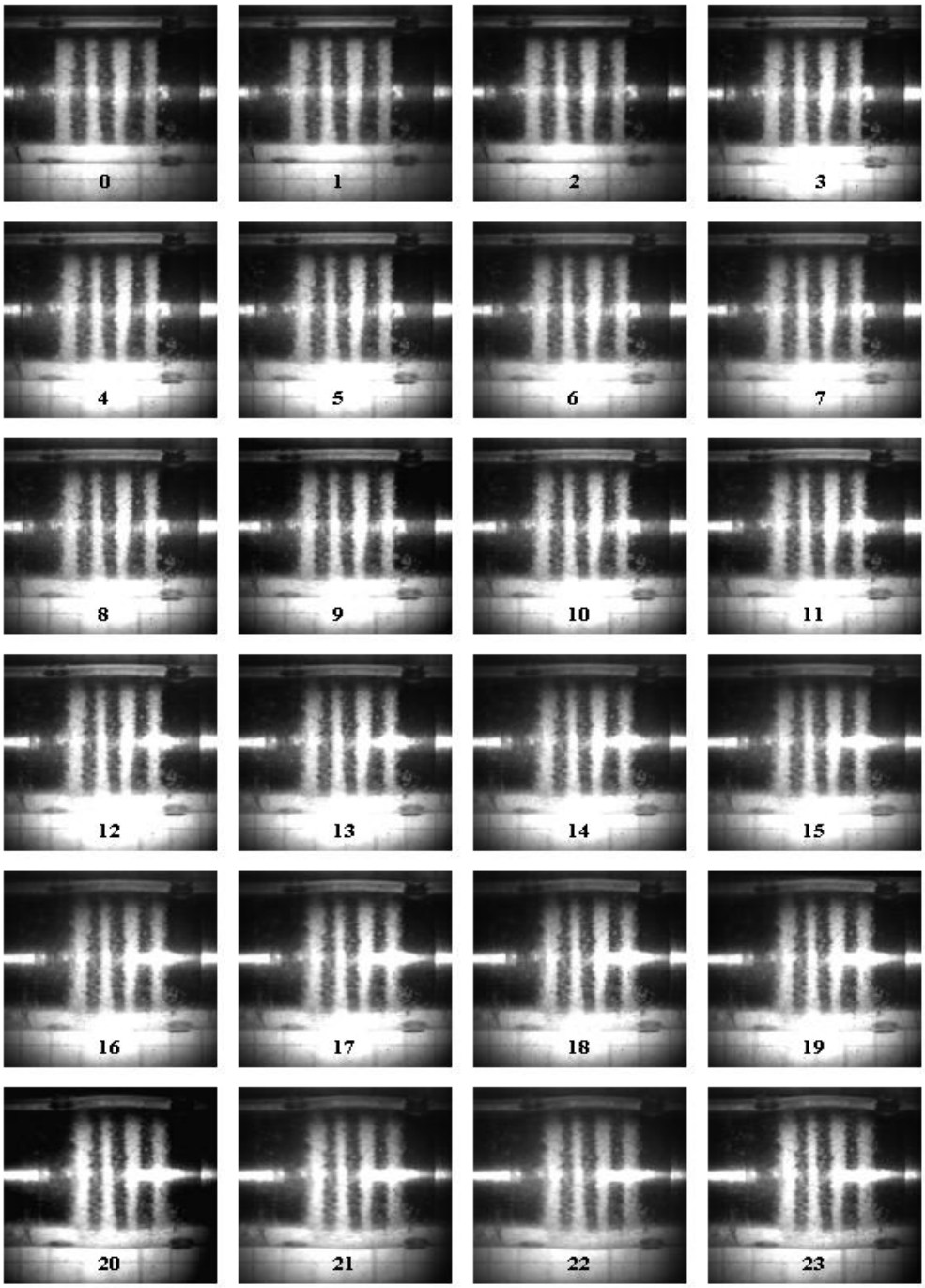

Figure 3-19. Dynamic deformation of a 15.2 mm long dry sand specimen (Duration: 12.4 microseconds). [Reprinted from Song, B., and Chen, W., 2006, "Dynamic Compressive Behavior of Sands," Unpublished technical report, School of Aeronautics and Astronautics and School of Materials Engineering, Purdue University. (Figure 5)]

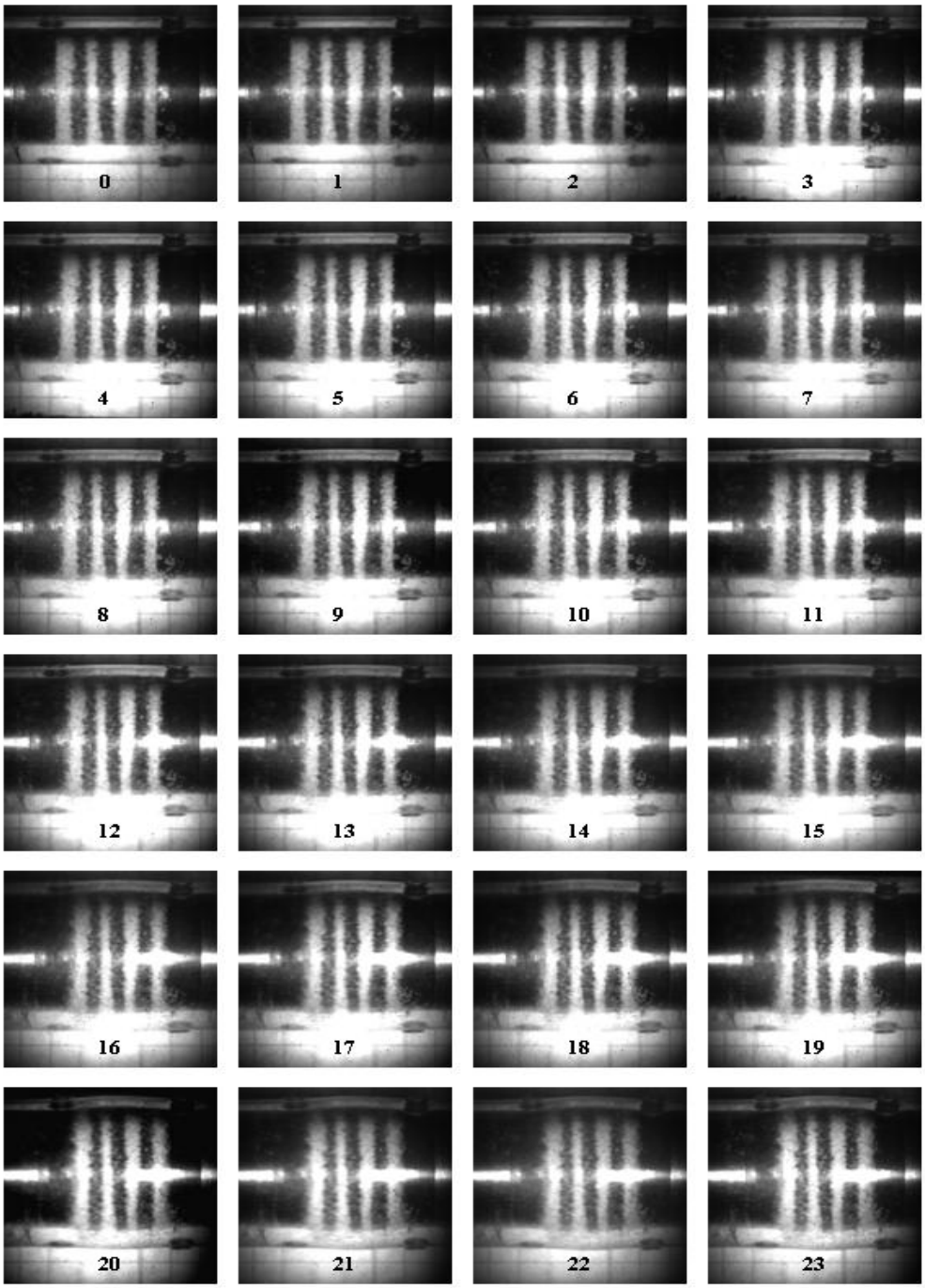

Figure 3-20. Dynamic deformation of a 13.1 mm long dry sand specimen (Duration: 12.6 microseconds). [Reprinted from Song, B., and Chen, W., 2006, "Dynamic Compressive Behavior of Sands," Unpublished technical report, School of Aeronautics and Astronautics and School of Materials Engineering, Purdue University. (Figure 6)]

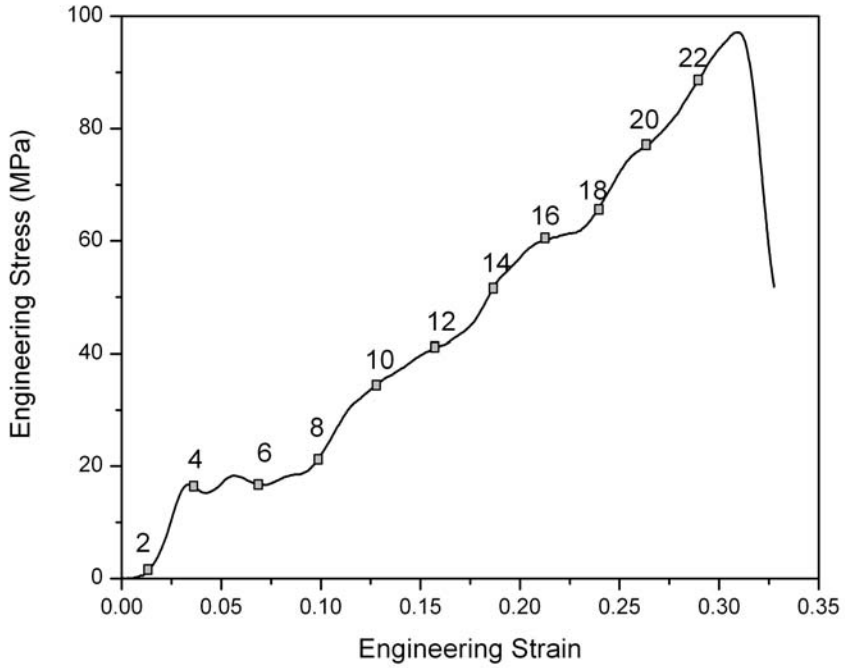

Figure 3-21. Engineering stress-strain curve for the 13.1-mm-long dry sand specimen. The square boxes on the plot indicate the image number from Figure 3-20. [Reprinted from Song, B., and Chen, W., 2006, "Dynamic Compressive Behavior of Sands," Unpublished technical report, School of Aeronautics and Astronautics and School of Materials Engineering, Purdue University. (Figure 7)]

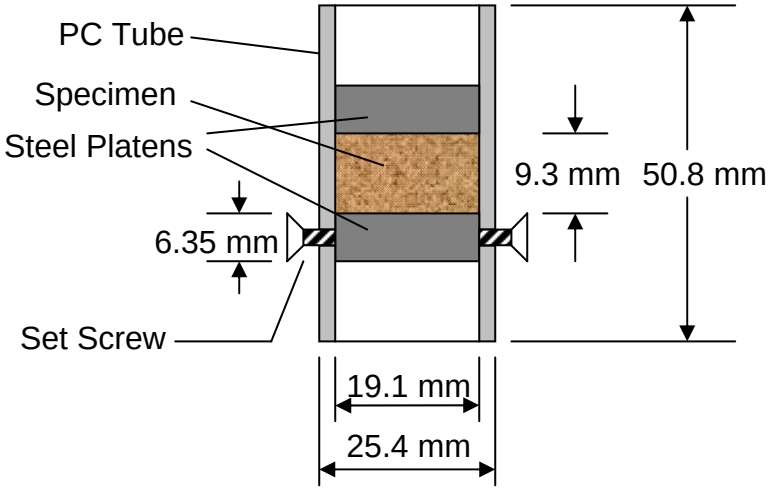

Figure 3-22. Sand specimen arrangement confined by a polycarbonate tube.

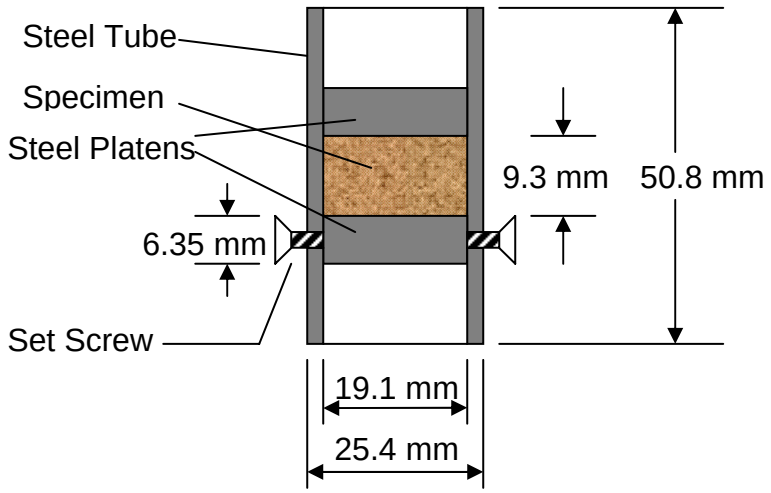

Figure 3-23. Sand specimen arrangement confined by a 4340 steel tube.

CHAPTER 4
EXPERIMENTAL RESULTS

4.1 Presentation of Data

High strain rate experiments using a modified SHPB were conducted on a fine grain sand to determine the effects of moisture content on the mechanical behavior. The sand specimens used a dry density of 1.50 g/cc for all experiments and can be considered to be in an undrained, remolded state. Because of the short duration of the dynamic tests, an undrained[2] state may be assumed. All experiments were conducted at a strain-rate of about 400/s for varying moisture contents and polycarbonate and steel confinements. To check/ensure the repeatability of the data, a minimum of five experiments were conducted for each moisture level, under each confinement method, except at 5% moisture content with steel confinement where four experiments were conducted. Repeated experiments of each moisture level were conducted to examine the repeatability of the data. As previously mentioned, due to the low wave speed of the material, a modified SHPB incorporating pulse shaping were used such that the specimen was loaded slower than in a conventional SHPB. A copper disc was mounted in between the striker and incident bar (Fig. 3-6). No strain gages were mounted on the confinement tubes.

One-dimensional wave theory was used to reduce all data collected from the modified SHPB (Chapter 3). The starting point of the reflected pulse, following the incident pulse, was obtained by using the determined wave speed of the bar material (~5,080 m/s) to calculate the time required for the incident pulse to travel from the strain gage to the specimen, be reflected at the bar/specimen interface, and travel back to the strain gage. Thus, this time is $T = 2L/C$,

[2] An undrained condition for the sand was determined to be a viable assumption by Dr. Stephen A. Akers of the U.S. Army Engineering Research and Development Center in Vicksburg, MS on March 14, 2007 through a personal communication.

where L is the distance from the strain gage center to the bar/specimen interface and C is the wave speed of the bar material. The starting point for the transmitted signal was determined in a similar fashion. The starting point of the transmitted pulse was determined using: $T = T_s + T_t + 1/2\,T_r$ where T_s is the transit time through the specimen, T_t is the time to travel from the specimen to the transmitter bar strain gage and T_r the transit time for the reflected pulse. These approximate starting times for the reflected and transmitted pulses are 1060 μs and 640 μs, respectively. These times were used in reducing the data for all experiments in this study.

Following the data reduction, all the stress-strain curves obtained for different moisture contents and confinement methods (both polycarbonate and steel confinement) were plotted together. Figures 4-1 to 4-6 show the stress-strain relationships under polycarbonate confinement while in Figures 4-7 to 4-13 are shown the stress-strain relationships in the case of steel confinement. For all experiments, the stress-strain curves were truncated by determining the maximum percent strain value where both stress-equilibrium and constant strain-rate were no longer satisfied simultaneously. The mean curves for each moisture content and confinement are plotted together in Figures 4-14 and 4-15. A rigorous statistical analysis was not conducted on the data, but in order to investigate the effects of moisture content for each confinement a two sigma standard deviation was determined for all of the mean curves in Figures 4-14 and 4-15. For example, using Figure 4-1 the error bars associated to its mean curve shown in Figure 4-14 were determined by finding the stresses of each curve in Figure 4-1 associated with specific percent strains. Then for each percent strain the standard deviation was determined for the error bars. The error bars in Figures 4-14 and 4-15 are not a strict statistical representation, but represent the range of the stress-strain data at a particular percent strain for each moisture content

and confinement. The percent strains used for the polycarbonate confinement are 1%, 3%, 5%, 7%, 8% and 9% and for the steel confinement are 1%, 3%, 5%, 7%, 8%.

The dry sand results shown in Figures 4-14 and 4-15 reported by Song et al. [28] were determined in the same manner with the exception of the standard deviation. The error bars shown for the dry sand data represents the range of data obtained for those experiments. The data associated with the dry sand mean curves presented in Figures 4-14 and 4-15 are shown in Figures 4-16 and 4-17 for polycarbonate and steel confinements, respectively. Although the dry sand test were conducted at a slightly higher strain-rate as shown in Figure 4-18, no significant strain-rate effects were apparent for dry sand in the strain-rate range covered by Song et al. [28]. All dry sand results by Song et al. [28] were conducted using the identical material, SHPB, and specimen preparation method.

The results in Figures 4-14 and 4-15 indicate that dry sand is stiffer than the moist/partially saturated sand under the testing conditions utilized for these experiments. The stress-strain relationships in Figures 4-1 thru 4-6 show significant spikes in stress between 1% and 3% strain. The same spikes in stress are also evident in Figures 4-7 thru 4-13, but more amplified since a stiffer confinement is used. These are occurring between 2% and 4% strain. One of the possible sources of these spikes is the contact conditions between the loading platens and the sand specimen. Researchers in Sandia National Laboratories recently found that by placing a thin copper sheet between the sand and the platens could reduce the amplitudes of the spikes[3].

[3] This technique of using the copper sheet between the steel platen and sand was investigated by Dr. Vicent K. Luk of Sandia National Laboratories, Albuquerque, NM. The results of this investigation were discovered through a personal communication with Dr. Luk on March 27, 2007.

The trends shown in Figures 4-14 and 4-15 where moisture addition makes the sand more compressible (less stiff), appears to be in contradiction. The following sections will present and discuss hypotheses that might be used to give an interpretation of the data and to possibly answer questions regarding the trends observed experimentally.

4.2 Discussion of Results

4.2.1 Moisture Effects

Figures 4-1 thru 4-6 presents the stress-strain data obtained in all tests where polycarbonate confinement was applied. To facilitate the analysis, for each moisture content a mean stress-strain curve was determined. Figure 4-14 shows the mean stress-strain curves corresponding to the various moisture contents in comparison with the dry sand data. Given that error bars overlap significantly, it is difficult to determine accurately the effect of moisture content on the behavior. Indeed, the 4% moisture content stiffness is comparable to 7% and 9% moisture content curves. Still, based on the results presented in Figure 4-14, it can be concluded that as the moisture content decreases the material stiffness becomes greater. Figures 4-7 thru 4-13 presents the stress-strain data obtained in all tests where steel confinement was applied. Figure 4-15 show the mean curves with error bars for various moisture contents in comparison with dry sand data. No apparent trend between moisture contents is observable. However, ignoring the error bars associated with the mean curves, a trend is observed if several changes in the data are performed. If test SDDT-45 is removed from Figure 4-7 for 3% moisture content under steel confinement its respective mean curves in Figure 4-15 would decrease making the response less stiff. If test SDDT-75 is removed from Figure 4-10 for 9% moisture content under the same confinement its respective mean curve in Figure 4-15 would raise, so the response is stiffer than in the 3% moisture content case. If the assumption is made that these particular experiments are anomalies within the data, a more defined trend is apparent. If this is the case,

stiffness' for 3% and 9% moisture contents would be nearly equal. In addition, the stiffness would decrease from 3% to 7% moisture content, respectively, and increase with increasing the moisture contents in the range 9% to 20%, respectively. Although this treatment shows a more definitive trend the 11% moisture content mean curve is still equivalent in stiffness to the 3% and 9% moisture contents ones. The stress-strain curve at 11% moisture content shown in Figure 4-11 illustrates that the response has two stiffness regimes. The cause of this is not yet known, but if a mean curve is created to represent each stiffness regime of Figure 4-11 then for 11% moisture content, would have a stiffness representing the lower stiffness regime associated with 3% to 7% moisture content and mean curve representing the higher stiffness regime associated with 9% to 20% moisture content. If this is possible then 9% moisture content is very close to the transition regime at 11% moisture content showing a shifting of the stiffness in the stress-strain response of the moist sand with steel confinement. However, the stress-strain response for each moisture content for a given confinement (Figures 4-14 and 4-15) are in general undistinguishable from one another indicating that small changes in moisture content does not affect the stiffness of moist sand.

4.2.2 Soil Mechanics Perspective

The apparent trends in Figures 4-14 and 4-15 indicate that dry sand is stiffer than moist/partially saturated sand for the given set of testing conditions. The porosity of a given particulate material is dependent on the shape of the particles and the particles size distribution. For example, if a fine sand material is used, as the one in this study, the specimen can be a two-phase or three-phase material. If the sand is dry the material can be considered as being two-phase: a solid phase corresponding to the sand skeleton and a gas phase associated to the pore air; if the material contains water or any other liquid (partially saturated) then it can be generally

considered a three phase material, but it is two-phase if fully saturated (all pores are filled with water).

In our study, the specimen consists of a sand skeleton and pores which may be filled with air or water. Pores in the sample, for a moist/partially saturated condition is a combination of the pore air and pore water. Generally, if the specimen is strained sufficiently, all pore air will be compressed out if drained conditions prevail or taken over by pore water if undrained conditions prevail. Once the pore air is removed the specimen is fully saturated and the water is immediately loaded. When the water is loaded the material will stiffen with no additional compression of the sample taking place because water is incompressible. A general illustration of this is shown in Figure 4-19. The experiments conducted in this study using steel confinement essentially approximate or closely simulate one-dimensional axial strain conditions. This condition allows only axial strain to occur with radial stress applied by the steel confinement to constrict lateral displacement. For uniaxial strain conditions the volume fraction of air voids in the specimen is directly related to the percent strain required to remove all air voids. When the percent strain is equal to the percent volume of air in the specimen the water will then be loaded and the material will stiffen. The moisture contents for the specimens tested in this study ranged from 3% to 20%. The corresponding percent volume of air associated with each of these moisture contents is tabulated in Table 4-1. It is shown that the percent volume of air voids decreases as the moisture content increases indicating that the minimum percent strain required to remove the air is ~13% for the 20% moisture content. The experiments conducted with both polycarbonate and steel confinements only strained the specimens to approximately 9% strain. With the maximum percent strains below the percent volume of air voids the effects of water should not be evident. Looking again at Figures 4-1 thru 4-13 the stress-strain curves

show no evidence of the material “locking up” where the specimen becomes completely saturated and water only is loaded.

The trends shown in Figures 4-14 and 4-15 do not necessarily agree with what one from a soil mechanics perspective would expect to see. Evaluating the trends is difficult since both the dry and moist/partially saturated sand were not adequately strained to experience the effects of water. For the low strains shown in Figures 4-14 and 4-15 one might expect the material response of the dry and moist/partially saturated sand to be the same since only air is being removed from the specimen. It might be possible when compressing moist/partially saturated sand at high strain-rates the interaction between the sand particles, pore air and pore water respond differently than under dry conditions. Interaction between dry sand particles may introduce more resistance due to higher friction between the particles creating higher resistance to the applied compressive load. Thus, the moist/partially saturated sand may experience less friction between the particles due to the pore water in the specimen being concentrated around the interparticale contacts (Craig [30]) providing lubrication between the particles. Additionally, as the pore air is being removed the sand particles and water could either rearrange themselves dramatically, changing the material structure or very little with no change in material structure.

A second possible explanation of the effects of moisture on the dynamic behavior is related to water as acting as a lubricant and thus reducing friction between the specimen and steel platens. If this is the case, then moist/partially saturated sand could be more compressible than dry sand due to greater friction being prevalent between dry sand and the incident bar acting to oppose the applied compressive load. Again, these theories cannot be verified due to the difficulties associated with acquiring measurements inside the sand specimen during a SHPB test. In addition, either of these hypotheses could be valid, or act separately to possibly influence

the material response or both may interact simultaneously. Again, these trends may change if different testing conditions or higher strain-rates are utilized.

4.2.3 Boundary Conditions

Testing sand using a SHPB is increasingly difficult due to fact that confinement needs to be applied to the specimen prior to loading. Thus, the specimen needs to be bounded radially and contained on both ends of the specimen by steel platens. Both types of boundaries on the specimen introduces it own set of problems.

The radial confinement introduces uncertainties associated with side-wall friction, bulging of the confinement tube (in the case of the polycarbonate confinement) and non-uniform radial loading along the length of the specimen. The polycarbonate confinement is more complex since the conditions are neither one-dimensional strain nor one-dimensional stress in the specimen during the loading event. The polycarbonate confinement during loading will produce bulging because the wall stiffness of the confinement is not sufficient to restrict the lateral displacements of the specimen created by the compressive loading. Thus, a non-uniform state of stress is created along the specimen outer diameter and longitudinally along its length. The radial loading along the length of the specimen will be greatest in the middle and taper off to the front and back edges of the specimen. This is clearly shown in Figures 3-17 thru 3-20. The bulging due to polycarbonate confinement permits the specimen diameter to increase allowing the sand structure to rearrange, thus changing the initial structure of the material. The polycarbonate confinement may create an additional problem concerned with drainage in the sample. As the polycarbonate confinement expands it will separate slightly radially from the ends of the specimen and steel platens allowing drainage of sand particles, pore air or pore water possibly changing the material structure of the specimen. Although, this is a possibility, no visual evidence supports that drainage of sand particles and pore water occurs, but the drainage of pore

air can not obviously be accounted for. If steel confinement is applied, the issue of non-uniform state of stress also arises for steel confinement, but the radial loading should be more uniform along the length of the specimen than in the case of the polycarbonate confinement since the steel confinement has an elastic modulus fifty times higher. In addition, since the steel confinement is stiffer than the polycarbonate confinement drainage effects, if any, should be minimal. The non-uniform state of stress in the specimen is further amplified by possible friction at the specimen/incident bar interfaces. The friction created at this interface will prohibit the specimen to deform radially at the ends of the specimen acting to stiffen the response. Typically lubricate is put at the interface of the loading mechanism and the specimen to reduce or eliminate this effect. The use of a porous material prohibits the application of lubrication since this could affect the material properties of the specimen. If friction is present the observed material response will not be the true response of the material since friction will increase the stiffness.

The friction associated with the incident bar/specimen interface is also coupled with side-wall friction that is present between the specimen outer diameter and the inner diameter of the confining tube. This type of friction is often called "side-wall friction" and introduces shear stresses along the entire length of the specimen. The shearing stresses oppose the compressive load being applied by the incident bar possibly giving a stiffer response of the material. The friction associated with this interaction event can neither be explained qualitatively nor quantitatively due to the inability to measure this during the dynamic event. The boundary conditions that are known to exist for these testing conditions is the non-uniform loading applied by the confinement along the length of the specimen and the side-wall friction that creates shear stresses.

4.2.4 Other Effects

Additional problems are concerned with friction between the steel platens and confinement tubes. The oscillations present in the stress-strain curves in Figures 4-1 thru 4-13 at the early percent strain indicates that maybe friction or the interaction between the platens and confinement produced this phenomenon. The steel platens were machined slightly smaller than the inner diameter of the confinement tubes to ensure the platens moved as freely as possible within the confinement. Additionally, the platens were faced flat on each side to ensure they are perpendicular to the center-line of the incident and transmitter bars. Although the platens were to be machined to this criteria does not eliminate the premise that they may not truly be flat or round. If the platens were indeed not flat on both faces then a possibility exists that the steel platen/sand specimen interface was not perpendicular to the incident bar center-line. The stress-strain curves indicate the oscillations are less amplified for the polycarbonate confinement than steel confinement. This could be sand draining around the steel platen in the polycarbonate confinement allowing sand particles to wedge between the steel platens and confinement. If the oscillations shown in Figures 4-1 thru 4-6 are a product of this phenomenon these oscillations would probably occur throughout the entire stress-strain curve or may produce more inconsistency in the stress-strain response. To ensure alignment between the steel platens and specimen pressure was applied using the incident/transmitter bars. This ensured the correct specimen length was acquired in conjunction with introducing some crude compaction to the specimen. This misalignment of the steel platens on the front and back faces of the specimen will create uneven loading across the specimen cross-section when loaded. It could cause the steel platens to realign with the bars possibly causing the oscillatory motion shown in the figures. When the platen is aligned then the oscillations would dissipate. This theory does not seem sound due to the consistency of the amplitudes and locations of the oscillations.

The confinements both have coefficient of frictions associated to them with steel being higher. The interaction between the sand and the confinements may introduce the oscillations shown in the before mentioned figures. The friction would inherently be greater between the sand particles and steel rather than the polycarbonate. Using the pulse shaping technique the load is gradually applied to the specimen with a ramp loading. Initially the load is low with the friction between the sand particles and the confinement being the greatest, but as the load gradual increases the static friction is overcome between the sand particles and confinement with the dynamic friction being lower. This would explain effectively why the oscillations are less amplified with the polycarbonate confinement rather than the steel confinement. Although any of these mentioned theories could prevail it is increasingly difficult to qualitatively or quantitatively verify any of these theories using the SHPB. The oscillations could be a culmination of several of these theories, but again this is not supportable.

4.2.5 Uniaxial Strain Tests

The dynamic testing of soils has been investigated minimally in the last four decades with various test equipment including the split-Hopkinson pressure bar, shock tubes, dynamic drop tests and flyer plate impacts being utilized. Although the focus of this study is limited to dynamic events only the trends from quasi-static to dynamic should remain the same while quantitatively the results will probably be different. To validate the results of this study well controlled experiments need to be conducted. Uniaxial strain tests have proven to be well controlled experiments with well defined boundary conditions. The testing conditions for a SHPB test is typically one-dimensional stress, but with the steel confinement utilized for this study these experiments will approximate a one-dimensional strain, although all boundary conditions are not fully defined.

A general uniaxial strain test loads the specimen in the axial direction and constrains the specimen in the lateral direction with the radial loading recorded. The specimen is assembled as shown in Figures 4-20 and 4-21. The specimen has three membranes placed around the specimen with the outer membrane coated with liquid synthetic rubber to prohibit deterioration from the confining fluid (Williams et al. [31]). The specimen is mounted with a Linear Variable Differential Transformer (LVDT) (Figure 4-21) to measure vertical movement or in the case of a uniaxial test the axial strain. A lateral deformeter is mounted at the specimen mid height to measure radial displacement. The lateral deformator has a LVDT mounted to a hinged ring so when the specimen is displaced radially the ring opens. The specimen is placed in a pressure vessel where a confining fluid is put into the pressure vessel to supply confinement and the axial loading is induced by a servo controlled loader. Additional information on the execution and instrumentation used for the uniaxial strain tests is given in Williams et al. [31].

The material evaluated in this study was used by Akers et al. [12], from the U.S. Army Engineering Research and Development Center (ERDC), to perform uniaxial strain tests at a dry condition and a moist/partially saturated condition. The specimens were 50 mm (2.0 inch) in diameter and 110 mm (4.33 inch) in length having an aspect ratio ~ 2 compared to an aspect ratio ~ 0.49 for the specimens in this study. The ERDC specimens had a dry density of 1.657 g/cc for the dry tests and 1.645 g/cc for the moist/partially saturated sand. The dry sand had a posttest moisture content of 0.5% for tests SD09 and SD09 with the moist/ partially saturated sand having a posttest moisture content of 7.3% and 7.7% for tests SW09 and SW11, respectively. Although the dry density is higher than the dry density used in this study a qualitative verification of trends is appropriate. The strain-rates accomplished with the uniaxial strain tests from Akers et al. [12] are approximately $10^{-4}s^{-1}$ to $10^{-5}\,s^{-1}$. The uniaxial stress-strain response of

dry and moist/partially saturated sand is shown in Figure 4-22. This figure clearly indicates that the moist/partially saturated sand is more compressible (less stiff) than the dry sand. In addition, test SW09 appears to be more compressible than SW11 supporting the fact that a lower moisture content was used as documented above. The loading of water or often called "lock-up" of the stress-strain curves presented in Figure 4-22 can be determined utilizing the stress paths in Figure 4-23. The stress paths for dry and moist/partially saturated sand are the same until a mean normal stress of approximately 238 MPa (~34.5 ksi) and 213 MPa (30.8 ksi) for tests SW09 and SW11, respectively, is reached and the water is loaded. The response following these values of mean normal stress have a slight slope and should approximate a Poisson's ratio of approximately 0.49, which is nearly incompressible, indicating that the water is supporting all the load. When the lock-up mean normal stress (MNS) and principal stress difference (PSD) are determined the corresponding axial stress can be obtained. The principal stress difference is known as,

$$\sigma_a - \sigma_r = PSD \tag{4-1}$$

where σ_a is the axial stress and σ_r is the radial stress. Accordingly the mean normal stress is known as,

$$\frac{\sigma_a + 2\sigma_r}{3} = MNS \tag{4-2}$$

Using the equations (4-1) and (4-2) there are two unknowns and so the corresponding axial stress can be determined. The calculated axial stress is then used with Figure 4-22 to locate the lock-up strain. The lock-up strains for tests SW09 and SW11 are 27% and 26%, respectively. The data presented in this study only acquired stress equilibrium and constant strain-rate simultaneously to approximately 9% strain. The comparison of trends between the data in this study and data obtained by Akers et al. [12] is only compared for stress and strain values up to 9% strain. A

verification is conducted to determine whether the MNS associated with 9% strain is within the region in Figure 4-23 where the stress paths are the same. The MNS can be obtained using Figure 4-24 where MNS is a function of volumetric strain. The uniaxial strain test is one-dimensional in strain, so all strain measured in the experiment is axial strain and is the same as volumetric strain. The average MNS from Figure 4-24 for 9% strain for dry and moist/partially saturated sand is 27.7 MPa (~4.0 ksi) and 21.5 MPa (~3.1 ksi), respectively. The PSD associated with each average MNS is well within the regime where the stress paths for dry and moist/partially saturated sand are the same. This validates that the trends found in this study and data obtained by Akers et al. [12] is the same qualitatively. The difference, quantitatively, between dry and moist/partially saturated sand for Akers et al. [12] data is approximately 6.2 MPa (~900 psi), which is smaller than the difference associated with the same moisture content for this study for steel confinement. However, this difference could be due to boundary effects as discussed earlier in this chapter.

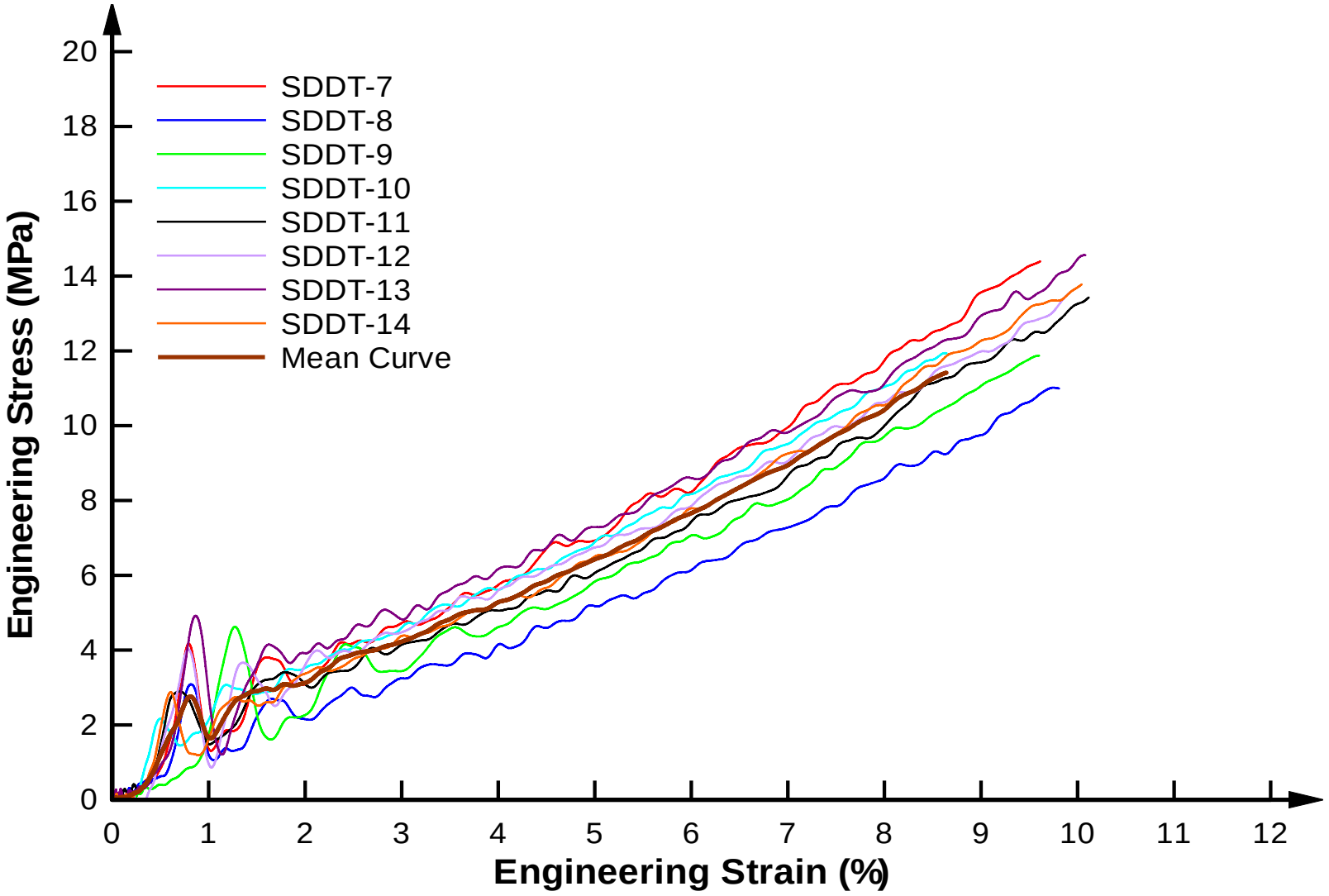

Figure 4-1. Stress-strain curve for 3% moisture content and polycarbonate confinement.

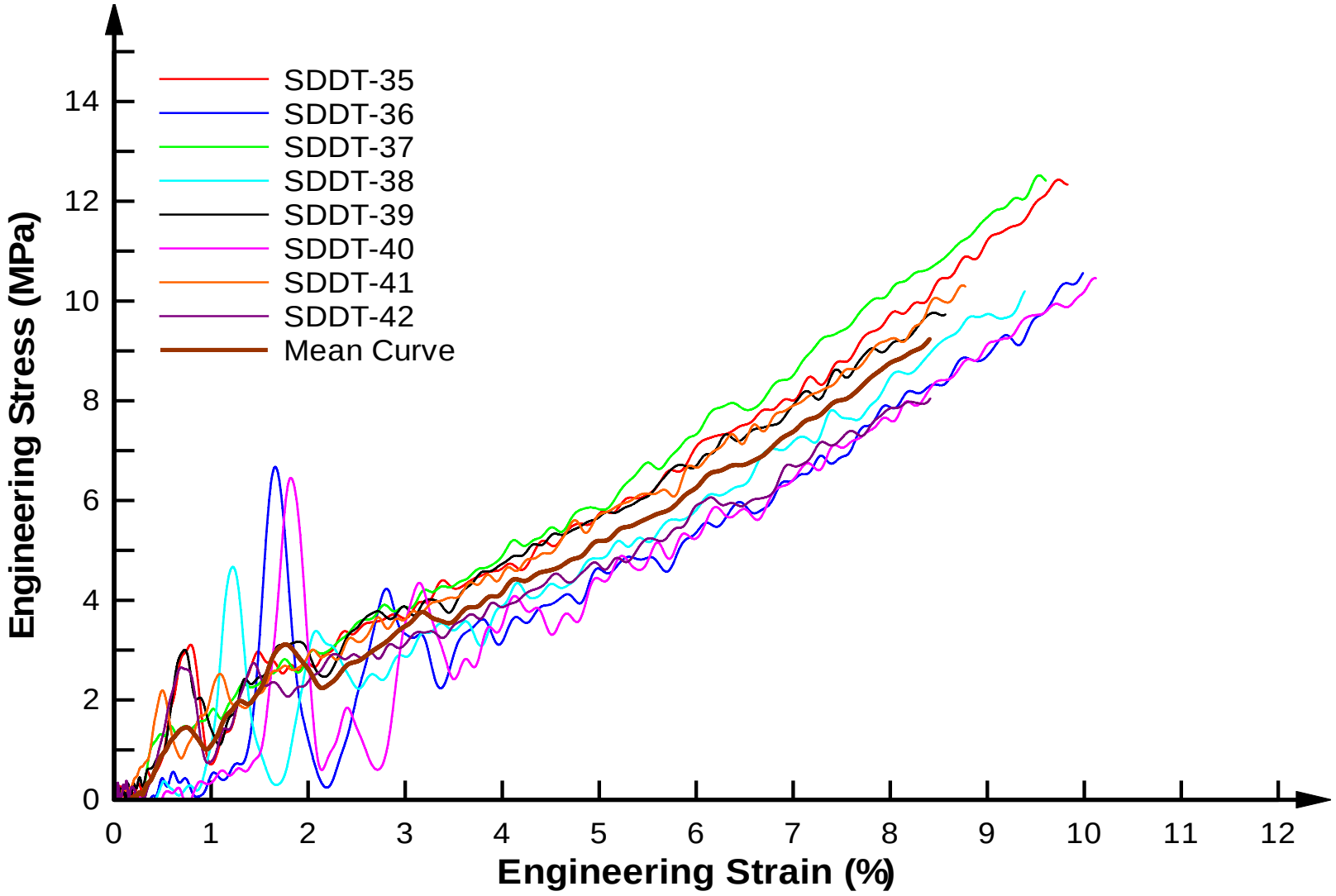

Figure 4-2. Stress-strain curve for 4% moisture content and polycarbonate confinement.

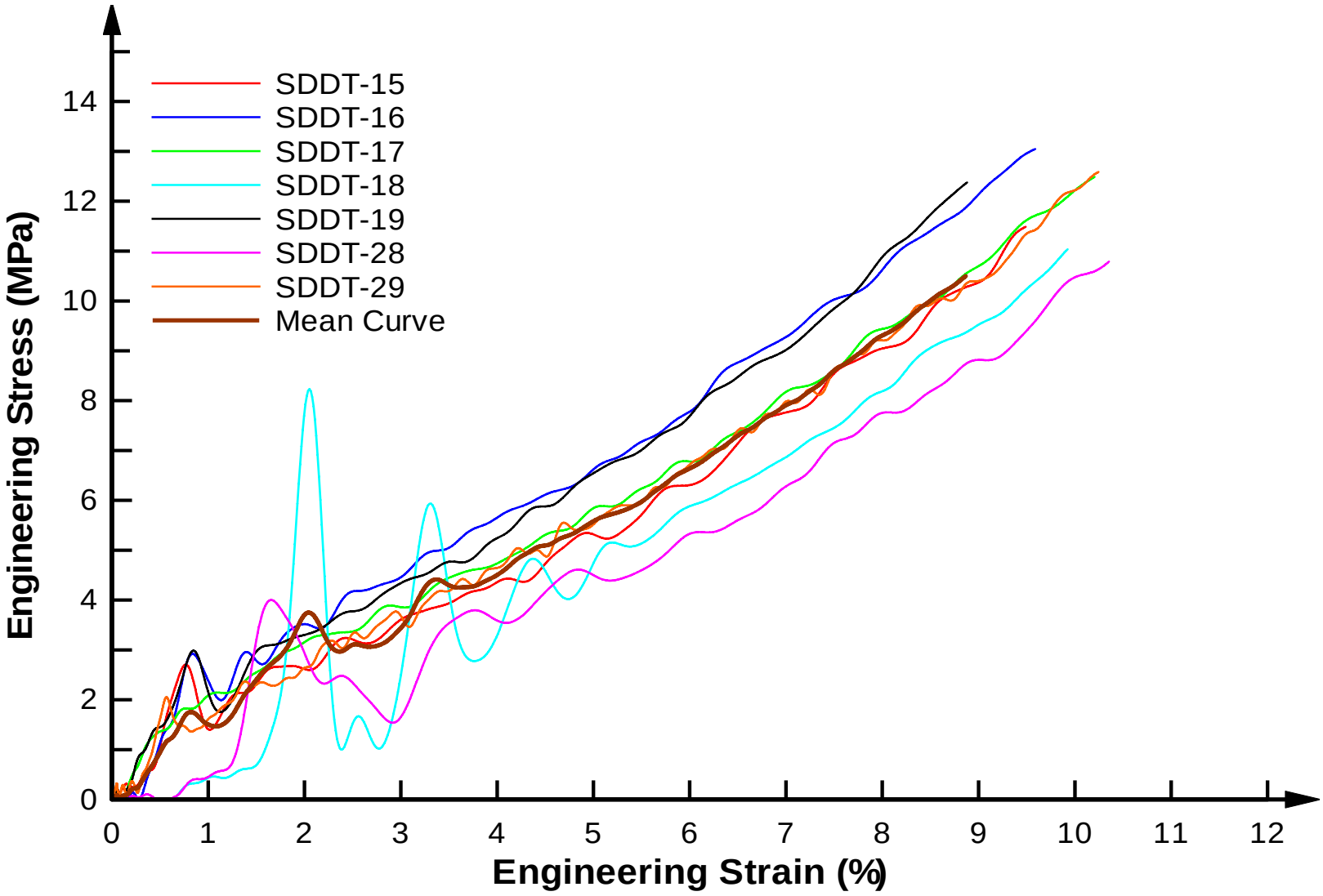

Figure 4-3. Stress-strain curve for 5% moisture content and polycarbonate confinement.

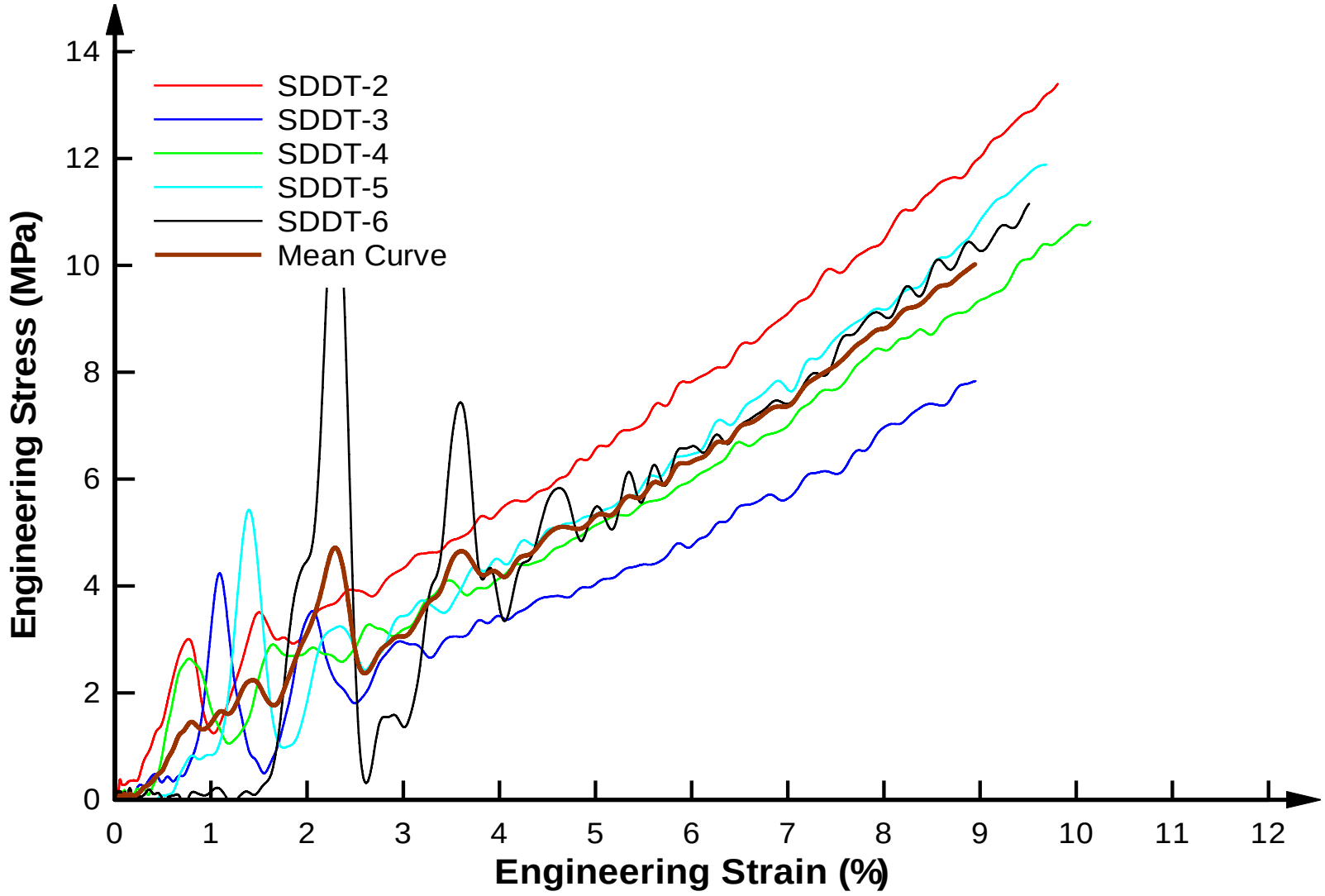

Figure 4-4. Stress-strain curve for 7% moisture content and polycarbonate confinement.

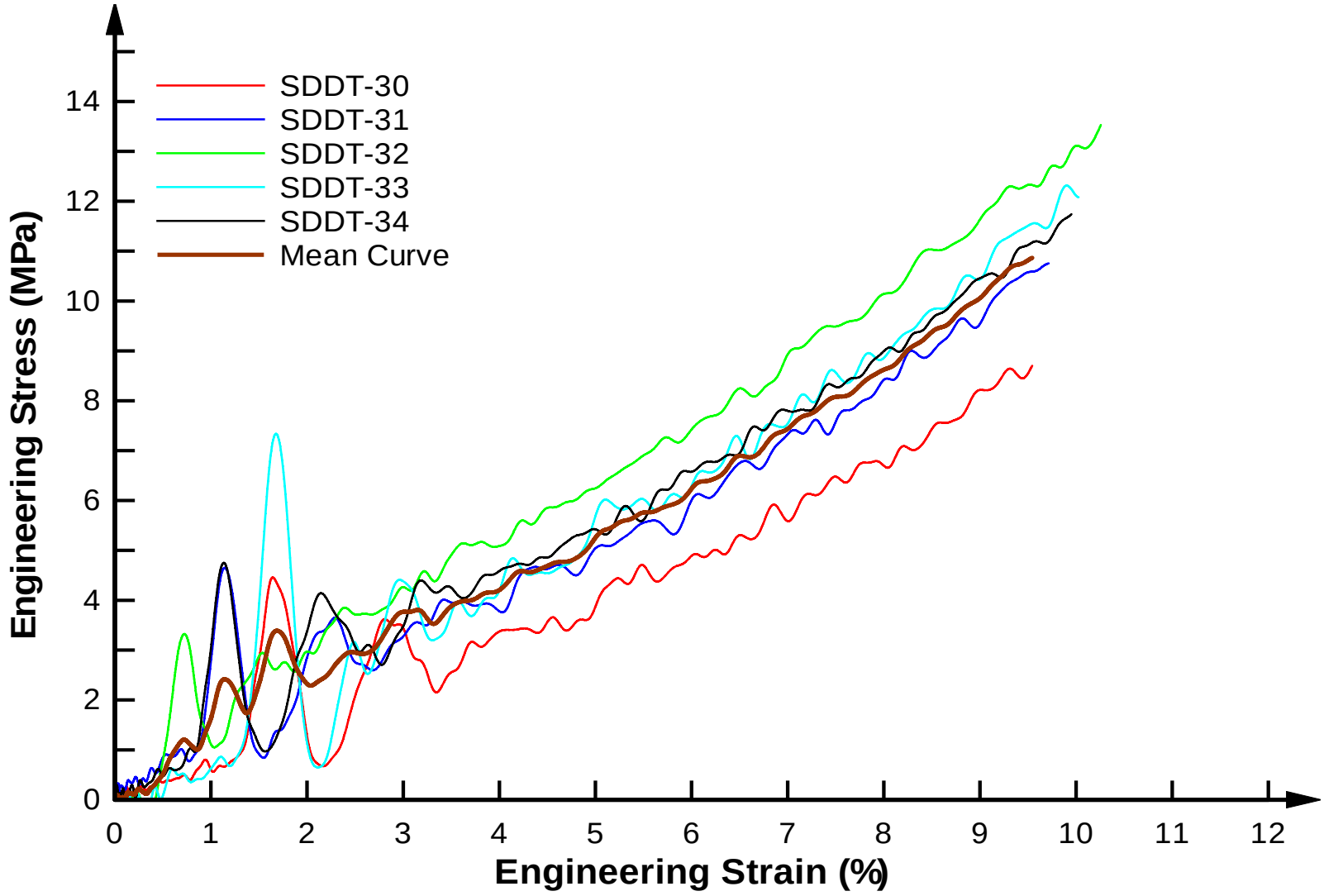

Figure 4-5. Stress-strain curve for 9% moisture content and polycarbonate confinement.

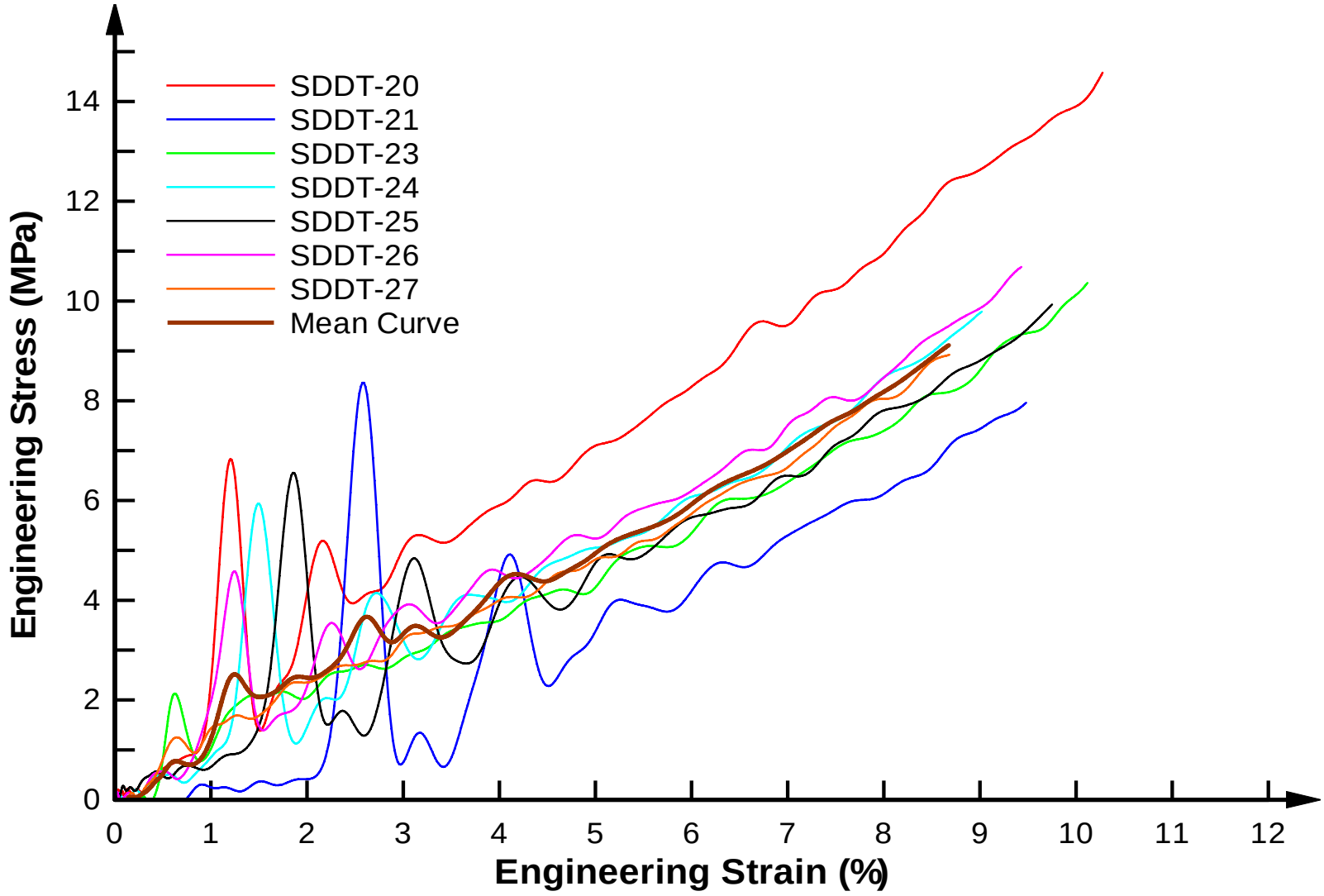

Figure 4-6. Stress-strain curve for 11% moisture content and polycarbonate confinement.

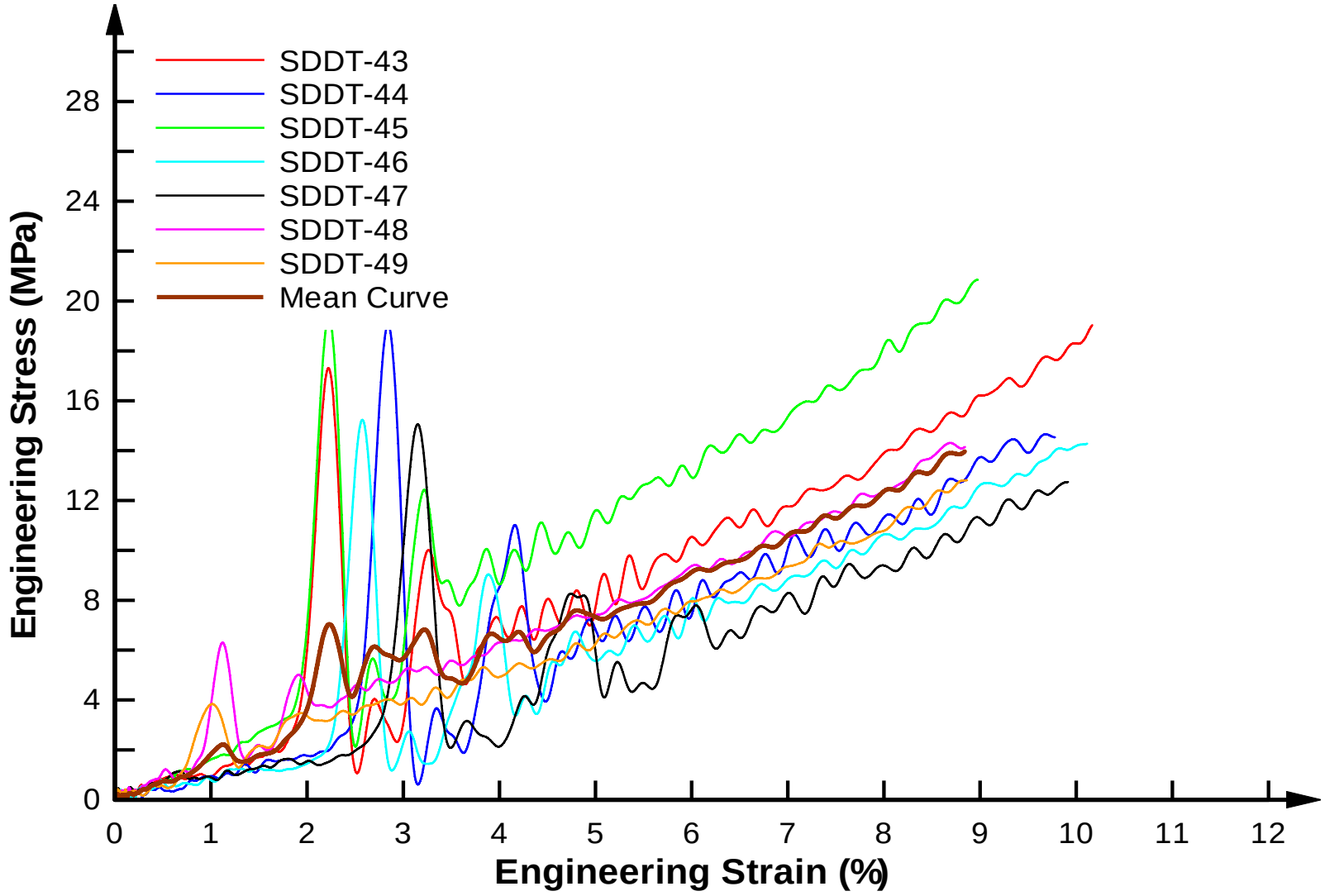

Figure 4-7. Stress-strain curve for 3% moisture content and steel confinement.

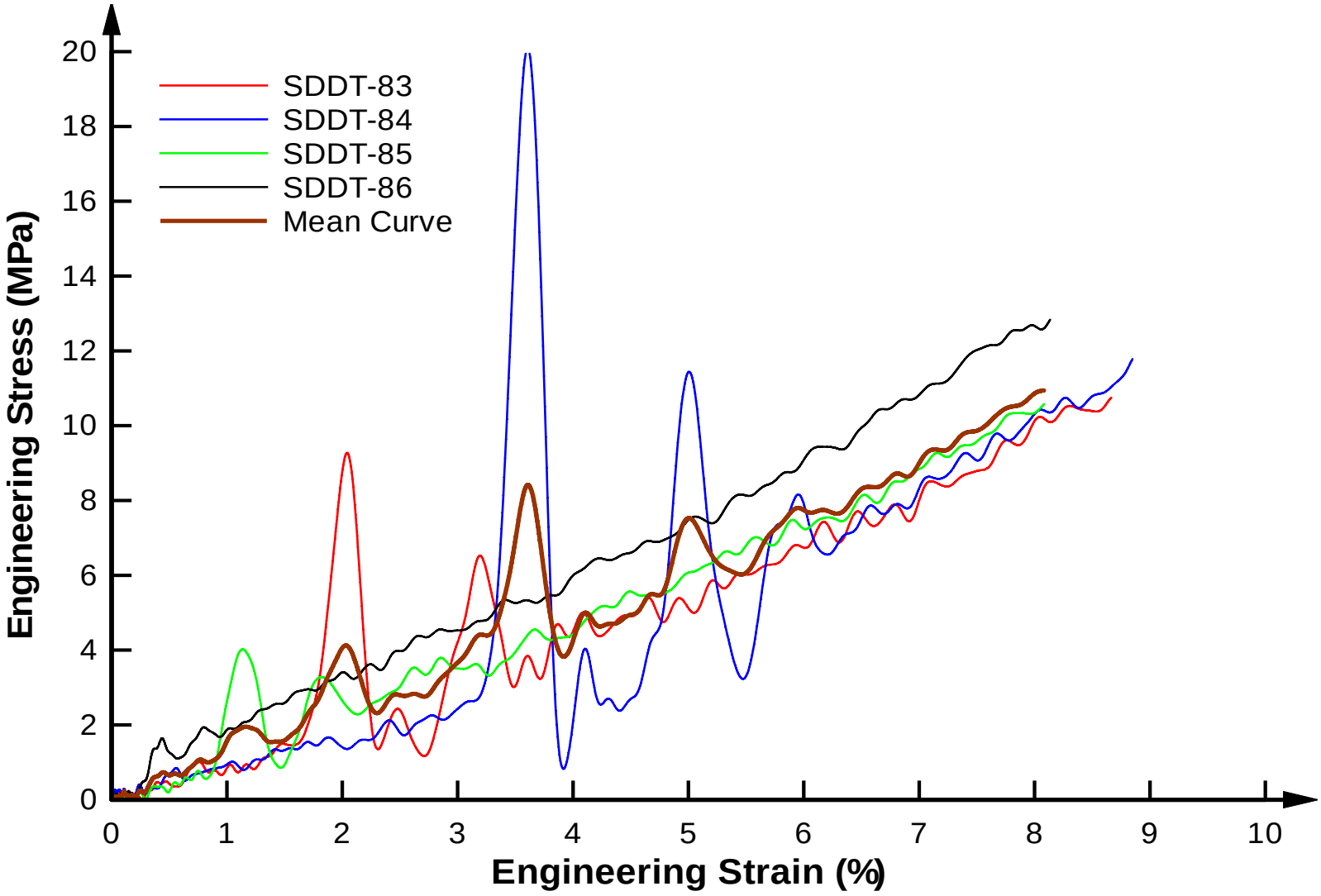

Figure 4-8. Stress-strain curve for 5% moisture content and steel confinement.

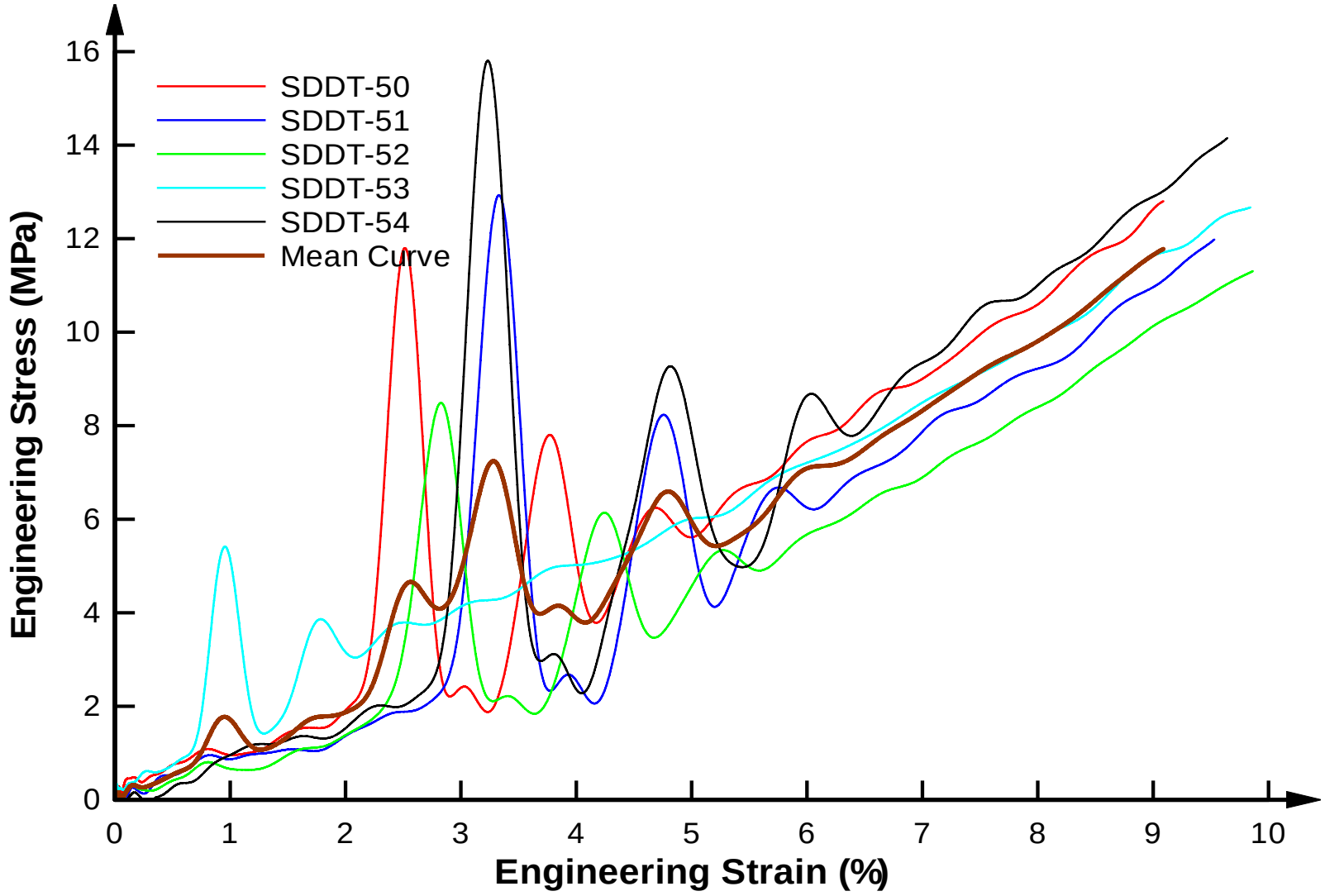

Figure 4-9. Stress-strain curve for 7% moisture content and steel confinement.

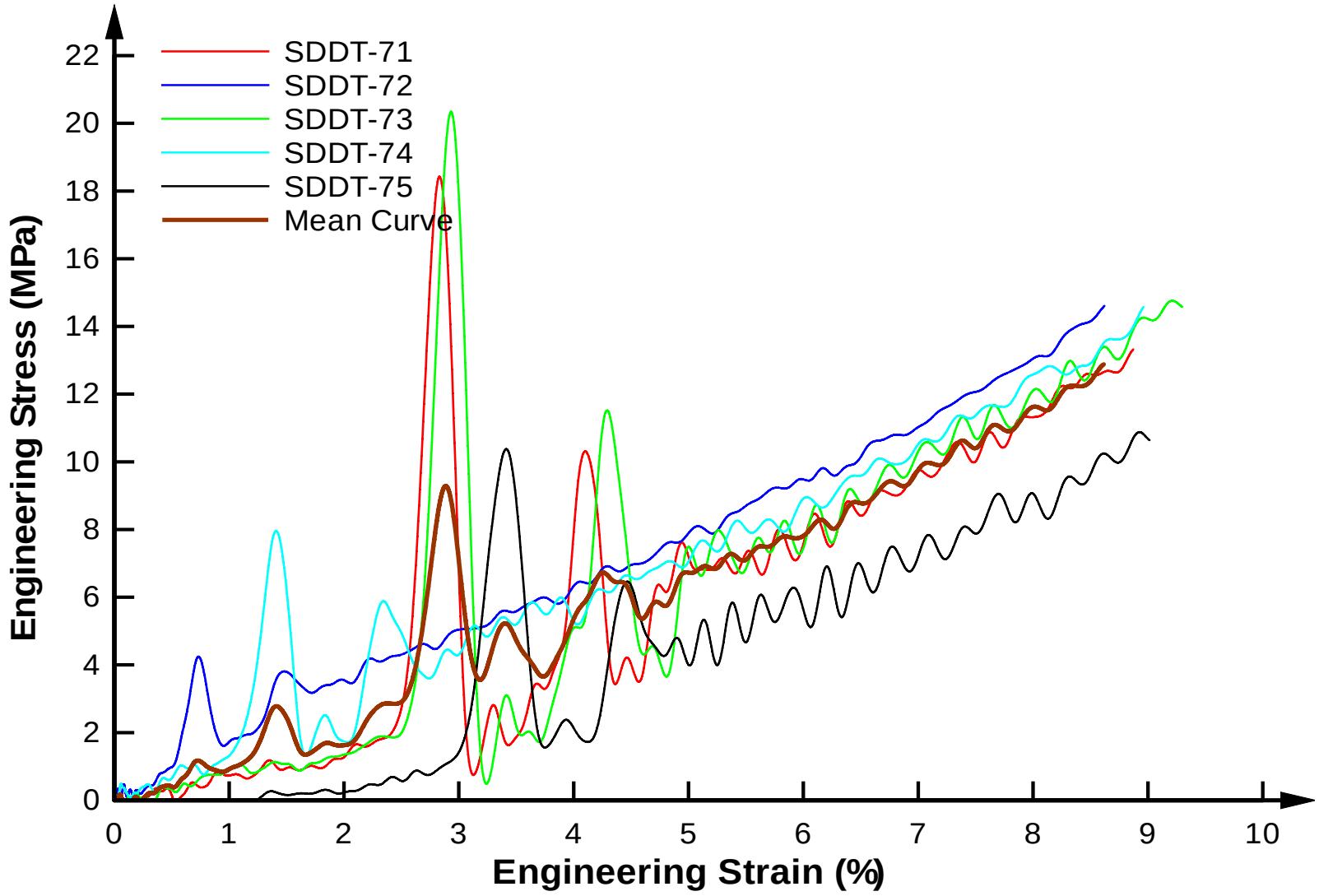

Figure 4-10. Stress-strain curve for 9% moisture content and steel confinement.

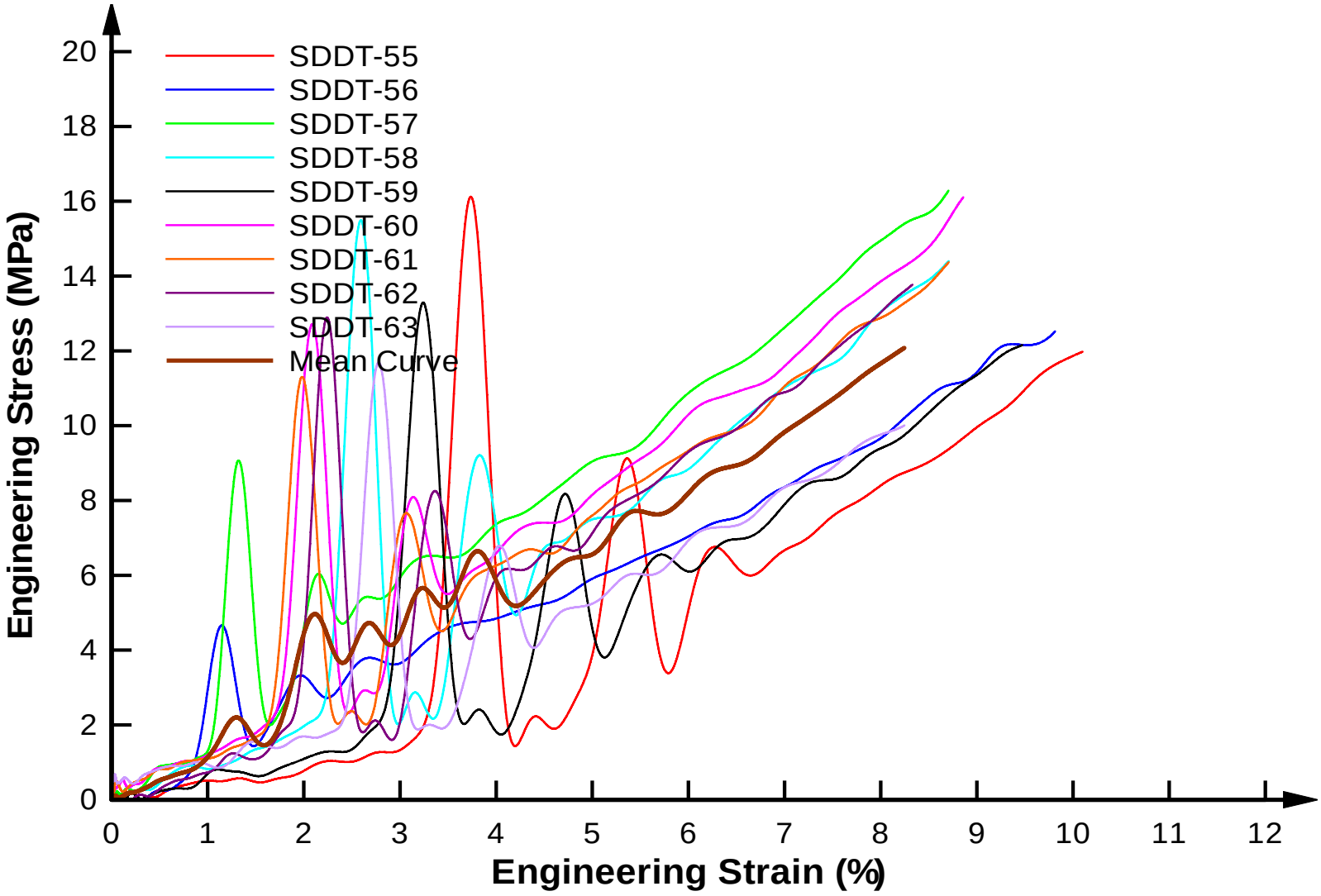

Figure 4-11. Stress-strain curve for 11% moisture content and steel confinement.

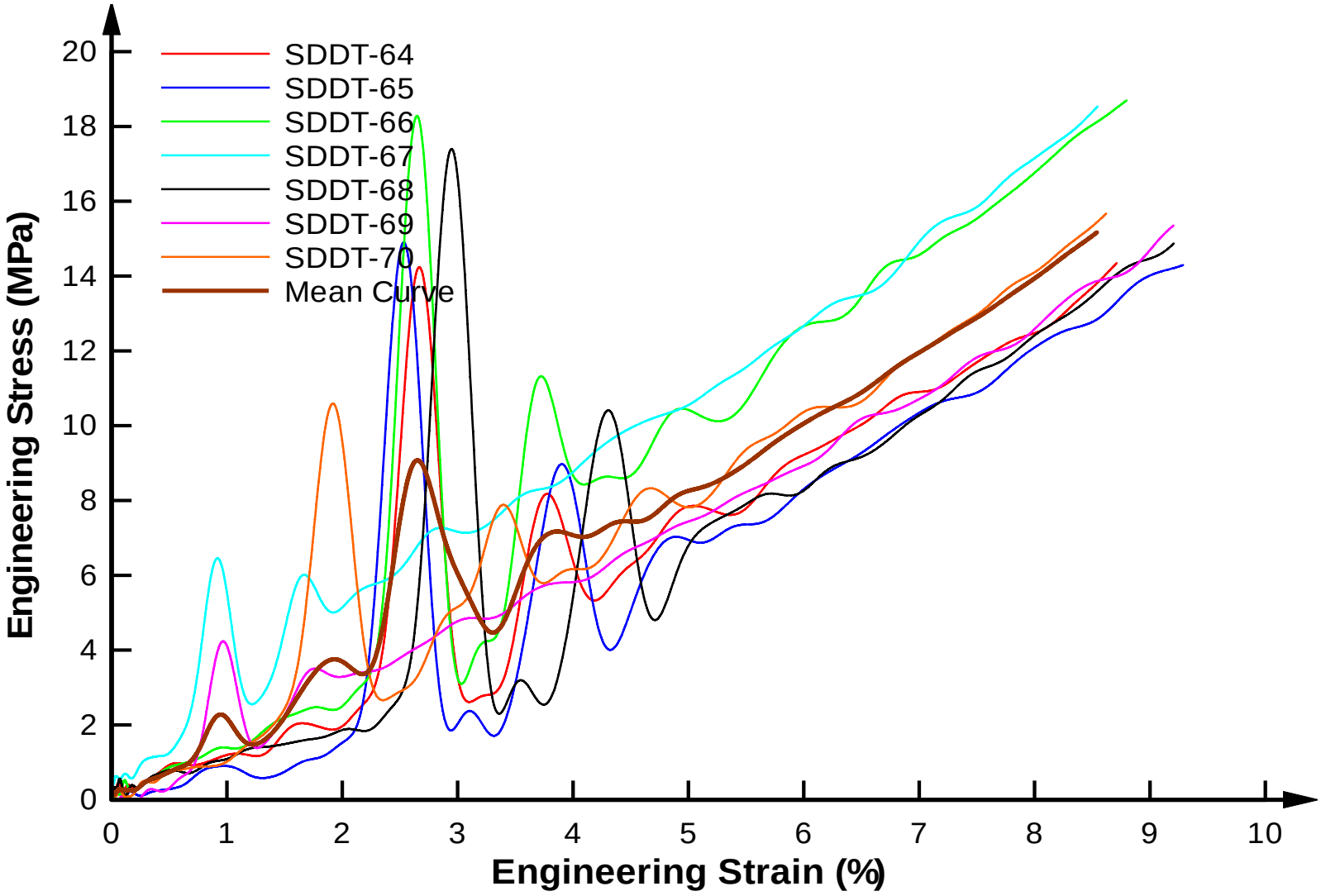

Figure 4-12. Stress-strain curve for 13% moisture content and steel confinement.

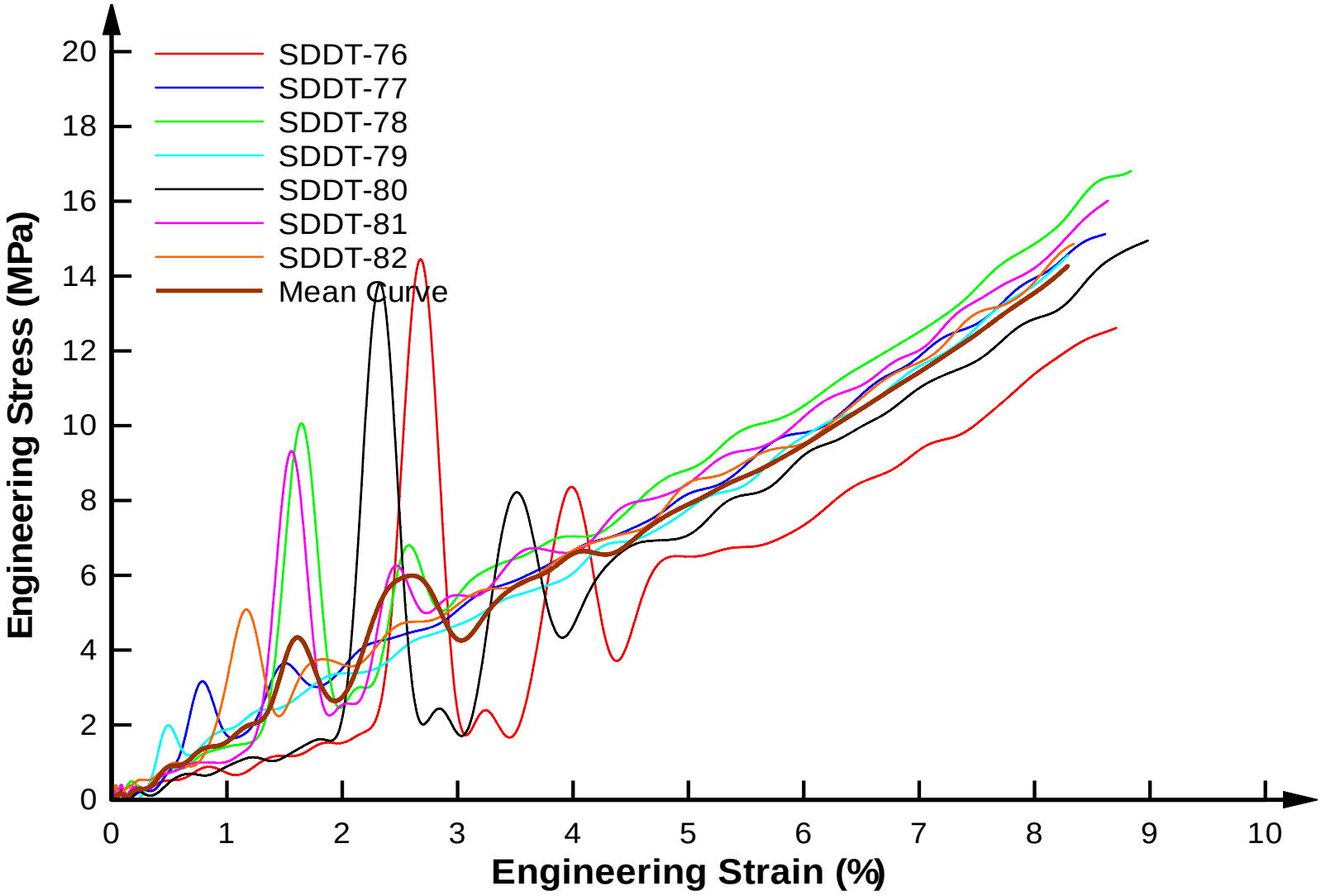

Figure 4-13. Stress-strain curve for 20% moisture content and steel confinement.

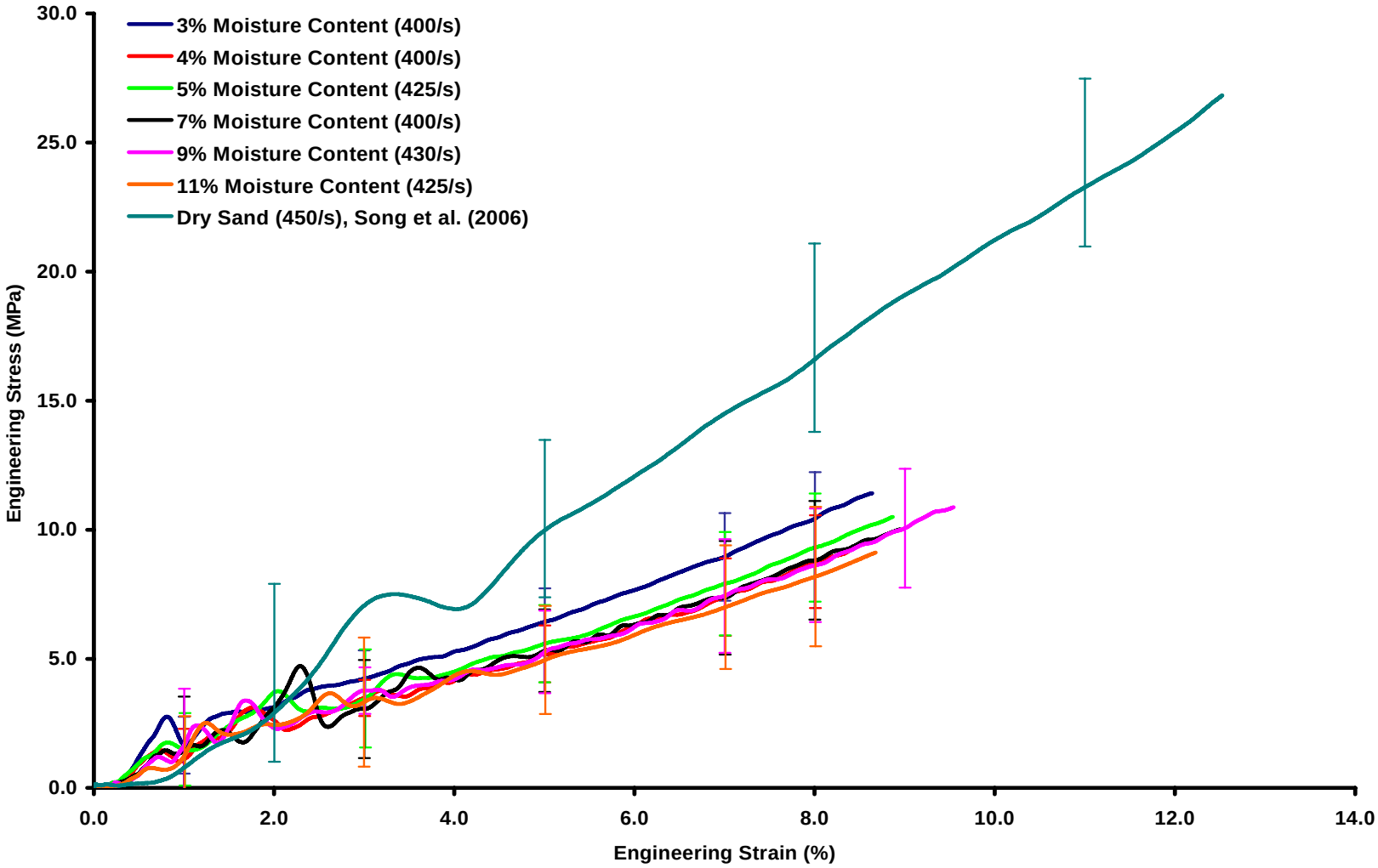

Figure 4-14. Mean stress-strain curves for Quikrete #1961 sand with polycarbonate confinement. [Dry sand data from Song, B., and Chen, W., 2006, "Dynamic Compressive Behavior of Sands," Unpublished technical report, School of Aeronautics and Astronautics and School of Materials Engineering, Purdue University. (Figure 15)]

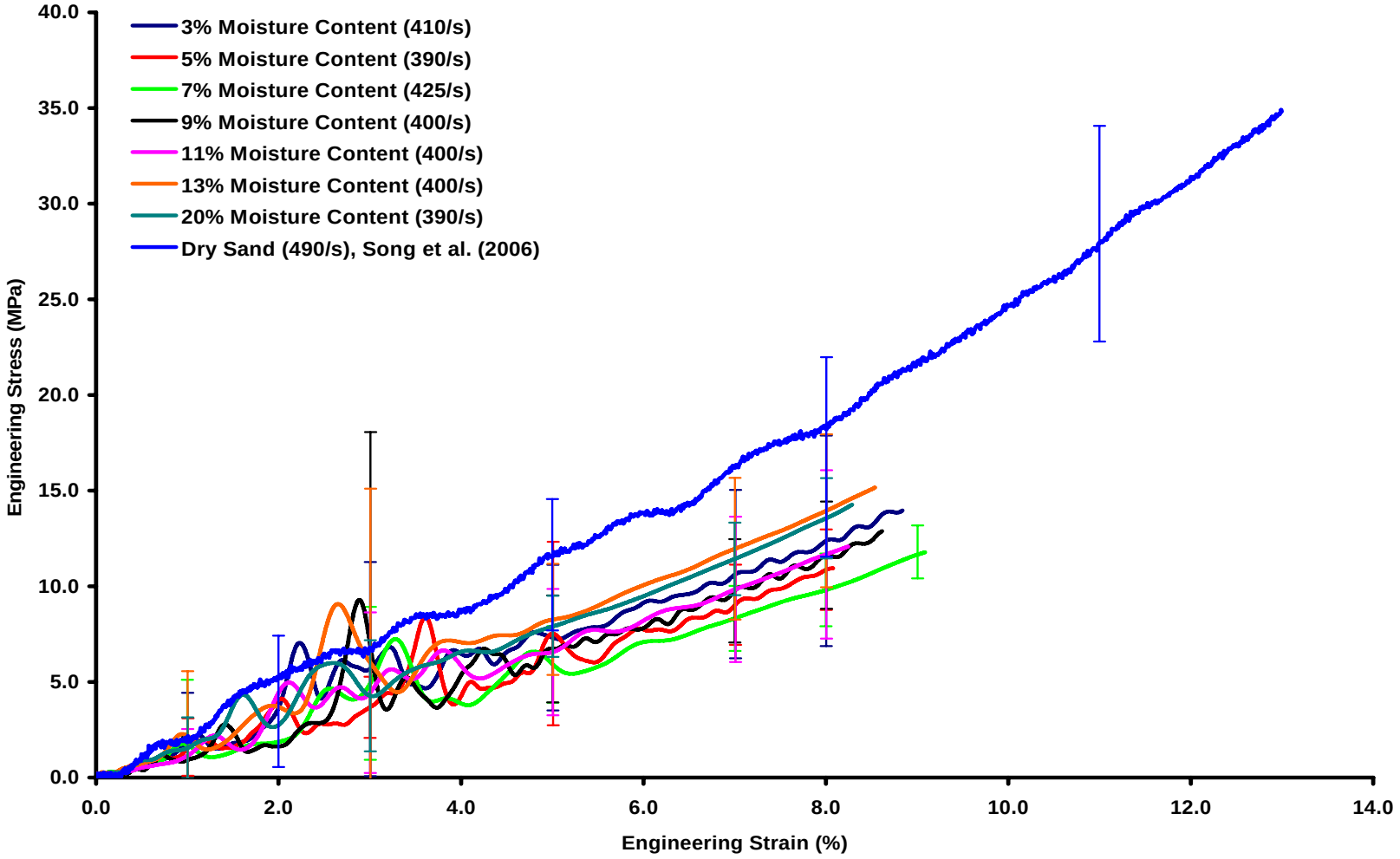

Figure 4-15. Mean stress-strain curves for Quikrete #1961 sand with steel confinement. [Dry sand data from Song, B., and Chen, W., 2006, "Dynamic Compressive Behavior of Sands," Unpublished technical report, School of Aeronautics and Astronautics and School of Materials Engineering, Purdue University. (Figure 25)]

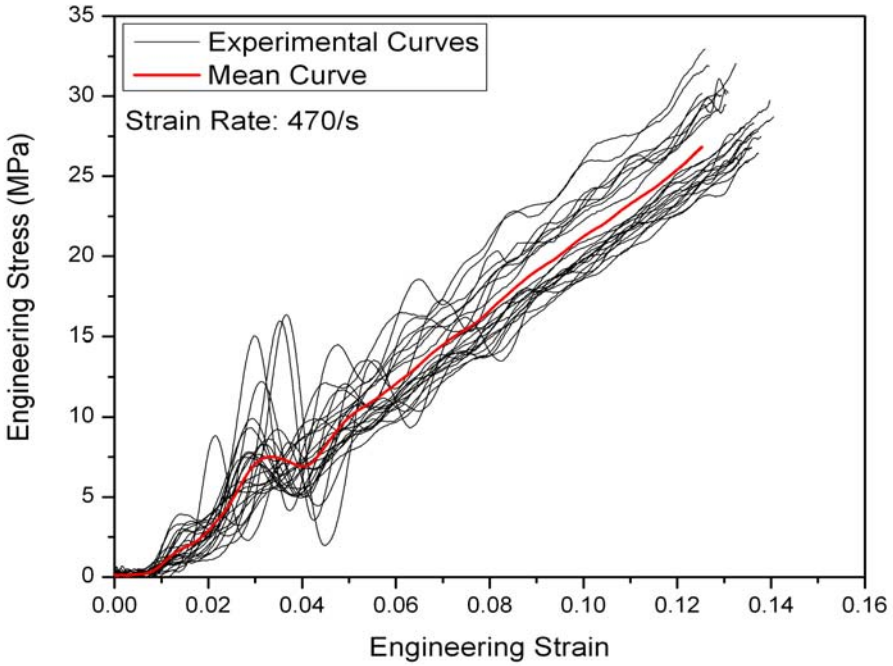

Figure 4-16. Stress-strain curves for Quikrete #1961 dry sand with polycarbonate confinement. [Reprinted from Song, B., and Chen, W., 2006, "Dynamic Compressive Behavior of Sands," Unpublished technical report, School of Aeronautics and Astronautics and School of Materials Engineering, Purdue University. (Figure 15)]

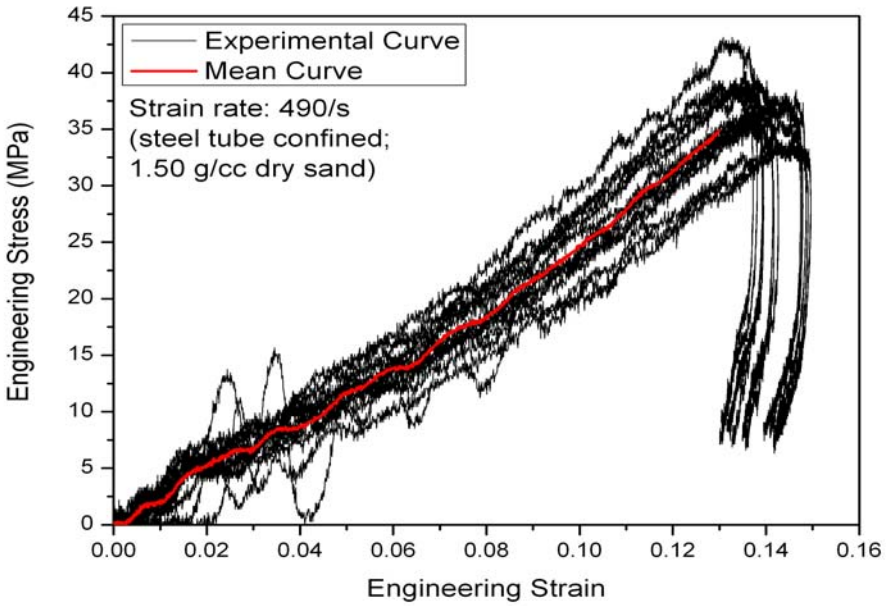

Figure 4-17. Stress-strain curves for Quikrete #1961 dry sand with steel confinement. [Reprinted from Song, B., and Chen, W., 2006, "Dynamic Compressive Behavior of Sands," Unpublished technical report, School of Aeronautics and Astronautics and School of Materials Engineering, Purdue University. (Figure 25)]

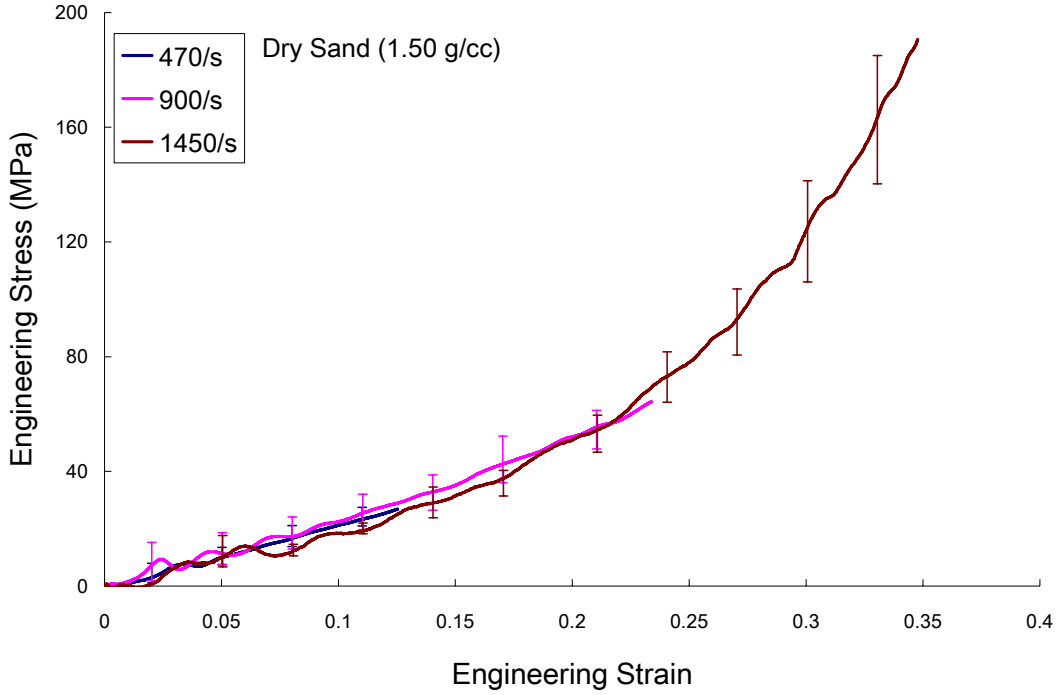

Figure 4-18. Stress-strain curves for Quikrete #1961 dry sand with polycarbonate confinement at various strain-rates. [Reprinted from Song, B., and Chen, W., 2006, "Dynamic Compressive Behavior of Sands," Unpublished technical report, School of Aeronautics and Astronautics and School of Materials Engineering, Purdue University. (Figure 19)]

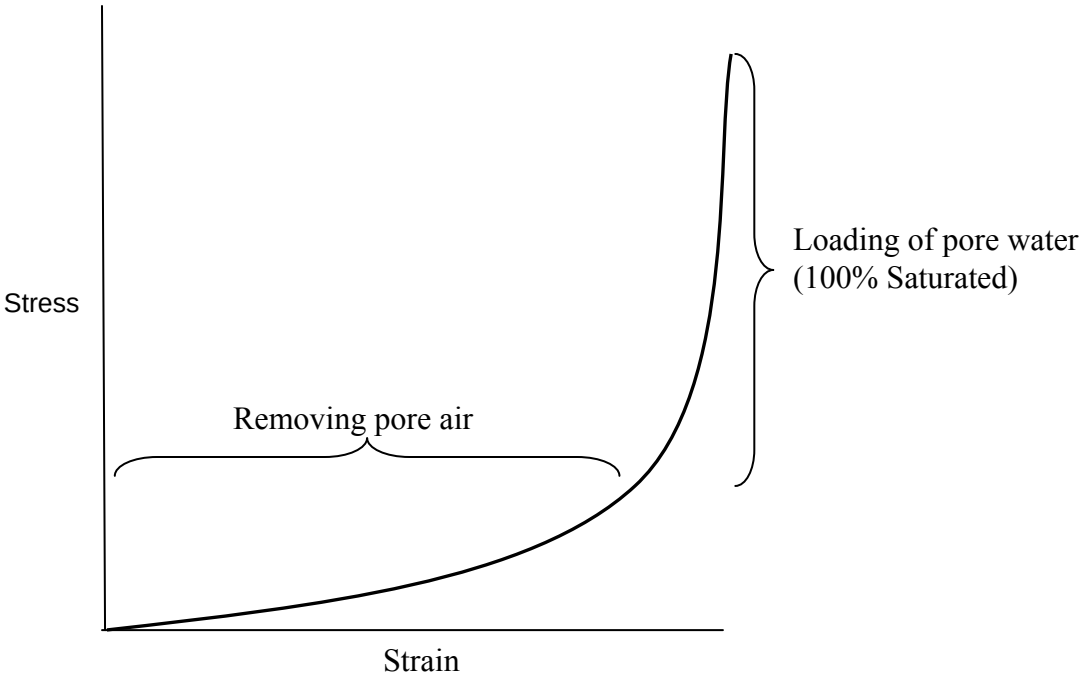

Figure 4-19. Loading phases of moist/partially saturated sand.

Table 4-1. Percent Volume of air for a given moisture content.

% Moisture	Wet Density	% Saturation	% Vol. of Air
3%	1.55 g/cc	11%	38.5
4%	1.56 g/cc	14%	37.0
5%	1.58 g/cc	18%	35.5
7%	1.61g/cc	25%	32.5
9%	1.64 g/cc	32%	29.5
11%	1.67 g/cc	39%	26.4
13%	1.70 g/cc	46%	23.4
20%	1.80 g/cc	70%	13.0

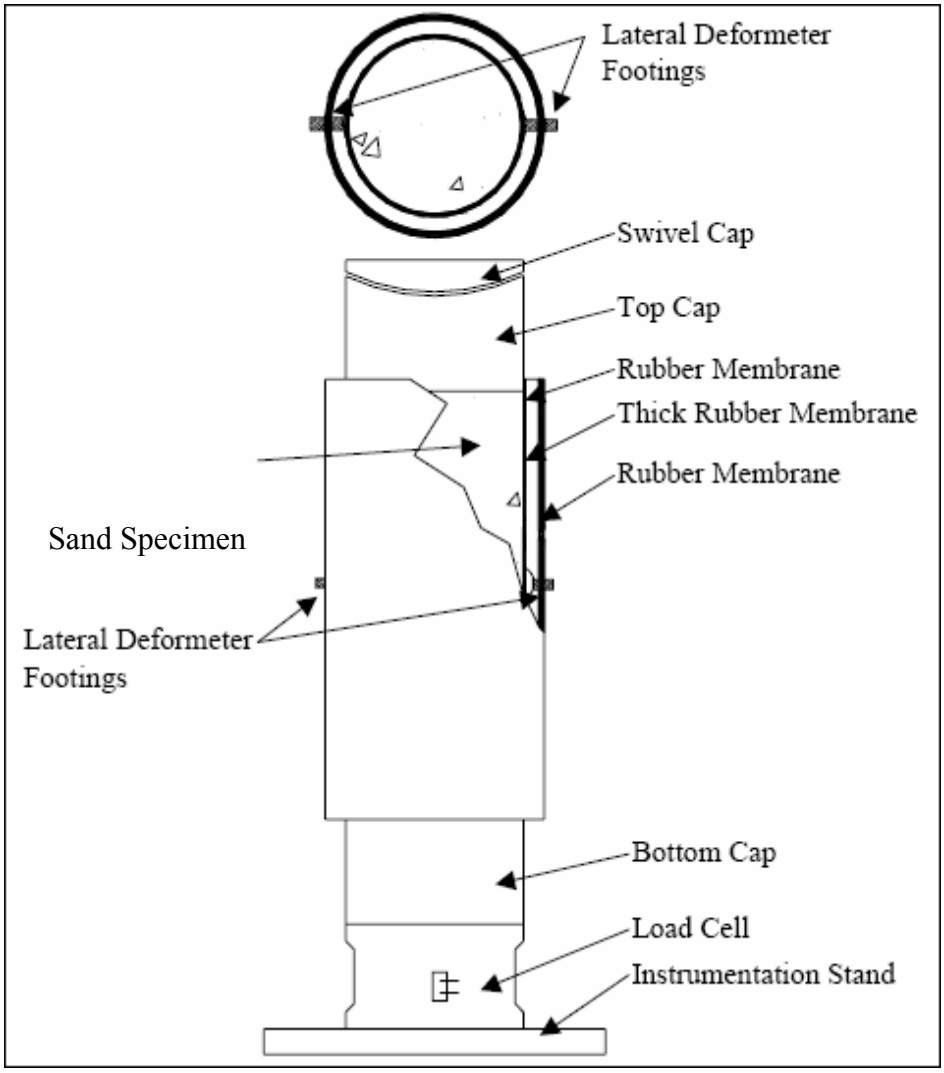

Figure 4-20. Uniaxial strain specimen assembly. [Reprinted from Williams, E.M., Akers, S.A., and Reed, P.A., 2006, "Laboratory Characterization of SAM-35 Concrete," ERDC/GSL TR-06-15, U.S. Army Engineering Research and Development Center, Geotechnical and Structures Laboratory, Vicksburg, MS. (Figure 1)]

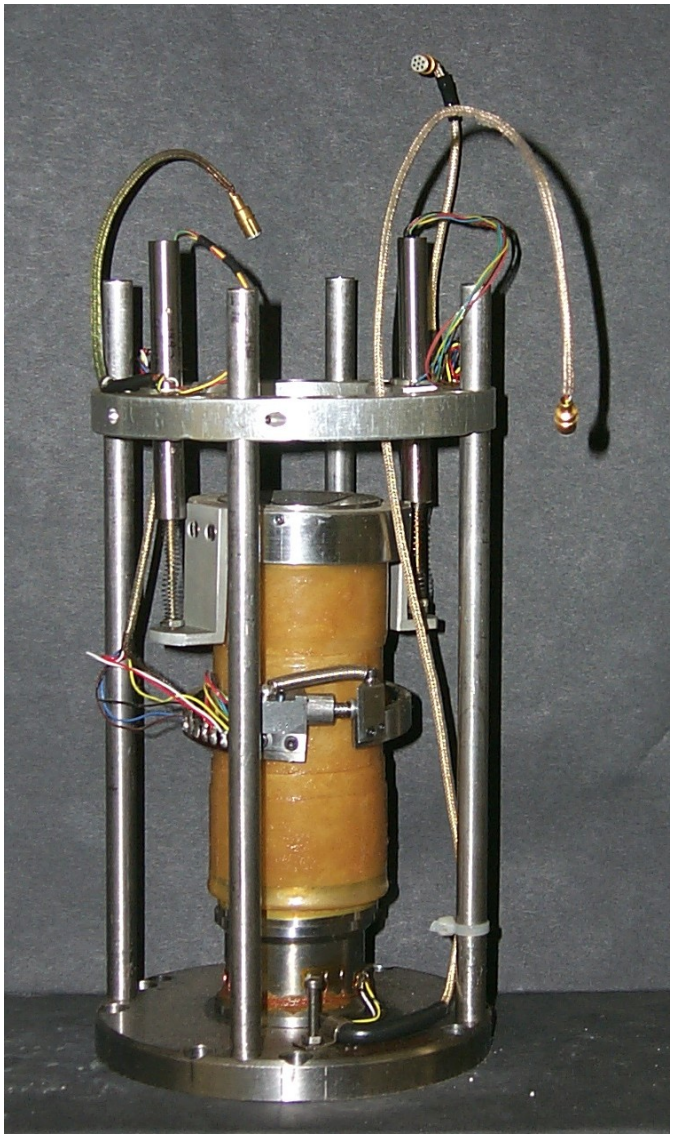

Figure 4-21. Uniaxial strain specimen assembly with instrumentation.

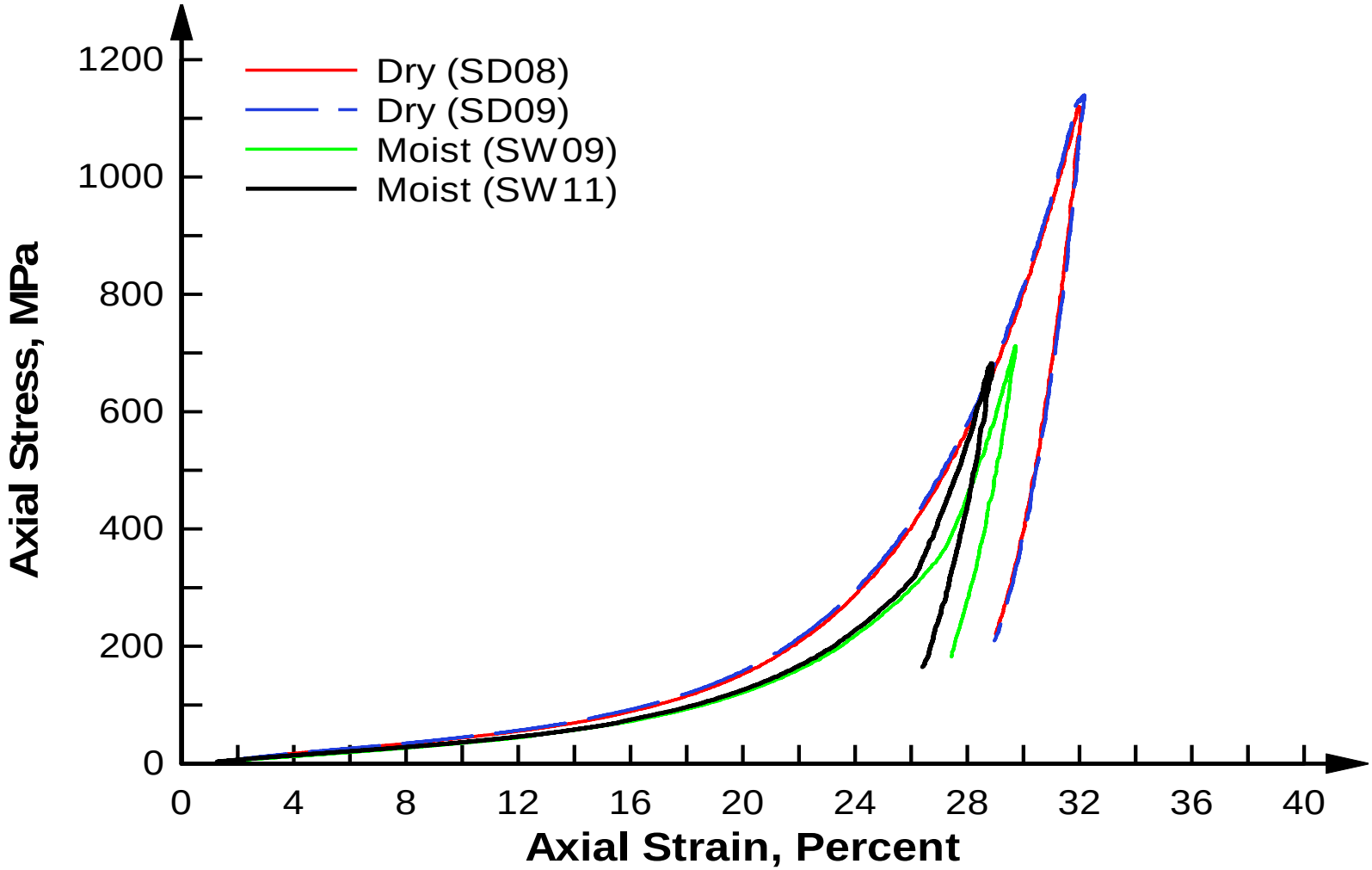

Figure 4-22. Uniaxial strain response for Quikrete #1961 sand. [Data from Akers, S.A., Williams, E.M., and Reed, P.A., 2007, "Quasi-static Characterization of Fine Sand," Unpublished technical report, U.S. Army Engineering Research and Development Center, Geotechnical and Structures Laboratory, Vicksburg, MS.]

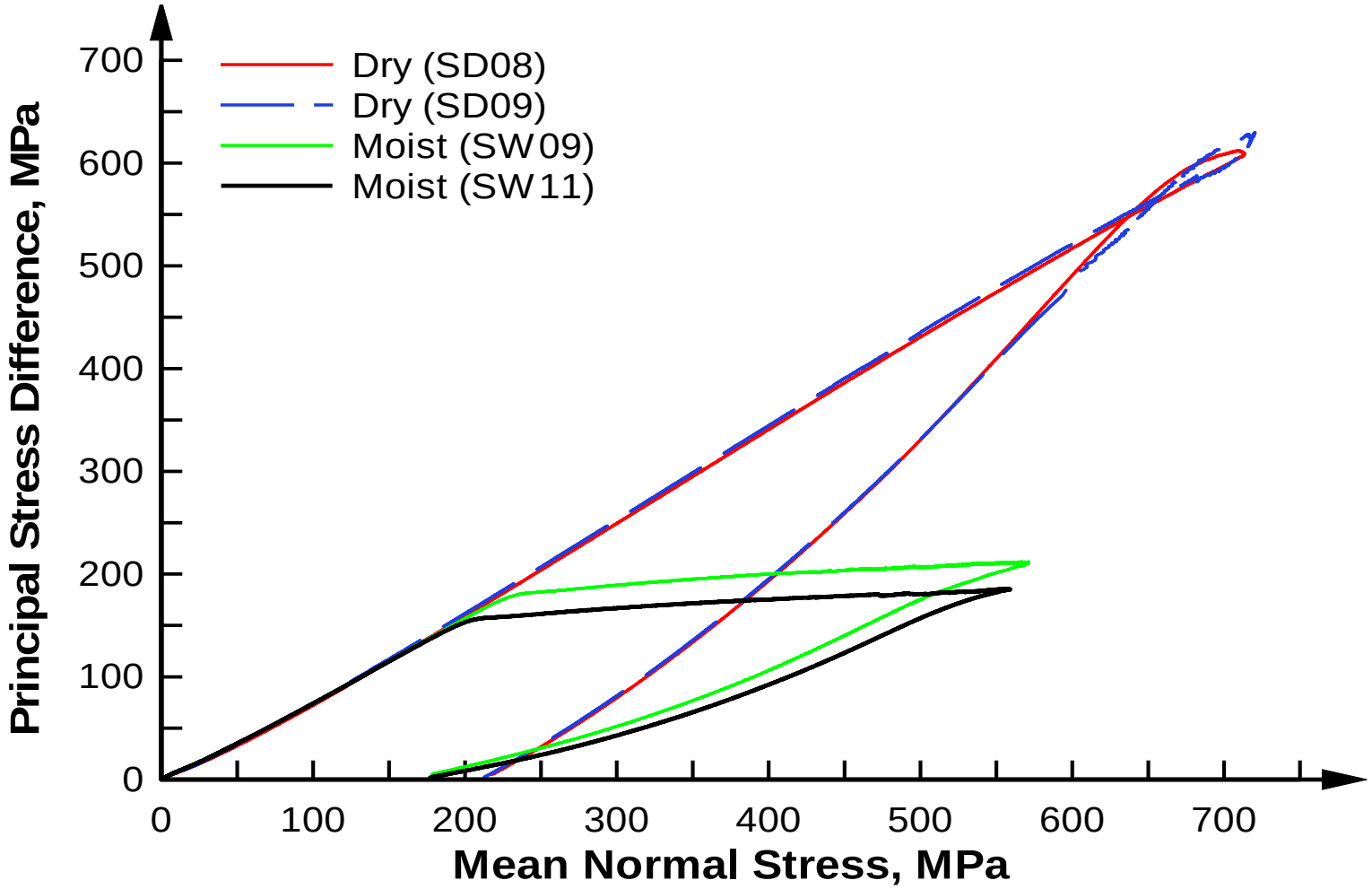

Figure 4-23. Stress paths for the uniaxial strain response of Quikrete #1961 sand. [Data from Akers, S.A., Williams, E.M., and Reed, P.A., 2007, "Quasi-static Characterization of Fine Sand," Unpublished technical report, U.S. Army Engineering Research and Development Center, Geotechnical and Structures Laboratory, Vicksburg, MS.]

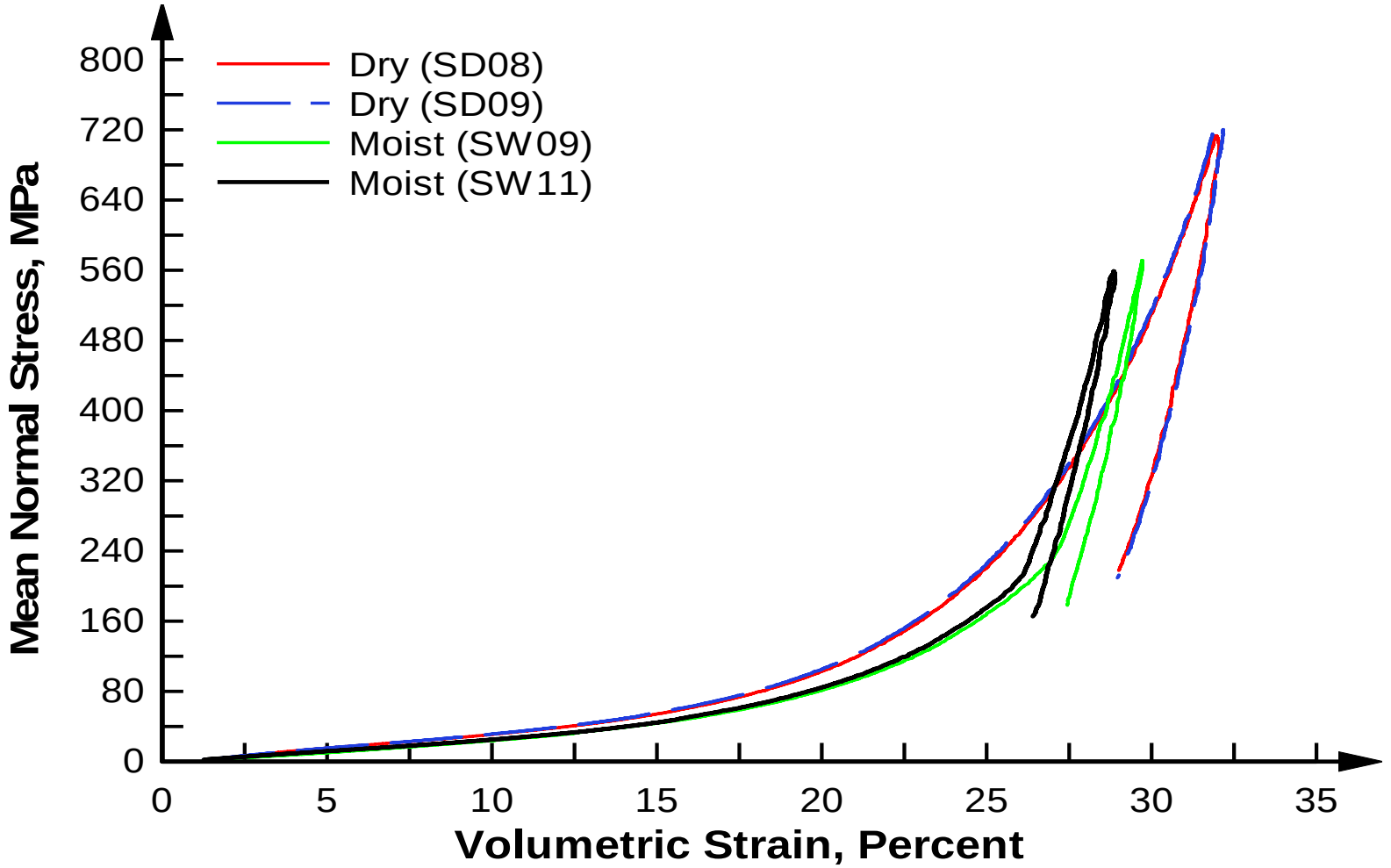

Figure 4-24. Mean Normal Stress vs. Volumetric Strain for the uniaxial strain response of Quikrete #1961 sand. [Data from Akers, S.A., Williams, E.M., and Reed, P.A., 2007, "Quasi-static Characterization of Fine Sand," Unpublished technical report, U.S. Army Engineering Research and Development Center, Geotechnical and Structures Laboratory, Vicksburg, MS.]

CHAPTER 5
CONCLUSIONS & RECOMMENDATIONS

5.1 Conclusions

An extensive and well defined experimental investigation was conducted on fine grain sand at various moisture contents. The experiments were conducted at one dry density and one strain-rate to assess the effects of varying moisture content on the dynamic compressive stress-strain behavior of fine sand. An experimental effort of this size has not been attempted by previous researchers to determine the effects of one single parameter on the response of sand. The research documented in this report coupled with research done by Song et al. [28] gives a comprehensive study of the material in this study for dry and moist/partially saturated conditions at one strain-rate. The research presented evaluated the material at a strain-rate of ~ 400 s^{-1} and at varying moisture contents from 3% to 20% and with two different levels of confinement. All experiments are considered to be in an undrained condition with the experiments using polycarbonate confinement having neither one-dimensional stress nor strain with the experiments using steel confinement approximating a one-dimensional strain condition. Results from quasi-static uniaxial strain experiments with the same material done by Akers et al. [12] suggests that moist/partially saturated sand is more compressible (less stiff) than dry sand.

In order to evaluate the moisture effects on the sand a modified split-Hopkinson pressure bar technique had to be implemented. Previous research (Veyera [3], and Felice et al. [1]) using a conventional SHPB was unable to acquire constant strain-rate (Figures 3-8 and 3-9, respectively) in the material possibly compromising there results. This study implemented the pulse shaping technique to create an incident pulse with a slower rise time to peak load to allow the specimen to acquire stress equilibrium and constant strain-rate due to the low wave speed of the material. The results of the experiments by using pulse shaping were presented in Figures 4-

14 and 4-15. These results suggest that the moist/partially saturated sand is softer than the dry sand.

The softening of the moist/partially saturated sand may be due to various frictional effects as discussed previously in Chapter 4. Although friction is more likely to be evident, qualitatively the results presented in this study show the same trends as uniaxial strain tests conducted by Akers et al. [12]. The friction, however, does present problems when evaluating the results quantitatively due to friction introducing resistance to the applied compressive load at the specimen ends. The friction inherent in the SHPB experiments are predominately created by the mechanical confinement applied to the specimen. It is known that friction exists between the confinement inner wall and specimen creating shear stresses. However, this cannot be experimentally verified due to difficulties with measuring friction during a SHPB experiment. Friction also exists between the steel platens and the ends of the specimen. This type of friction cannot be remedied since the specimen length has to be small to enable stress equilibrium and if lubrication is placed between the specimen and steel platen it will alter the material properties. An additional friction effect is caused by the interactions between particles. This friction will produce shear between the particles and act to stiffen the response of the material.

The results presented herein and previous work by Song et al. [28] used the same experimental method. Thus, the same frictional effects are present in both sets of data verifying that the qualitative response of the material is accurate. Therefore, the softening of the moist/partially saturated sand is probably due to water acting as lubrication between sand particles since the water in moist/partially saturated sand is typically concentrated in the interparticle contact areas where shear loads can be reduced. The oscillations in Figures 4-1 to 4-13 are probably due to several different effects interacting together. These effects could be

misalignment of the steel platens, interaction between the steel platens and the specimen and friction between the steel platens and confinement. These effects cannot be quantified or verified experimentally, but the oscillations occur prior to stress equilibrium and constant strain-rate not affecting the critical portion of the stress-strain curve.

In conclusion, this thesis presents a comprehensive investigation showing the effects of moisture content on sand at one high strain-rate. This data provides a better understanding of the dynamic behavior of sand for a given set of testing conditions that will provide future research with a foundation. Additionally, this study introduced a new SHPB experimental technique for assessing geo-materials dynamically while acquiring stress equilibrium and constant strain-rate simultaneously. Lastly, this data will provide necessary parameters for establishing the dynamic material behavior for constitutive modeling linking the quasi-static and dynamic strain-rate regimes.

5.2 Recommendations

The fundamental understanding of soils at high strain-rates is very limited at present. To establish a well defined constitutive relationship for soils the SHPB is essential to link the quasi-static regime and flyer plate impact regime. The complications with testing soils with a SHPB are many, but with additional investigation this method of testing will be very reliable for obtaining accurate dynamic data for geo-materials. To establish a sound experimental technique will require a comprehensive testing program. The recommendations mentioned below will aid in establishing a more refined testing technique using the SHPB for soils:

1. The confinement tube may need to be more rigid to ensure that a true one-dimensional strain condition is met.

2. Use a different confinement tube material with a lower coefficient of friction, or place a low-friction liner inside a stiff tube, acting to reduce friction between the platen and confinement and friction between the specimen and confinement reducing shear

stresses. Also, placing a liner, e.g. a thin copper sheet between the specimen and the platens, may improve the initial oscillations in the loading history.

3. Evaluate different methods of preparing sand specimens to determine the sensitivity of the data to specimen preparation. This will determine the most effective way to prepare the specimens and increase consistency in the specimen properties.

4. Study different specimen aspect ratios to determine if the stress-strain response is dependent or independent of aspect ratios.

5. Mount strain gages on the outer diameter of the confining tube to acquire a strain history. This can be coupled with FEA codes to determine the radial loading applied by the confinement.

6. Use momentum trapping to apply a single load to the specimen. This will enable the specimen properties to be evaluated following the experiment. The posttest particle size and distribution can be determined.

7. Conduct quasi-static tests using the same specimen preparation and confinement method. This would determine if friction and inertial effects play a significant role in the material response at the higher strain-rates.

To establish a constitutive model for a single type of soil (i.e. sand, clay, silt, sandy clay, etc.) an extensive testing program is required. A well-defined constitutive model needs to capture density effects, moisture effects and strain-rates effects. The tests to be performed to accomplish this are mentioned below:

1. Conduct triaxial quasi-static experiments for different moisture contents, densities and confining pressures. Frictional effects will be minimal with no inertial effects present.

2. Conduct dynamic triaxial experiments for different moisture contents, densities, confining pressures and strain-rates. The confining fluid may need to be gas rather than oil to restrict fluctuations in the confining pressure when the specimen displaces in the lateral direction.

3. Conduct Hydrostatic compression experiments for different moisture contents, densities and confining pressures.

4. Conduct uniaxial strain experiments for different moisture contents, densities and aspect ratios.

5. Conduct SHPB experiments with dry and moist sand using a latex membrane. This would approximate a one-dimensional stress state better representing a true SHPB experiment. This could simulate an in-situ top layer soil with minimal confinement.

6. Perform load induced grain refining and grain packing changes. Implementing momentum trapping the specimen would experience a single load rather than being loaded multiple times due to wave reflections. The posttest specimen would be reevaluated to establish the evolution in grain size and distribution. Evaluate specimens using similar material with different particle sizes to determine if the grain refinement and packing influences the stress-strain behavior.

LIST OF REFERENCES

[1] Felice, C.W., Gaffney, E.S., Brown, J.A., and Olsen, J.M., 1987, "Dynamic High Stress Experiments on Soil," Geotechnical Testing Journal, GTJODJ, **10**, No. 4, pp. 192-202.

[2] Hampton, D., and Wetzel, R.A., 1966, "Stress Wave Propagation in Confined Soils," AFWL-TR-66-56, Air Force Weapons Laboratory, Kirkland AFB, New Mexico.

[3] Veyera, G.E., 1994, "Uniaxial Stress-Strain Behavior of Unsaturated Soils at High Strain Rates," WL-TR-93-3523, Wright Laboratory Flight Dynamics Directorate, Tyndall AFB, FL.

[4] Kolsky, H., 1949, "An Investigation of the Mechanical Properties of Materials at very High Rates of Loading," Proc. Phys. Soc. London, **B62**, pp. 676-700.

[5] Kolsky, H., 1963, "*Stress Waves in Solids*," Dover Publications Inc., New York, NY.

[6] Nemat-Nasser, S., 2000, "Introduction to High Strain Rate Testing," *Mechanical Testing and Evaluation,* Metals Handbook, American Society for Metals, Materials Park, OH, **8**, pp. 427-446.

[7] Pierce, S., 1989, "High Intensity Compressive Stress Wave Propagation through Unsaturated Sands," Master Thesis, Colorado State University, Fort Collins, Co.

[8] Charlie, W.A., Ross, C.A., and Pierce, S.J., 1990, "Split-Hopkinson Pressure Bar Testing of Unsaturated Sand," Geotechnical Testing Journal, GTJODJ, **13**, No. 4, pp. 291-300.

[9] Ross, C.A., Nash, P.T., and Friesenhahan, C.J., 1986, "Pressure Waves in Soils Using a Split-Hopkinson Pressure Bar," ESL-TR-86-29, Engineering and Services Laboratory, Air Force Engineering and Services Center, Tyndall AFB, FL.

[10] Felice, C.W., Brown, J.A., Gaffney, E.S., and Olsen, J.M., 1987, "An Investigation into the High Strain-rate Behavior of Compacted Sand Using the Split-Hopkinson Pressure Bar Technique, *Proc., 2nd Symp. on the Interaction of Non-Nuclear Munitions With Structures*, Panama City Beach, FL, pp. 391-396.

[11] Lee, M.Y., Luk, V.K., and Bronowski, D.R., 2006, "Quasi-static Characterization of Fine Sand," *Fall meeting of TCG-XI*, Eglin AFB, FL.

[12] Akers, S.A., Williams, E.M., and Reed, P.A., 2007, "Quasi-static Characterization of Fine Sand," Unpublished technical report, U.S. Army Engineering Research and Development Center, Geotechnical and Structures Laboratory, Vicksburg, MS.

[13] Whitman, R.V., Roberts, J.E., and Mao, S., 1960, "Report 4: One-Dimensional Compression and Wave Velocity Tests," Contract No. DA-22-079-eng-224, U.S. Army Engineer Waterways Experiment Station, CE, Vicksburg, MS.

[14] Whitman, R.V., 1970, "The Response of Soils to Dynamic Loadings: Report 26, Final Report," Contract Report No. 3-26, U.S. Army Waterways Experiment Station, Vicksburg, MS.

[15] Durbin, W.L., 1964, "Study of the Dynamic Stress-Strain and Wave Characteristics of Soils," URS for U.S.A. Engr. Waterways Experiment Station (Contract DA-22-079-eng-373) Rpt. 2, Contract Rpt. 3-91.

[16] Duffy, J., Campbell, J.D., and Hawley, R.H., 1971, "On the Use of a Torsional Split Hopkinson Bar to Study Rate Effects in 1100-0 Aluminum," ASME Trans. J. Appl. Mech., **37**, pp. 83-91.

[17] Ellwood, S., Griffiths, L.J., and Parry, D.J., 1982, "Materials Testing at High Constant Strain Rates," J. Phys. E: Sci. Instrum., **15**, pp. 280-282.

[18] Christensen, R.J., Swanson, S.R., and Brown, W.S., 1972, "Split-Hopkinson-bar Tests on Rock under Confining Pressure," Exp. Mech., pp. 508-513.

[19] Frantz, C.E., Follansbee, P.S., and Wright, W.T., 1984, " Experimental Techniques with the Split Hopkinson Pressure Bar," *Proceedings of the 8th International Conference on High Energy Rate Fabrication,* Pressure Vessel and Piping Division, ASME, pp. 229-236, Texas, TX.

[20] Nemat-Nasser, S., Isaacs, J.B., and Starrett, J.E., 1991, "Hopkinson Techniques for Dynamic Recovery Experiments," Proc. R. Soc. London, Ser. A, **A435**, pp. 371-391.

[21] Frew, D.J, Forrestal, M.J., and Chen, W., 2005, "Pulse Shaping Techniques for Testing Elastic-Plastic Materials with a Split Hopkinson Pressure Bar," Exp. Mech., **45**, pp. 186-195.

[22] Frew, D.J, Forrestal, M.J., and Chen, W., 2002, "Pulse Shaping Techniques for Testing Brittle Materials with a Split Hopkinson Pressure Bar," Exp. Mech., **42**, pp. 93-106.

[23] Hopkinson, B., 1914, "A Method of Measuring the Pressure Produced in the Detonation of High Explosives or by the Impact of Bullets," Philos. Trans. R. Soc. London, Ser. *A*, **213**, pp. 437-456.

[24] Davies, R.M., 1948, "A Critical Study of the Hopkinson Pressure Bar," Philos. Trans. R. Soc. London, Ser. A, **240**, pp. 375-457.

[25] Gray, G.T., 2000, "Classic Split-Hopkinson Pressure Bar Testing," *Mechanical Testing and Evaluation*, Metals Handbook, American Society for Metals, Materials Park, OH, **8**, pp. 462-476.

[26] Gray, G.T., 1997, "High-Strain-Rate Testing of Materials: The Split-Hopkinson Pressure Bar," LA-UR-97-4419, Los Alamos National Laboratory, Santa Fe, New Mexico.

[27] Gray, G.T., and Blumenthal, W.R., 2000, "Split Hopkinson Pressure Bar Testing of Soft Materials," *Mechanical Testing and Evaluation*, Metals Handbook, American Society for Metals, **8**, Materials Park, OH, pp. 488-496.

[28] Song, B., and Chen, W., 2006, "Dynamic Compressive Behavior of Sands," Unpublished technical report, School of Aeronautics and Astronautics and School of Materials Engineering, Purdue University.

[29] Davies, E.D.H., and Hunter, S.C., 1963, "Dynamic Compression of Solids by the Method of the Split Hopkinson Pressure Bar," J. Mech. Phys. Solids, **11**, pp. 155-179.

[30] Craig, R.F., 1987, "*Soil Mechanics*," 4th Edition, Chapman & Hall, 2-6 Boundary Row, London SE1 8HN, UK.

[31] Williams, E.M., Akers, S.A., and Reed, P.A., 2006, "Laboratory Characterization of SAM-35 Concrete," ERDC/GSL TR-06-15, U.S. Army Engineering Research and Development Center, Geotechnical and Structures Laboratory, Vicksburg, MS.

BIOGRAPHICAL SKETCH

Bradley E. Martin was born in Pensacola, FL, on December 16, 1975. He graduated with a Bachelor of Science in mechanical engineering from the University of South Alabama in 2001. Upon graduation, he was hired at Ingalls Shipbuilding in Pascagoula, MS, as a Life Cycle Engineer. Bradley, in August 2001, was hired by General Dynamics-OTS in Niceville, FL, as a Design Engineer where he primarily conducted penetration and sled track experiments. In June 2002, he was hired by the Air Force Research Laboratory (AFRL) Eglin AFB, FL, at the Damage Mechanisms Branch. Bradley is still currently working for the AFRL conducting applied research for the Department of Defense. While working for AFRL, he has completed a Master of Engineering degree at the University of Florida in August of 2007.